Time-Resolved Total Internal Reflection Fluorometry Study on Chemical and Structural Characteristics at Liquid/Liquid Interfaces

Shoji Ishizaka

Division of Chemistry, Graduate School of Science, Hokkaido University,

2001

Contents

Chapter 1

Introduction

1.1 Introduction

Chemistry at a liquid/liquid interface is the fundamental basis for various sciences, and it has been well recognized that an interface of two immisible liquid/liquid plays essential roles in chromatography, a phase-transfer catalysis, solvent extraction, and so forth.[1-13] Furthermore, liquid/liquid interfacial systems have been also widely used in applied sciences (i.e., foods, photographs, paints, cosmetics, and so forth). Biological cells are an another example of liquid/liquid systems, in which two water phases are separated by an organic membrane wall and various chemical reactions proceed across the membrane wall. Therefore, directional mass/electron transfer across liquid/liquid interfaces has been studied as a model of biological systems.[14-18] Recently, liquid/liquid interfacial systems have also received current interests in reference to a model of molecular/ion recognition processes in biological systems.[19-25] All these interfacial phenomena are supposed to be dependent on nature of a liquid/liquid interface, so that detailed understanding of chemical and structural characteristics of liquid/liquid interfaces at a microscopic level would afford wide benefit for further advances in various sciences. Nonetheless, very little is known about chemical and

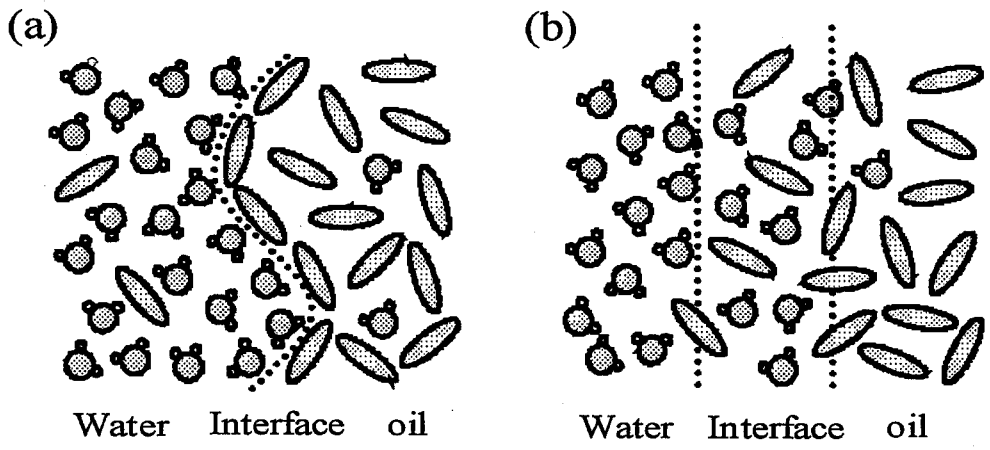

Figure 1-1 Model of sharp (a) and diffuse (b) boundary between two immiscible solvent.

structural characteristics of a liquid/liquid interface at a microscopic level.

So far, experimental studies on liquid/liquid interfaces have been conducted on the basis of thermodynamic,[26-29] spectroscopic[30-41] and electrochemical techniques,[42-155] and fundamental knowledge about the properties of liquid/liquid interfaces has been accumulated in the past decades. However, experimental results obtained by these studies do not necessarily provide microscopic or molecular-level characteristics at the interface, since these studies are based essentially on bulk measurements. In the field of electrochemistry, as an example, mass/electron transfer processes across liquid/liquid interfaces have been studied extensively.[42-155] Although such approaches were very successful to elucidate kinetic mechanisms of interfacial processes, characteristic features of the chemistry at an interface in nanometer resolution cannot be obtained. One basic issue, thus remained unsolved, is the thickness and/or roughness of a liquid/liquid interface. For instance, Schiffrin and Girault studied ground-state electron transfer at a liquid/liquid interface and reported that the interfacial region was considered to be a "mixed-solvent" region, which was thick enough to be considered as the third phase.[70] On the other hand, another view of the interface has been provided by the study on ion transfer kinetics across liquid/liquid interfaces by means of faradaic impedance measurements at equilibrium potentials. These studies predicted that the existence of a "sharp inner layer" at the phase boundary.[76] These two models are schematically illustrated in Figure 1-1 as limiting cases of a liquid/liquid interface. To date, however, there is no clear experimental evidence on these models. A clearer picture of liquid/liquid phenomena is obtained only by exact knowledge about the structural characteristics at a liquid/liquid interface. Experimental approaches other than those mentioned above are needed to reveal an unambiguous picture of the microscopic structures at a liquid/liquid interface.

Recent advances in molecular dynamics simulations have provided invaluable information about molecular level characteristics of the interface.[156-205] As an example, Benjamin and his co-workers have reported the structures of water/CCl_4 and water/1,2-dichloroethane (DCE) interfaces on the basis of molecular dynamics computer simulations, and demonstrated that a water/DCE interface is molecularly sharp; there is no-mixed solvent layer between the two phases.[156,157,161,180] However, they have also pointed out that the physical property of the interface is characterized by thermally capillary waves[206-209] generated at the sharp interface and, the interface is quite rough at a short time scale. Such an information is very important to elucidate further the liquid/liquid interfacial structures including its dynamics. Nonetheless, complementary studies with experiments are limited, so that predictions by the simulations are still controversial and worth checking experimentally.

Among the past decades, new experimental techniques were developed and applied to studying interfacial processes at a liquid/liquid boundary: nonlinear optical techniques (second harmonic generation (SHG)[210-216] and sum frequency generation (SFG)[217-229]), neutron specular reflectivity measurements[230-234], a quasi-elastic laser scattering (QELS)[235-240], and total-internal-reflection (TIR) spectroscopy.[241-263] Although nonlinear optical techniques have afforded new insight about the characteristics of liquid/liquid interfaces such as molecular orientations and hydrogen bonding structures of water at the interface, dynamic motions of a solute molecule at an interface cannot be observed. On the other hand, neutron specular reflectivity measurements can afford new insight about the thickness of the interfacial layer. Nonetheless, it is very difficult to discuss dynamic motions of a molecule at the interface. QELS provides information about the role of thermal capillary waves in physical properties of the interface. However, its time-resolution is in a rage of milliseconds so that dynamic aspects of the structure in

nanometer cannot be obtained. On the other hand, it is well known that both nanometer and nanosecond ~ picosecond resolutions at an interface can be achieved by TIR fluorescence spectroscopy. In different from steady-state fluorescence spectroscopy, fluorescence dynamics is highly sensitive to microscopic environments, so that time-resolved TIR fluorometry at liquid/liquid interfaces is worth exploring to obtain a clearer picture of the interfacial phenomena.

One of the interesting targets to be studied on a liquid/liquid interface is characteristics of dynamic motions of a molecule at the interface. Dynamic molecular motions at a liquid/liquid interface are considered to be influenced by a subtle change in the chemical/physical properties of the interface, particularly in a nanosecond ~ picosecond time regime, so that time-resolved spectroscopy is expected to be highly potential to study nature of a liquid/liquid interface. As an example of such a study, Wirth and Burbage reported in-plane and out-of-plane reorientation dynamics of Acridine Orange at water/oil interfaces on the basis of fluorescence depolarization measurements and, demonstrated that out-of-plane reorientation of the dye was influenced by surface roughness, while the in-plane reorientational dynamics was almost independent of the viscosity of the oil phase.[242] Although a fluorescence depolarization technique is certainly promising to obtain an inside look at a liquid/liquid interface, the number of the study along the line is still limited. Furthermore, their study was conducted by using a frequency domain technique. In order to obtain more detailed information, therefore, fluorescence dynamic anisotropy measurements of a dye adsorbed on water/oil interfaces are worth exploring on the basis of a picosecond time-correlated single photon counting technique.[264]

1.2 Experimental Approaches of the Study

In the present study, the following experimental approaches were employed to study characteristics of water/oil interfaces.

Dynamic fluorescence anisotropy is based on rotational reorientation of the excited dipole of a probe molecule, and its correlation time(s) should depend on local environments around the molecule. For a dye molecule in an isotropic medium, three-dimensional rotational reorientation of the excited dipole takes place freely.[265-274] At a liquid/liquid interface, on the other hand, the out-of-plane motion of a probe molecule should be frozen when the dye is adsorbed on a sharp liquid/liquid interface (i.e., two-dimension in respect to the molecular size of a probe), while that will be allowed for a relatively thick liquid/liquid interface (i.e., three-dimension).[243, 275] Thus, by observing rotational freedom of a dye molecule (i.e., excited dipole), one could discuss thickness of a water/oil interface and the correlation time(s) provides information about the chemical/physical characteristics of the interface, including dynamical behavior of the interfacial structure. Dynamic fluorescence anisotropy measurements are thus expected to provide new insight about a liquid/liquid interface, not obtained by conventional spectroscopies.

It is worth noting, however, that liquid/liquid interfacial structures would be governed by various factors, so that a complementary study other than fluorescence dynamic anisotropy is required to obtain further detailed information about the characteristics at a liquid/liquid interface. As a new and novel approach, therefore, excitation energy transfer dynamics and the relevant structural (fractal) dimension analysis were also introduced to elucidate the structure of a liquid/liquid interface.

Dipole-dipole (Förster-type) excitation energy transfer between an energy donor (D)

and an acceptor (A) both adsorbed on a liquid/liquid interface is considered here. When diffusional motions of D and A are inhibited as in the case for strong binding of the molecules to the surface by adsorption, excitation energy transfer quenching dynamics of D by A reflects structural dimension around D and A through spatial distributions of the components.[276,277] Actually, the method has been applied to study nanometer-scale morphologies in Langmuir-Blodgett films,[278,279] vesicles,[279,280] polymers,[281-284] and silica gels.[285-287] Therefore, it is expected that a study on excitation energy transfer dynamics provides invaluable information about the characteristics at a liquid/liquid interface, along with a complementary study on the same system by fluorescence dynamic anisotropy.

1.3 Theoretical Background of the Experiments

In order to study interfacial phenomena at a liquid/liquid boundary at a microscopic level, surface selective or depth-resolved measurements at an interface are absolutely necessary. Among several methods, total internal reflection spectroscopy is a powerful means to obtain an inside look at an interfacial layer in several tens to several hundreds nanometers. In this study, therefore, total internal reflection (TIR) spectroscopy was employed to follow chemical and physical characteristics at liquid/liquid interfaces. The basic theory of TIR of light is thus briefly reviewed in the followings.

1.3.1 Total Internal Reflection (TIR)

Whenever electromagnetic radiation is incident at an interface separating two media, a part of the beam is *reflected* back into a medium *1*, while the part continues into a medium *2*, but with an altered direction of propagation. This latter phenomenon is termed *refraction*. Figure 1-2 depicts this situation, where the subscripts i, t and r refer to the incident, transmitted, and reflected beams, respectively. The radiation is incident from a medium of a lesser refractive index (n_1) upon a medium of a greater refractive index (n_2); $n_2 > n_1$. In such a case, a phenomenon of reflection is termed *external reflection*, and a real angle of refraction, θ_t, exists for all possible choices of the angle of incidence, θ_i, with the condition of $\theta_t < \theta_i$. On the other hand, under the refractive index condition of $n_1 > n_2$, a phenomenon of reflection is termed *internal reflection,* and it is obvious from Snell's law that the angle of refraction becomes imaginary for values of the

angle of incidence such that $\theta_i > \sin^{-1}(n_2 / n_1)$. The angle above which this refracted wave ceases to be real is termed the *critical angle*, θ_c;

$$\theta_c = \sin^{-1}(n_2 / n_1) \tag{1.1}$$

In the case of $\theta_i > \theta_c$, the reflectivity becomes unity for both the parallel and perpendicular components. This phenomenon is appropriately termed *total internal reflection*.[288,289]

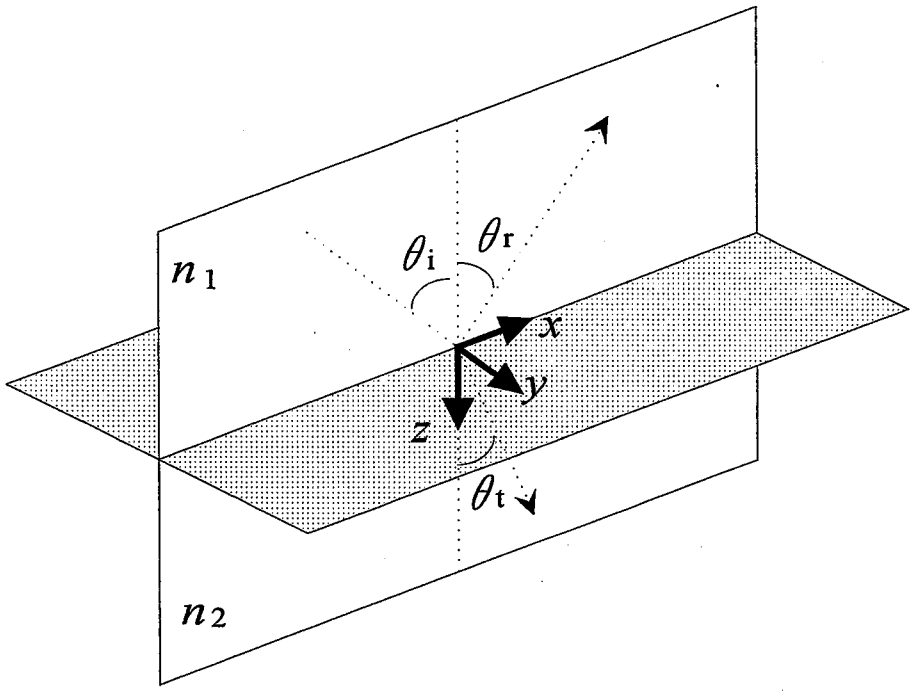

Figure 1-2 Schematic representation of refraction and reflection of a plane electromagnetic wave at a boundary. The surface normal is taken along the *z* axis, and the incident beam is assumed to be in the *x*-*z* plane (plane of incidence).

1.3.2 Evanescent Wave

In terms of the relative index of refraction, $n = (n_2 / n_1) < 1$, the following expressions follow from Snell's law for angles of incidence greater than the critical angle:

$$\sin\theta_t = (1/n)\sin\theta_i \tag{1.2}$$

$$\cos\theta_t = \left[1-(1/n^2)\sin^2\theta_i\right]^{1/2} = i\left[(1/n^2)\sin^2\theta_i - 1\right]^{1/2} \tag{1.3}$$

Using these values in Fresnel's formula, the amplitude of the reflected beam perpendicular to the plane of incidence ($A_{r\perp}$) is given by eq. (1.4),

$$A_{r\perp} = A_{i\perp}\frac{(1/n)\cos\theta_i - i\left[(1/n^2)\sin^2\theta_i - 1\right]^{1/2}}{(1/n)\cos\theta_i + i\left[(1/n^2)\sin^2\theta_i - 1\right]^{1/2}} \tag{1.4}$$

which is equivalent to

$$A_{r\perp} = A_{i\perp}\exp(-i\delta_\perp) \tag{1.5}$$

where

$$\tan\left(\frac{\delta_\perp}{2}\right) = \frac{\left[(1/n^2)\sin^2\theta_i - 1\right]^{1/2}}{(1/n)\cos\theta_i} \tag{1.6}$$

Thus, the perpendicular component of a reflected wave whose incidence in the *x-z* plane is

$$E_{r\perp} = A_{i\perp}\exp\left[i\left\{\omega t - k(x\sin\theta_i - z\cos\theta_i) - \delta_\perp\right\}\right] \tag{1.7}$$

In a similar way, those of the parallel components are expressed as

$$A_{r//} = A_{i//} \frac{\cos\theta_i - (i/n)\left[(1/n^2)\sin^2\theta_i - 1\right]^{1/2}}{\cos\theta_i + (i/n)\left[(1/n^2)\sin^2\theta_i - 1\right]^{1/2}} \tag{1.8}$$

or

$$E_{r//} = A_{i//} \exp\left[i\left\{\omega t - k(x\sin\theta_i - z\cos\theta_i) - \delta_{//}\right\}\right] \tag{1.9}$$

where

$$\tan\left(\frac{\delta_{//}}{2}\right) = \frac{(1/n)\left[(1/n^2)\sin^2\theta_i - 1\right]^{1/2}}{\cos\theta_i} \tag{1.10}$$

Hence, the components of **E** parallel and perpendicular to the plane of incidence undergo phase retardations $\delta_{//}$ and $\delta_{\perp}$, respectively, although the amplitudes are unaltered by reflection. If the incident wave is plane polarized, the incident components are in phase, while those of the reflected wave are not, so that elliptical polarization is produced. The magnitude of the phase shift for $\theta_i > \theta_c$ is,

$$\tan\left(\frac{\delta_{//}}{2} - \frac{\delta_{\perp}}{2}\right) = \frac{\cos\theta_i\left[(1/n^2)\sin^2\theta_i - 1\right]^{1/2}}{(1/n)\sin^2\theta_i} \tag{1.11}$$

The above-mentioned phase shift for the angle of incidence greater than the critical angle implies the existence of a resultant field in the first medium at the interface. In order that the boundary conditions remain satisfied, there must be a resultant disturbance in the second phase. It can readily be shown that this disturbance is of the nature of an exponentially damped wave which penetrates into the second medium. This wave is termed *evanescent wave*.

The depth of penetration of an evanescent wave into the second medium (d_p) can be quantitatively defined in terms of the distance required for the electric field intensity to decrease to $1/e$ of its initial value,

$$d_p = \left(\frac{\lambda}{2\pi}\right)\left(n_1^2 \sin^2 \theta_i - n_2^2\right)^{-1/2} \tag{1.12}$$

where λ is the wavelength of the radiation in the first medium. However, we actually deal with the intensity of the light rather than that of the electric field in the TIR fluorometry, which is proportional to a square of the electric field. More practical formula of the penetration depth of an evanescent wave is defined as follows. [290]

$$d_p = \left(\frac{\lambda}{4\pi}\right)\left(n_1^2 \sin^2 \theta_i - n_2^2\right)^{-1/2} \tag{1.13}$$

Equation (1.13) shows that the depth of penetration depends on the wavelength and the angle of an incident beam. Thus, an appropriate choice of the angle of an incident light beam enables one depth-resolved measurement of an interface.

1.4 Purpose and Content of the Thesis

The purpose of the thesis is to elucidate structures of liquid/liquid interfaces on the basis of time-resolved total-internal reflection fluorescence spectroscopy and discuss the interfacial characteristics at a molecular level.
The thesis consists of six chapters.

In Chapter 1, historical backgrounds of the studies on liquid/liquid interfaces were overviewed and, the experimental strategies of the study on the interfaces were described. Furthermore, the principal of Total-Internal Reflection Spectroscopy necessary to discuss the experimental results obtained by this study was outlined.

In Chapter 2, fluorescence dynamics of a 1-pyrene sulfonate anion (PSA) adsorbed on a water/1,2-dichloroethane (DCE) interface was described. In TIR fluorometry, a penetration depth of an incident evanescent wave possesses a finite value, so that fluorescence characteristics of the dye in a bulk phase are superimposed more or less to those at an interface. After describing general features of the fluorescence spectra and the dynamics of PSA at a water/DCE interface, separation of the interfacial and bulk fluorescence characteristics of PSA will be demonstrated

In Chapter 3, fluorescence dynamic anisotropy of Sulforhodamine 101 (SR101) at water/ phthalate esters (PE) interfaces was described and the structures of the interface were discussed on the basis of the rotational reorientation times of SR101.

In Chapter 4, the experiments were focused to reveal the structures of water/carbon tetrachloride (CCl_4) and water/1,2-dichloroethane (DCE) interfaces. Fluorescence

dynamic anisotropy and excitation energy transfer quenching of Sulforhodamine 101 (SR101) at water/CCl_4 and water/DCE interfaces were introduced to the experiments and, thickness and/or roughness of the interfaces were discussed in detail.

In Chapter 5, Sulforhodamine B (SRB) was used as a probe molecule to investigate the interfacial polarity. Since SRB is surface active and possesses a high fluorescence quantum yield, the dye is very suitable for TIR fluorescence measurements at a liquid/liquid interface. Furthermore, it has been reported that the non-radiative decay rate constant (k_{nr}) of Rhodamine B (RB) is sensitive to a medium polarity and, $\ln(k_{nr})$ is linearly correlated to $E_T(30)$.[291,292] On the basis of fluorescence dynamic measurements of SRB adsorbed on a water/oil interface, a relationship between interfacial thickness/roughness and the polarity at the interface was discussed.

In Chapter 6, the results of the study were summarized and future perspective of the research was discussed.

1.5 References and Notes

(1) Surakitbanharn, Y.; Muralidharan, S.; Freiser, H.; *Anal. Chem.* **1991**, *63*, 2642.

(2) Chen, F.; Ma, H.; Freiser, H.; Muralidharan, S. *Langmuir* **1995**, *11*, 3235.

(3) Starks, C.M.; Liotta, C.; *Phase Transfer Catalysis*; Academic Press: London, 1978.

(4) Demlow, E.V. and Demlov, S.S., *Phase Transfer Catalysis: 2nd revised edition*, Verlag Chemie, Weinheim, 1983.

(5) Cunnane, V.J.; Schiffrin, D.J.; Beltran, C.; Geblewicz, G.; Solomon, T. *J Electroanal. Chem.*, **1988**, *247*, 203

(6) Carter, S.P.; Freiser, H. *Anal. Chem.* **1979**, *51*, 1100.

(7) Watarai, H.; Cunningham, L.; Freiser, H. *Anal. Chem.* **1982**, *54*, 2390.

(8) Watarai, H.; Takahashi, M.; Shibata, K. *Bull. Chem. Soc. Jpn.* **1986**, *59*, 3469.

(9) Watarai, H. *Bunseki Kagaku* **1996**, *45*, 725-744.

(10) Watarai, H. *J. Chromatography* **1997**, *780*, 93-102.

(11) Shi, C.; Anson, F. C. *Anal. Chem.* **1998**, *70*, 3114–3118.

(12) Shao, Y.; Mirkin, M.V. *Anal. Chem.* **1998**, *70*, 3155–3161.

(13) Ma, M.; Cantwell, F.F. *Anal. Chem.* **1999**, *71*, 388–393.

(14) Girault, H.H.; Schiffrin, D.J. In *Electroanalytical Chemistry*; Bard, A. J., Ed.; Marcel Dekker: New York, 1989; Vol 15, Chapter 1.

(15) Volkov, A.G.; Deamer, D.W., Eds. *Liquid-Liquid interfaces*; CRC Press: Boca Raton, FL, 1996.

(16) Cheng, Y.; Schiffrin, D.J. *J. Chem. Soc., Faraday Trans.* **1994**, *90*, 2517.

(17) Cheng, Y.; Cunnane, V.J.; Kontturi, A.K.; Schiffrin, D.J. *J. Phys. Chem.* **1996**, *100*, 15470.

(18) Maeda, K.; Nishihara, M.; Ohde, H.; Kihara, S. *J. Electroanalytical Chemistry*; **1998**, *14*, 85-88.

(19) Wipff, G.; Lauterbach, M. *Supramolecular Chem.* **1995**, *6*, 187.

(20) Guilbaud, P.; Wipff, G. *New Journal of Chem.* **1996**, *20*, 631-642.

(21) Troxler, L.; Wipff G. *Anal. Sci.* **1998**, *14*, 43-56.

(22) Shioya, T.; Nishizawa, S.; Teramae, N. *J. Am. Chem. Soc.* **1998**, *120*, 11534-11535.

(23) Muzet, N.; Engler, E.; Wipff G. *J. Phys. Chem. B* **1998**, *102*, 10772-10788.

(24) Ohashi, A.; Tsukahara, S.; Watarai H. *Anal. Chim. Acta.* **1999**, *394*, 23-31.

(25) Teramae, N.; Uchida, T.; Yamaguchi, A.; Nochi, K.; Yamashita, T.; Shioya, T. *Bunseki Kagaku* **1999**, *48*, 1063-1075.

(26) Kakiuchi, T., Senda, M. *Bull. Chem. Soc. Jpn.* **1983**, *56*, 2912.

(27) Girault, H.H.; Schiffrin, D.J. *J. Electroanalytical Chemistry*; **1984**, *170*, 127.

(28) Hunsel, J.V.; Bleys, G.; Joos, P. *J. Colloid Interface Sci.* **1986**, 114, 432.

(29) Kakiuchi, T.; Nakanishi, M.; Senda, M. *Bull. Chem. Soc. Jpn.* **1988**, *61*, 1845.

(30) Watarai, H.; Sasaki, K.; Takahashi, K.; Murakami, J. *Talanta* **1995**, *42*, 1691–1700.

(31) Chiba, Y.; Watarai, H. *Bull. Chem. Soc. Jpn.* **1996**, *69*, 341–347.

(32) Nagatani, H.; Watarai, H. *Anal. Chem.* **1996**, *68*, 1250–1253.

(33) Nagatani, H.; Watarai, H. *Chem. Lett.* **1997**, *2*, 167-168.

(34) Nagatani, H.; Watarai, H. *J. Chem. Soc. Faraday Trans.* **1998**, *94*, 247-252.

(35) Onoe, Y.; Tsukahara, S.; Watarai, H. *Bull. Chem. Soc. Jpn.* **1998**, *71*, 603–608.

(36) Ohashi, A.; Tsukahara, S.; Watarai, H. *Anal. Chim. Acta* **1998**, *364*, 53-62.

(37) Nagatani, H.; Watarai, H. *Anal. Chem.* **1998**, *70*, 2860–2865.

(38) Ohashi, A.; Tsukahara, S.; Watarai, H. *Anal. Chim. Acta* **1999**, *394*, 23-31.

(39) Nagatani, H.; Watarai, H. *Chem. Lett.* **1999**, *7*, 701-702.

(40) Nagatani, H.; Watarai, H. *Anal. Chim. Acta* **2000**, *419*, 107-114.

(41) Webster, R.D.; Dryfe, R.A.W.; Coles, B.A.; Compton, R.G. *Anal. Chem.* **1998**, *70*, 792–800.

(42) Gavach, C.; Henry, F.J. *J. Electroanal. Chem.* **1974**, *54*, 361.

(43) Guaninazzi, M.; Silvestri, G.; Serravalle, G. *J. Chem. Soc. Chem. Commun.* **1975**, 200.

(44) Koryta, J.; Vanysek, P.; Brezina, M. *J. Electroanal. Chem.* **1977**, *75*, 211.

(45) Gavach, C.; Seta, P.; d'Epenoux, B. *J. Electroanal. Chem.* **1977**, *83*, 225.

(46) Samec, Z.; Marecek, V.; Koryta, J.; Khalil, M.W. *J. Electroanal. Chem.* **1977**, *83*, 393.

(47) Samec, Z.; Marecek, V., Weber, J. *J. Electroanal. Chem.* **1979**, *96*, 245.

(48) Samec, Z. *J. Electroanal. Chem.* **1979**, *99*, 197.

(49) Samec, Z.; Marecek, V.; Weber, J.; Homolka, D. *J. Electroanal. Chem.* **1979**, *99*, 385.

(50) Samec, Z.; Marecek, V.; Weber, J. *J. Electroanal. Chem.* **1979**, *100*, 841.

(51) Samec, Z. *J. Electroanal. Chem.* **1979**, *103*, 1.

(52) Samec, Z.; Marecek, V., Weber, J. *J. Electroanal. Chem.* **1979**, *103*, 11.

(53) Koryta, J. *Electroanchim. Acta* **1979**, *24*, 293.

(54) Samec, Z. *J. Electroanal. Chem.* **1980**, *111*, 211.

(55) Homolka, D.; Hung, L.Q.; Hofmanova, A.; Khalil, J; Koryta, J.; Marecek, V.; Samec, Z.; Sen, S.K.; Vanysek, P.; Weber, J.; Brezina, M. *Anal. Chem.* **1980**, *52*, 1606.

(56) Samec, Z.; Marecek, V.; Weber, J.; Homolka, D. *J. Electroanal. Chem.* **1981**, *126*, 105.

(57) Melroy, O.R.; Buck, R.P; *J. Electroanal. Chem.* **1982**, *136*, 19.

(58) Osakai, T.; Kakiuchi, T.; Senda, M. *Bull. Chem. Soc. Jpn.* **1984**, *57*, 370.

(59) Marecek, V.; Samec, Z. *J. Electroanal. Chem.* **1985**, *185*, 263.

(60) Samec, Z.; Marecek, V.; Homolka, D. *J. Electroanal. Chem.* **1985**, *187*, 31.

(61) Girault, H.H.; Schiffrin, D.J. *J. Electroanal. Chem.* **1985**, *195*, 213.

(62) Gennett, T.; Milner, D.F.; Weaver, M.J. *J. Phys. Chem.* **1985**, *89*, 2787.

(63) Buck, R.P.; Bronner, W.E. *J. Electroanal. Chem.* **1986**, *197*, 179.

(64) Kihara, S.; Suzuki, M.; Maeda, K.; Ogura, K.; Umetani, S.; Matsui, M.; Yoshida, Z. *Anal. Chem.* **1986**, *58*, 2954.

(65) Samec, Z.; Marecek, V. *J. Electroanal. Chem.* **1986**, *200*, 17.

(66) Kihara, S.; Suzuki, M.; Maeda, K.; Ogura, K.; Matsui, M.; Yoshida, Z. *J. Electroanal. Chem.* **1986**, *210*, 147.

(67) Kakiuchi, T.; Nishiwaki, Y.; Osakai, T.; Senda, M. *Bull. Chem. Soc. Jpn.* **1986**, *59*, 781.

(68) Hanzlik, J.; Samec, Z.; Hovolka, J. *J. Electroanal. Chem.* **1987**, *216*, 303.

(69) Samec, Z.; Marecek, V.; Holub, K; Racinsky, S.; Hajkova, P. *J. Electroanal. Chem.* **1987**, *225*, 65.

(70) Girault, H. H. *J. Electroanchim. Acta* **1987**, *132*, 383.

(71) Girault, H.H.; Schiffrin, D.J. *J. Electroanal. Chem.* **1988**, *244*, 15.

(72) Geblewicz, G.; Schiffrin, D.J. *J. Electroanal. Chem.* **1988**, *244*, 27.

(73) Girault, H.H. *J. Electroanal. Chem.* **1988**, *257*, 47.

(74) Koryta, J. *Electroanchim. Acta* **1988**, *33*, 189.

(75) Kihara, S.; Suzuki, M.; Maeda, K.; Ogura, K.; Matsui, M.; Yoshida, Z. *J. Electroanal. Chem.* **1989**, *271*, 107.

(76) Wandlowski, T.; Marecek, V.; Holub, K; Samec, Z. *J. Phys. Chem.* **1989**, *93*, 8204.

(77) Samec, Z.; Brown, A.R.; Yellowlees, L.J.; Girault, H.H. *J. Electroanal. Chem.* **1990**, *288*, 245.

(78) Kakiuchi, T.; Senda, M. *J. Electroanal. Chem.* **1991**, *300*, 432.

(79) Maeda, K.; Kihara, S.; Suzuki, M.; Matsui, M. *J. Electroanal. Chem.* **1991**, *303*, 171.

(80) Cheng, Y.; Schiffrin, D.J. *J. Electroanal. Chem.* **1991**, *314*, 153.

(81) Senda, M.; Kakiuchi, T.; Osakai, T, *Electroanchim. Acta* **1991**, *36*, 253.

(82) Chen, Q.Z.; Iwamoto, K.; Seno, M. *Electroanchim. Acta* **1991**, *36*, 291.

(83) Matsuda, H.; Yamada, Y.; Kanamori, K.; Kudo, Y. Takeda, Y. *Bull. Chem. Soc. Jpn.* **1991**, *64*, 1497.

(84) Kihara, S.; Maeda, K.; Suzuki, M.; Sohrin, Y.; Shirai, O.; Matsui, M. *Anal. Sci.* **1991**, *7*, 1415.

(85) Kakiuchi, T. *J. Electroanal. Chem.* **1992**, *322*, 55.

(86) Kakiuchi, T.; Noguchi, J.; Senda, M. *J. Electroanal. Chem.* **1992**, *327*, 63.

(87) Samec, Z.; Marecek, V. *J. Electroanal. Chem.* **1992**, *333*, 319.

(88) Kakiuchi, T.; Noguchi, J.; Senda, M. *J. Electroanal. Chem.* **1992**, *336*, 137.

(89) Osakai, T.; Himeno, S.; Saito, A. *J. Electroanal. Chem.* **1993**, *360*, 299.

(90) Cheng, Y.; Schiffrin, D.J. *J. Chem. Soc., Faraday Trans.* **1993**, *89*, 199.

(91) Wang, H.; Yao, Y.; Wang, E. *J. Electroanal. Chem.* **1994**, *372*, 21.

(92) Senda, M. *J. Electroanal. Chem.* **1994**, *378*, 215-220.

(93) Senda, M. *Anal. Sci.* **1994**, *10*, 649.

(94) Wang, H.; Yu, Z.; Wang, E. *J. Electroanal. Chem.* **1995**, *380*, 69.

(95) Beattie, P.D.; Wellington, R.G.; Girault, H.H. *J. Electroanal. Chem.* **1995**, *396*, 317.

(96) Katano, H.; Maeda, K. Senda, M. *J. Electroanal. Chem.* **1995**, *396*, 391.

(97) Osborne, M. D.; Girault, H. H. *Electroanalysis* **1995**, *7*, 425-434.

(98) Senda, M. *Denki Kagaku* **1995**, *63*, 368-372.

(99) Osborne, M. D.; Girault, H. H. *Electroanalysis* **1995**, *7*, 714-721.

(100) Cunnane, V. J.; Geblewicz, G.; Schiffrin, D. J. *Electroanchim. Acta* **1995**, *40*, 3005-3014.

(101) Kakiuchi, T. *Electroanchim. Acta* **1995**, *40*, 2999-3003.

(102) Senda, M. *Electroanchim. Acta* **1995**, *40*, 2993-3007.

(103) Kntturi, K.; Manzanares, J.A.; Murtomaki, L. *Electroanchim. Acta* **1995**, *40*, 2979.

(104) Indenbon, A.V. *Electroanchim. Acta* **1995**, *40*, 2985.

(105) Samec, Z.; Kakiuchi, T.; Senda, M. *Electroanchim. Acta* **1995**, *40*, 2971.

(106) Dassie, S.A.; Yudi, L.M.; Baruzzi, A.M. *Electroanchim. Acta* **1995**, *40*, 2953.

(107) Volkov, A. G.; Gugeshashvili, M. I.; Deamer, D. W. *Electroanchim. Acta* **1995**, *40*, 2849-2868.

(108) Wei, C.; Bard, A. J.; Mirkin, M. V. *J. Phys. Chem.* **1995**, *99*, 16033-16042.

(109) Solomon, T.; Bard, A. J. *J. Phys. Chem.* **1995**, *99*, 17487-17489.

(110) Selzer, Y.; Mandler, D. *J. Electroanal. Chem.* **1996**, *409*, 15-17.

(111) Tsionski, M.; Bard, A. J.; Mirkin, M. V. *J. Phys. Chem.* **1996**, *100*, 17881-17888.

(112) Shao, Y. H.; Mirkin, M. V.; Rusling, J. F. *J. Phys. Chem. B* **1997**, *101*, 3202-3208.

(113) Cheng, Y. F.; Schiffrin, D. J. *J. Electroanal. Chem.* **1997**, *429*, 37-45.

(114) Slevin, C. J.; Unwin, P. R. *Langmuir* **1997**, *13*, 4799-4803.

(115) Katano, H; Senda, M. *Bull. Chem. Soc. Jpn.* **1997**, *70*, 2489-2493.

(116) Tsionski, M.; Bard, A. J.; Mirkin, M. V. *J. Am. Chem. Soc.* **1997**, *119*, 10785-10792.

(117) Kontturi, K.; Manzanares, J. A.; Murtomaki, L.; Schiffrin, D. J. *J. Phys. Chem. B* **1997**, *101*, 10801-10806.

(118) Suzuki, M.; Matsui, M. Kihara, S. *J. Electroanal. Chem.* **1997**, *438*, 147-151.

(119) Senda, M.; Kubota, Y.; Katano, H. *Anal. Sci.* **1997**, *13*, 285-288.

(120) Shao, Y. H.; Mirkin, M. V. *J. Electroanal. Chem.* **1997**, *439*, 137-143.

(121) Delville, M. H.; Tsionsky, M.; Bard, A.J. *Langmuir* **1998**, *14*, 2774-2779.

(122) Lagger, G.; Tomaszewski, L.; Osborne, M.D.; Seddon, B.J.; Girault, H.H *J. Electroanal. Chem.* **1998**, *451*, 29-37.

(123) Shao, Y. H.; Mirkin, M. V. *Anal. Chem.* **1998**, *70*, 3155-3161.

(124) Shi, C. N.; Anson, F. C. *Anal. Chem.* **1998**, *70*, 3114-3118.

(125) Quinn, B.; Lahtinen, R.; Murtomaki, L.; Kontturi, K. *Electroanchim. Acta* **1998**, *44*, 47-57.

(126) Ohde, H.; Maeda, K.; Yoshida, Y.; Kihara, S. *Electroanchim. Acta* **1998**, *44*, 23-28.

(127) Wilke, S.; Zerihun, T. *Electroanchim. Acta* **1998**, *44*, 15-22.

(128) Katano, H.; Senda, M. *Bull. Chem. Soc. Jpn.* **1998**, *71*, 2359-2363.

(129) Fermin, D.J.; Ding, Z.F.; Duong, H.D.; Brevet, P.F.; Girault, H.H. *J. Phys. Chem. B* **1998**, *102*, 10334-10341.

(130) Shao, Y. H.; Mirkin, M. V. *J. Phys. Chem. B* **1998**, *102*, 9915-9921.

(131) Kuzmin, M.G.; Soboleva, I.V.; Kotov, N.A. *Anal. Sci.* **1999**, *15*, 3-16.

(132) Zu, Y.B.; Fan, F.R.F.; Bard, A.J. *J. Phys. Chem. B* **1999**, *103*, 6272-6276.

(133) Barker, A.L.; Unwin, P.R.; Amemiya, S.; Zhou, J.F.; Bard, A.J. *J. Phys. Chem. B* **1999**, *103*, 7260-7269.

(134) Liu, B.; Mirkin, M. V. *J. Am. Chem. Soc.* **1999**, *121*, 8352-8355.

(135) Katano, H.; Senda, M. *Bull. Chem. Soc. Jpn.* **1999**, *72*, 2085-2090.

(136) Murtomaki, L.; Kontturi, K.; Schiffrin, D.J. *J. Electroanal. Chem.* **1999**, *474*, 89-93.

(137) Slevin, C.J.; Unwin, P.R. *Langmuir* **1999**, *15*, 7361-7371.

(138) Zhang, J.; Unwin, P.R. *J. Phys. Chem. B* **2000**, *104*, 2341-2347.

(139) Barker, A.L.; Unwin, P.R. *J. Phys. Chem. B* **2000**, *104*, 2330-2340.

(140) Katano, H.; Kuboyama, H.; Senda, M. *J. Electroanal. Chem.* **2000**, *483*, 117-123.

(141) Amemiya, S.; Ding, Z.F.; Zhou, J.F.; Bard, A.J. *J. Electroanal. Chem.* **2000**, *483*, 7-17.

(142) Nakatani, K.; Chikama, K; Kim, H.-B.; Kitamura, N. *Chem. Lett.* **1994**, *4*, 793-796.

(143) Kitamura, N.; Nakatani, K.; Kim, H.-B.; *Pure & Appl. Chem.* **1995**, *67*, 79-86.

(144) Nakatani, K.; Suto, T.; Wakabayashi, M.; Kim, H.-B.; Kitamura, N. *J. Phys. Chem.* **1995**, *99*, 4745-4749.

(145) Nakatani, K.; Chikama, K; Kim, H.-B.; Kitamura, N. *Chem. Phys. Lett.* **1995**, *237*, 133-136.

(146) Nakatani, K.; Terui, N.; Kitamura, N. *Bull. Chem. Soc. Jpn.* **1996**, *69*, 997–1001.

(147) Nakatani, K.; Wakabayashi, M.; Chikama, K; Kitamura, N. *J. Phys. Chem.* **1996**, *100*, 6749-6754.

(148) Nakatani, K.; Terui, N.; Hasebe, K.; Kitamura, N. *Chem. Lett.* **1996**, *6*, 457-458.

(149) Chikama, K; Nakatani, K.; Kitamura, N. *Chem. Lett.* **1996**, *6*, 665-666.

(150) Nakatani, K.; Sudo, M.; Kitamura, N. *J. Phys. Chem. B* **1998**, *102*, 2908-2913.

(151) Chikama, K; Nakatani, K.; Kitamura, N. *Bull. Chem. Soc. Jpn.* **1998**, *71*, 1065–1070.

(152) Nakatani, K.; Suzuki, T.; Shitara, S.; Kitamura, N. *Langmuir* **1998**, *14*, 595–601.

(153) Nakatani, K.; Chikama, K; Kim, H.-B.; Kitamura, N. *Advances in Photochemistry*, Vol. 25, Eds., D. C. Neckers, D. H. Volman and G. von Bunau, John-Wiley & Sons, New York, 173-223 (1999).

(154) Nakatani, K.; Sudo, M.; Kitamura, N. *Anal. Chem.* **2000**, *72*, 339–342.

(155) Terui, N.; Nakatani, K.; Kitamura, N. *J. Electroanal. Chem.* **2000**, *494*, 41-46.

(156) Benjamin, I. *J. Chem. Phys.* **1992**, *97*, 1432–1445.

(157) Benjamin, I. *Science* **1993**, *261*, 1558–1560.

(158) Michael, D.; Benjamin, I. *J. Phys. Chem.* **1995**, *99*, 1530–1536.

(159) Klopfer, K. j.; Vanderlick, T. K. *Colloids & Surf. A-Phys. & Eng. Aspects* **1995**, *96*, 171-179.

(160) Toxvaerd, S.; Stecki, J.; *J. Chem. Phys.* **1995**, *102*, 7163-7168.

(161) Schweighofer, K. J.; Benjamin, I. *J. Phys. Chem.* **1995**, *99*, 9974–9985.

(162) Schweighofer, K. J.; Benjamin, I. *J. Electroanal. Chem.* **1995**, *391*, 1-10.

(163) Michael, D.; Benjamin, I. *J. Phys. Chem.* **1995**, *99*, 16810–16813.

(164) Cheng, C. K., Kier, L. B. *J. Chem. Info. & Comput. Sci.* **1995**, *35*, 1054-1059.

(165) Stecki, J.; Toxvaerd, S. *J. Chem. Phys.* **1995**, *103*, 4352-4359.

(166) Stecki, J.; Toxvaerd, S. *J. Chem. Phys.* **1995**, *103*, 9763-9771.

(167) Xantheas, S. S.; Dang, L. X. *J. Phys. Chem.* **1996**, *100*, 3989-3995.

(168) Chang, T. M.; Dang, L. X. *J. Chem. Phys.* **1996**, *104*, 6772-6783.

(169) Wipff, G.; Engler, E.; Guilbaud, P.; Lauterbach, M.; Troxlerl, L.; Varnek, A. *New Journal of Chem.* **1996**, *20*, 403-417.

(170) Padilla, P.; Stecki, J.; *J. Chem. Phys.* **1996**, *104*, 7249-7254.

(171) Guilbaud, P.; Wipff, G. *New Journal of Chem.* **1996**, *20*, 631-642.

(172) Wilson, M. A.; Pohorille, A. *J. Am. Chem. Soc.* **1996**, *118*, 6580-6587.

(173) Varnek, A.; Wipff, G. *J. Comput. Chem.* **1996**, *17*, 1520-1531.

(174) Chang, T. M.; Dang, L. X. *Chem. Phys. Lett.* **1996**, *263*, 39-45.

(175) Benjamin, I. *Chem. Rev.* **1996**, *96*, 1449-1475.

(176) Urbinavillalba, G.; Landrove, R.M.; Guaregua, J.A. *Langmuir* **1997**, *13*, 1644-1652.

(177) Varnek, A.; Troxler, L.; Wipff, G. *Chem.-A Euro. J.* **1997**, *3*, 552-560.

(178) Schweighofer, K. J.; Essmann, U.; Berkowitz, M. *J. Phys. Chem. B* **1997**, *101*, 3793-3799.

(179) Schweighofer, K. J.; Essmann, U.; Berkowitz, M. *J. Phys. Chem. B* **1997**, *101*, 10775-10780.

(180) Michael, D.; Benjamin, I. *J. Chem. Phys.* **1997**, *107*, 5684–5693.

(181) Benjamin, I. *Annu. Rev. Phys. Chem.* **1997**, *48*, 407-451.

(182) Watarai, H.; Gotoh, M.; Gotoh, N. *Bull. Chem. Soc. Jpn.* **1997**, *70*, 957–964.

(183) Lauterbach, M.; Engler, E.; Muzet, N.; Troxler, L.; Wipff G *J. Phys. Chem. B* **1998**, *102*, 245-256.

(184) Michael, D.; Benjamin, I. *Electrochim. Acta* **1998**, *44*, 133-138.

(185) Troxler, L.; Wipff, G. *Anal. Sci.* **1998**, *14*, 43-56.

(186) Onoe, Y.; Watarai, H. *Anal. Sci.* **1998**, *14*, 237-239.

(187) Watarai, H. *Pure & Applied Chem.* **1998**, *70*, 1889-1893.

(188) Lauterbach, M.; Engler, E.; Muzet, N.; Troxler, L.; Wipff, G. *J. Phys. Chem. B* **1998**, *102*, 245.

(189) Chang, T. M.; Dang, L. X. *J. Chem. Phys.* **1998**, *108*, 818–819.

(190) Michael, D.; Benjamin, I. *J. Phys. Chem. B* **1998**, *102*, 5145-5151.

(191) Michael, D.; Benjamin, I. *J. Electroanal. Chem.* **1998**, *450*, 335-345.

(192) Kohlmeyer, A.; Hartnig, C.; Spohr, E. *J. Mol. Liquid.* **1998**, *78*, 233-253.

(193) Muzet, N.; Engler, E.; Wipff, G. *J. Phys. Chem. B* **1998**, *102*, 10772-10788.

(194) Fernandes, PA.; Cordeiro, M.N.D.S.; Gomes, J.A.N.F. *Theochem-J. Molecular Structure* **1999**, 463, 151-156.

(195) Diaz-Herrera, E.; Alejandre, J.; Ramirez-Santiago, G.; Forstmann, F. *J. Chem. Phys.* **1999**, *110*, 8084-8089.

(196) Dang, L. X. *J. Chem. Phys.* **1999**, *110*, 10113-10122.

(197) Bresme, F.; Quirke, N. *Phys. Chem. Chem. Phys.* **1999**, *1*, 2149-2155.

(198) Fernandes, PA.; Cordeiro, M.N.D.S.; Gomes, J.A.N.F. *J. Phys. Chem. B* **1999**, *103*, 6290-6299.

(199) Dang, L. X. *J. Phys. Chem. B* **1999**, *103*, 8195-8200.

(200) Benjamin, I. *J. Phys. Chem. A* **1999**, *102*, 9500-9506.

(201) Benjamin, I. *J. Chem. Phys.* **1999**, *110*, 8070-8079.

(202) Schweighofer, K. J.; Benjamin, I. *J. Phys. Chem. A* **1999**, *103*, 10274-10279.

(203) Bresme, F.; Quirke, N. *J. Chem. Phys.* **2000**, *112*, 5985-5990.

(204) Fernandes, PA.; Cordeiro, M.N.D.S.; Gomes, J.A.N.F. *J. Phys. Chem. B* **2000**, *104*, 2278-2286.

(205) Schweighofer, K. J.; Benjamin, I. *J. Chem. Phys.* **2000**, *112*, 1474-1482.

(206) Buff, F.P.; Lovett, R.A.; Stillinger, Jr. F.H. *Phys. Rev. Lett.* **1965**, *15*, 621-623.

(207) Braslau, A.; Pershan, P.S.; Swislow, G.; Ocko, B.M.; Als-Nielsen, J. *Phys. Rev. A* **1988**, 38, 2457-.2470

(208) Pershan, P.S. *Faraday Discuss. Chem. Soc.* **1990**, *89*, 231-245.

(209) Simpson, G. J.; Rowlen, K. L. *Chem. Phys. Lett.* **1999**, *309*, 117-122.

(210) Grubb, S. G.; Kim, M. W.; Rasing, T.; Shen, Y. R. *Langmuir* **1988**, *4*, 452.

(211) Conboy, J.C.; Daschbach, J.L.; Richmond, G.L. *J. Phys. Chem.* **1994**, *98*, 9688-9692.

(212) Conboy, J. C.; Daschbach, J. L.; Richmond, G. L. *Appl. Phys. A-Solids & Surfaces* **1994**, *59*, 623-629.

(213) Conboy, J. C.; Richmond, G. L. *Electrochim. Acta* **1995**, *40*, 2881-2886.

(214) Carwford, M. J.; Frey, J. G.; Vandernoot, T. J.; Zhao, Y. G. *J. Chem. Soc. Faraday Trans.* **1996**, *92*, 1369-1373.

(215) Naujok, R. R.; Paul, H. J.; Corn, R. M. *J. Phys. Chem.* **1996**, *100*, 10497-10507.

(216) Rinuy, J.; Piron, A.; Brevet, P. F.; Blanchard, D. M.; Girault, H. H. *Chemistry-A European J.* 2000, 6, 3434-3441.

(217) Corn, R. M.; Higgins, D. A. *Chem. Rev.* **1994**, *94*, 107.

(218) Du, Q.; Freysz, E.; Shen, Y. R. *Science* **1994**, *264*, 826.

(219) Messmer M. C.; Conboy, J. C.; Richmond, G. L. *J. Am. Chem. Soc.* **1995**, *117*, 8039-8040.

(220) Conboy, J. C.; Messmer, M. C.; Richmond, G. L. *J. Phys. Chem.* **1996**, *100*, 7617-7622.

(221) Walker, R. A.; Conboy, J. C.; Richmond, G. L. *Langmuir* **1997**, *13*, 3070-3073.

(222) Conboy, J. C.; Messmer, M. C.; Richmond, G. L. *J. Phys. Chem. B* **1997**, *101*, 6724-6733.

(223) Gragson, D. E.; Conboy, J. C.; Richmond, G. L. *Langmuir* **1997**, *13*, 4804-4806.

(224) Gragson, D. E.; Richmond, G. L. *J. Phys. Chem. B* **1998**, *102*, 569-576.

(225) Gragson, D. E.; Richmond, G. L. *J. Am. Chem. Soc.* **1998**, *120*, 366.

(226) Walker, R. A.; Gruetzmacher, J. A.; Richmond, G. L. *J. Am. Chem. Soc.* **1998**, *120*, 6991-7003.

(227) Walker, R. A.; Gragson, D. E.; Richmond, G. L. *Colloids & Surf. A-Phys. & Eng. Aspects* **1999**, *154*, 175-185.

(228) Smiley, B. L.; Richmond, G. L. *Biopolymers* **2000**, *57*, 117-125.

(229) Brown, M. G.; Raymond, E. A.; Allen, H. C. Scatena, L. F.; Richmond, G. L. *J. Phys. Chem. A* **2000**, *104*, 10220-10226.

(230) Lee, L. T.; Langevin, D.; Farnoux, B. *Phys. Rev. Lett.* **1991**, *67*, 2678.

(231) Penfold, J.; Richardson, R.M.; Zarbakhsh, A.; Webster, J.R.P.; Bucknall, D.G.; Rennie, A.R.; Jones, R.A.L.; Cosgrove, T.; Thomas, R.K.; Higgins, J.S.; Fletcher,

P.D.I.; Dickinson, E.; Roser, S.J.; Mclure, I.A.; Hillman, A.R.; Richards, R.W.; Staples, E.J.; Burgess, A.N.; Simister, E.A.; White, J.W. *J. Chem. Soc., Faraday Trans.* **1997**, *93*, 3899-3917.

(232) Wang, R. M.; Schlenoff, J. B. *Macromolecules* **1998**, *31*, 494-500.

(233) Clifton, B. J.; Cosgrove, T.; Richardson, R. M.; Zarbakhsh, A.; Webster, J. R. P. *Physica B* **1998**, *248*, 289-296.

(234) Zarbakhsh, A.; Bowers. J.; Webster, J. R. P. *Measurement Sci. & Technology* **1999**, *10*, 738-743.

(235) Zhang, Z. H.; Tsuyumoto, I.; Takahashi, S.; Kitamori, T.; Sawada, T. *J. Phys. Chem. A* **1997**, *101*, 4163-4166.

(236) Takahashi, S.; Tsuyumoto, I.; Kitamori, T.; Sawada, T. *Electrochim. Acta* **1998**, *44*, 165-169.

(237) Tsuyumoto, I.; Noguchi, N.; Kitamori, T.; Sawada, T. *J. Phys. Chem. B* **1998**, *102*, 2684.

(238) Uchiyama, Y.; Tsuyumoto, I.; Kitamori, T.; Sawada, T. *J. Phys. Chem. B* **1999**, *103*, 4663-4665.

(239) Uchiyama, Y.; Fujinami, M.; Sawada, T.; Tsuyumoto, I. *J. Phys. Chem. B* **2000**, *104*, 4699-4702.

(240) Uchiyama, Y.; Kitamori, T.; Sawada, T.; Tsuyumoto, I. *Langmuir* **2000**, *16*, 6597-6600.

(241) Morrison, L. E.; Weber, G. *Biophys. J.* **1987**, *52*, 367.

(242) Wirth, M. J.; Burbage J. D. *J. Phys. Chem.* **1992**, *96*, 9022.

(243) Kovaleski, J. M.; Wirth, M. J. *J. Phys. Chem.* **1995**, *99*, 4091.

(244) Kovaleski, J. M.; Wirth, M. J. *J. Phys. Chem.* **1996**, *100*, 10304.

(245) Watarai, H.; Saitoh, Y. *Chem. Lett.* **1995**, *4*, 283-284.

(246) Okamura, R.; Hinoue, T.; Watarai, H. *Anal. Sci.* **1996**, *12*, 393–397.

(247) Nakatani, K.; Ishizaka, S.; Kitamura, N. *Anal. Sci.* **1996**, *12*, 701–705.

(248) Watarai, H.; Funaki F. *Langmuir* **1996**, *12*, 6717-6720.

(249) Bessho, K.; Uchida, T.; Yamauchi, A.; Shioya, T.; Teramae, N. *Chem. Phys. Lett.* **1997**, *264*, 381.

(250) Saitoh, Y.; Watarai, H. *Bull. Chem. Soc. Jpn.* **1997**, *70*, 351–358.

(251) Tupy, M.J.; Blanch, H.W.; Redke C. *J. Ind. & Eng. Chem. Res.* **1998**, *37*, 3159-3168

(252) Tsukahara, S.; Watarai, H. *Langmuir* **1998**, *14*, 7072-7075.

(253) Tsukahara, S.; Yamada, Y.; Hinoue, T.; Watarai, H. *Bunseki Kagaku* **1998**, *47*, 945-952.

(254) Ishizaka, S.; Nakatani, K.; Habuchi, S.; Kitamura, N. *Anal. Chem.* **1999**, *71*, 419–426.

(255) Ishizaka, S.; Habuchi, S.; Kim, H.-B.; Kitamura, N. *Anal. Chem.* **1999**, *71*, 3382–3389.

(256) Tsukahara, S.; Watarai, H. *Chem. Lett.* **1999**, *1*, 89-90.

(257) Fujiwara, M.; Tsukahara, S.; Watarai, H. *Phys. Chem. Chem. Phys.* **1999**, *1*, 2949-2951.

(258) Murad, MM. *J. Fluorescence* **1999**, *9*, 257-263.

(259) Gajraj, A.; Ofoli, R.Y. *Langmuir* **2000**, *16*, 4279-4285.

(260) Nagatani, H.; Iglesias, R. A.; Fermin, D. J.; Brevet, R. F.; Girault, H. H. *J. Phys. Chem. B* **2000**, *104*, 6869-6876.

(261) Jones, M. A.; Bohn, P. W. *Anal. Chem.* **2000**, *72*, 3776–3783.

(262) Tsukahara, S.; Yamada, Y.; Watarai, H. *Langmuir* **2000**, *16*, 6787-6794.

(263) Gajraj, A.; Ofoli, R.Y. *Langmuir* **2000**, *16*, 8085-8094.

(264) O'Connor, D.V.; Phillips, D. *Time-Correlated Single Photon Counting*; Academic Press: New York, 1986.

(265) Rice, S.A.; Kenney-Wallace, G.A. *Chem. Phys.* **1980**, *47*, 161-170.

(266) Barkley, M.D.; Kowalczyk, A.A.; Brand, L. *J. Chem. Phys.* **1981**, *75*, 3581-3593.

(267) Waldeck, D.H.; Fleming, G.R. *J. Phys. Chem.* **1981**, *85*, 2614-2617.

(268) Dote, J.L.; Schwartz, R.N. *J. Phys. Chem.* **1981**, *85*, 3756-3758.

(269) Moog, R.S.; Ediger, M.D.; Boxer, S.G.; Fayer, M.D. *J. Phys. Chem.* **1982**, *86*, 4694-4700.

(270) Phillips, L.A.; Webb, S.P.; Yeh, S.W.; Clark, J.H. *J. Phys. Chem.* **1985**, *89*, 17-19.

(271) Christensen, R.L.; Drake, R.C; Phillips, D. *J. Phys. Chem.* **1986**, *90*, 5960-5967.

(272) Visser, A.J.W.G.; Arie van Hoek, K.V.; Santema, J.S. *J. Phys. Chem.* **1988**, *92*, 759-765.

(273) Flom, S.R.; Fendler, J.H. *J. Phys. Chem.* **1988**, *92*, 5908-5913.

(274) Jiang, Y.; Blanchard, G. J. *J. Phys. Chem.* **1994**, *98*, 6436-6440.

(275) Wirth, M. J.; Burbage J. D. *Anal. Chem.* **1991**, *63*, 1311.

(276) Klafter, J.; Blumen, A. *J. Chem. Phys.* **1984**, *80*, 875–877.

(277) Klafter, J.; Blumen, A. *J. Lumin.* **1985**, *34*, 77–82.

(278) Tamai, N.; Yamazaki, T.; Yamazaki, I. *Chem. Phys. Lett.* **1988**, *147*, 25–29.

(279) Yamazaki, I.; Tamai, N.; Yamazaki, T. *J. Phys. Chem.* **1990**, *94*, 516–525.

(280) Tamai, N.; Yamazaki, T.; Yamazaki, I.; Mizuma, A.; Mataga, N. *J. Phys. Chem.* **1987**, *91*, 3503–3508.

(281) Lin, Y.; Nelson, M. C.; Hanson, D. M. *J. Chem. Phys.* **1987**, *86*, 1586–1592.

(282) Tcherkasskaya, O.; Spiro, J. G.; Ni, S.; Winnik, M. A. *J. Phys. Chem.* **1996**, *100*, 7114–7121.

(283) Yekta, A.; Spiro, J. G.; Winnik, M. A. *J. Phys. Chem. B* **1998**, *102*, 7960–7970.

(284) Kim, H. -B.; Habuchi, S.; Kitamura, N. *Anal. Chem.* **1999**, *71*, 842–848.

(285) Rojanski, D.; Huppert, D.; Bale, H. D.; Dacai, X.; Schmidt, P. W.; Farin, D.; Seri-Levy, A.; Avnir, D. *Phys. Rev. Lett.* **1986**, *56*, 2505–2508.

(286) Levitz, P.; Drake, J. M. *Phys. Rev. Lett.* **1987**, *58*, 686–689.

(287) Rojanski, D.; Huppert, D.; Avnir, D. *Chem. Phys. Lett.* **1987**, *139*, 109–115.

(288) Wendlandt, W. WM.; Hecht, H. G. "*Reflectance Spectroscopy*", John Wiley and Sons, New York, 1966

(289) Masuhara, H.; De Schryver, F.C.; Kitamura, N.; Tamai, N.; "*Microchemistry; Spectroscopy and Chemistry in Small Domains*", North-Holland, Amsterdam, 1994.

(290) Hamai. S.; Tamai, N.; Masuhara, H. *J. Phys. Chem.* **1995**, *99*, 4980.

(291) Casey, K. G.; Quitevis, E. L. *J. Phys. Chem.* **1988**, *92*, 6590–6594.

(292) Casey, K. G.; Onganer, Y.; Quitevis, E. L. *J. Photochem. Photobiol. A: Chem.* **1992**, *64*, 307–314.

Chapter 2

Time-Resolved Total Internal Reflection Fluorometry of 1-Pyrene Sulfonate Anion at Liquid/Liquid Interface

2.1 Introduction

It is well known that pyrene derivatives exhibit excimer or dimer fluorescence in addition to monomer fluorescence,[1-6] so that the fluorescence spectrum and its dynamics of the derivative at an interface will be different from those in the bulk phase, in particular, when the dye adsorbs on a liquid/liquid interface. Such a behavior of a pyrene derivative could be used to sense characteristics of a water/oil interface. In this study, a 1-pyrene sulfonate anion (PSA) was used as a fluorescence probe to study the structure at a water/1,2-Dichloroethane (DCE) interface on the basis of a time-resolved TIR technique.[7] In TIR fluorometry, however, a penetration depth of an incident evanescent wave possesses a finite value, so that fluorescence characteristics of a bulk phase are superimposed more or less to those at an interface.[3, 8] Therefore, clear information about the interface cannot be obtained. In different from steady-state fluorescence spectra, however, fluorescence dynamics is expected to be highly sensitive to microscopic environments, so that time-resolved TIR fluorometry would extract information on chemical characteristics at the interface. On the basis of such experimental ideas and approaches, characteristic behavior of fluorescence dynamics of PSA at a water/DCE interface was studied in detail. In this chapter, after describing general features of the fluorescence spectra and the dynamics of PSA at the interface, an experimental approach to separate the interfacial and bulk fluorescence characteristics of PSA is demonstrated.

2.2 Experimental

i) *Time - Resolved Total Internal Reflection Fluorometry*

A sodium salt of 1-pyrene sulfonic acid (PSA; Molecular Probes Inc.) was purified by recrystallizations from a water/ethanol (2/5-volume ratio) mixture. Water was purified by deionization and distillation (Advantec, GSR-200). 1,2-Dichloroethane (DCE; Dojindo, Sp grade) was used without further purification.

A DCE-saturated aqueous PSA solution (concentration ([PSA]) = 1.0 or 3.0 mM (1 M = 1 mol dm^{-3})) was poured onto a water-saturated DCE layer in a Pyrex tube (inner diameter = 17 mm). The lower inside of the tube was treated with dichlorodimethylsilane to construct a flat water/DCE interface, and the tube was thoroughly washed with DCE and then with water prior to experiments. Spectroscopic measurements were performed after the sample solution in the tube being kept standing over 100 min.

For TIR spectroscopy, pulses from an N_2 laser (Laser Photonics, NitroDye Laser, 337 nm, fwhm 500 ps, 10 Hz) were irradiated to the water/DCE interface through the DCE phase as illustrated in Figure 2-1. In the present experiments, the incident angle of the laser beam to the interface was fixed at 80° (critical total-reflection angle = 67°). The penetration depth (d_p) of the laser beam was calculated to be ~50 nm on the basis of the incident angle and the known refractive indices of DCE (n_1; 1.44) and water (n_2; 1.33)[9]; $d_p = \lambda/\{ 4\pi(n_1^2\sin^2\theta - n_2^2)^{1/2}\}$, where λ and θ are the wavelength (337 nm) and the incident angle (80°) of the laser beam, respectively. The fluorescence spectrum of PSA was measured by a polychromator (ISA Jobin-Ybon, HR320-150G / mm) – multichannel

detector (Princeton Instruments, IRY-512G) set. For dynamic spectroscopy, the fluorescence from the sample cell was passed through glass filters (360 – 380 nm or 450 – 600 nm) and detected by a streak camera (Hamamatsu Photonics, C4334, time resolution; ~500 ps under the combination with the N_2 laser). All of the experiments were conducted at room temperature (~ 23°C).

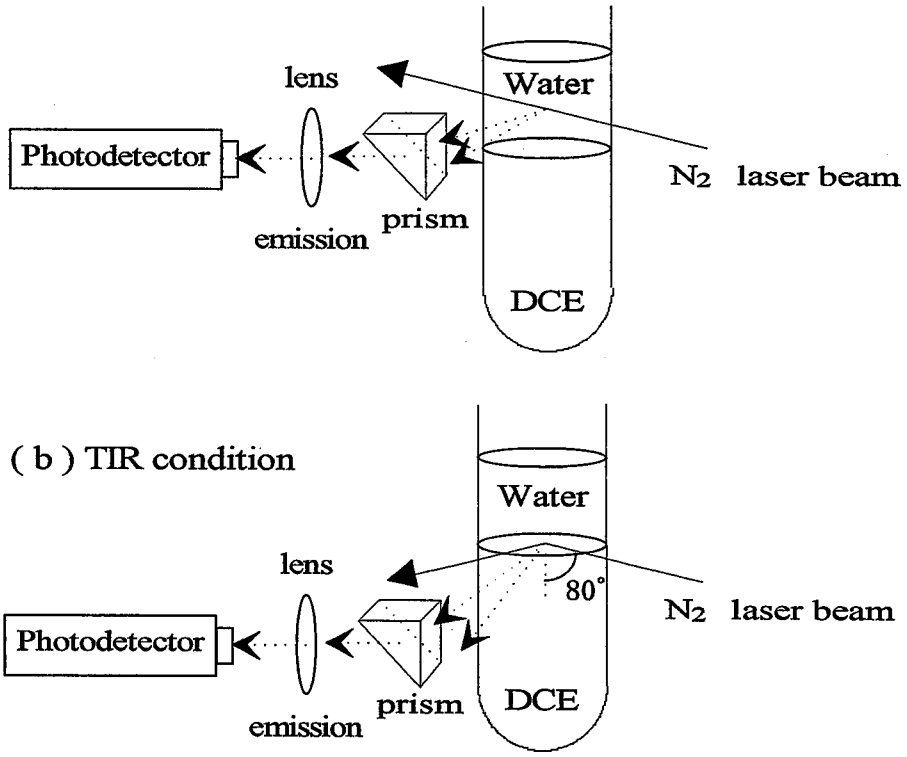

Figure 2-1 Apparatus for the fluorescence measurements under the normal (a) and TIR (b) conditions

ii) *Interfacial Tension Measurements (Pendant Drop Method)*

The interfacial tension (γ) at a water/DCE interface was measured by a pendant drop method[10, 11]. A DCE solution was dropped into an aqueous PSA solution in a glass cell (20 × 20 × 25 mm) through a Pyrex tube (inner diameter = 0.75 mm, outer diameter = 1.71 mm), which was pretreated with dichlorodimethylsilane, as illustrated in Figure 2-2. The shape of a pendant droplet was monitored by a CCD camera. In order to obtain a sharp image, a pendant droplet was irradiated with parallel and monochromatic light (Nikon; W-Lamp, band-pass filter; 450 nm). All measurements were performed over 30 min after the pendant droplet was formed at room temperature (21.5 ± 0.5°C).

The γ value at each [PSA] was determined by eq. (2.1) and (2.2).

$$\gamma = \frac{\Delta\rho g d_e^2}{H} \tag{2.1}$$

$$\frac{1}{H} = f(S) = f\left(\frac{d_s}{d_e}\right) \tag{2.2}$$

In these equations, $\Delta\rho$ is a density difference between DCE ($d^{20} \sim 1.2531$) and water ($d^{21} \sim 0.998$)[9], g is an acceleration of gravity, d_e is an equatorial diameter of a droplet and d_s is the diameter of a droplet measured at a distance d_e from the bottom of the droplet, as indicated in Figure 2-3. The shape of a pendant droplet was described by a ratio $S = d_s/d_e$, which was an experimentally measurable quantity. A quantity of $1/H$ is a function of S and was determined by the relationship between $1/H$ and S as reported previously[12].

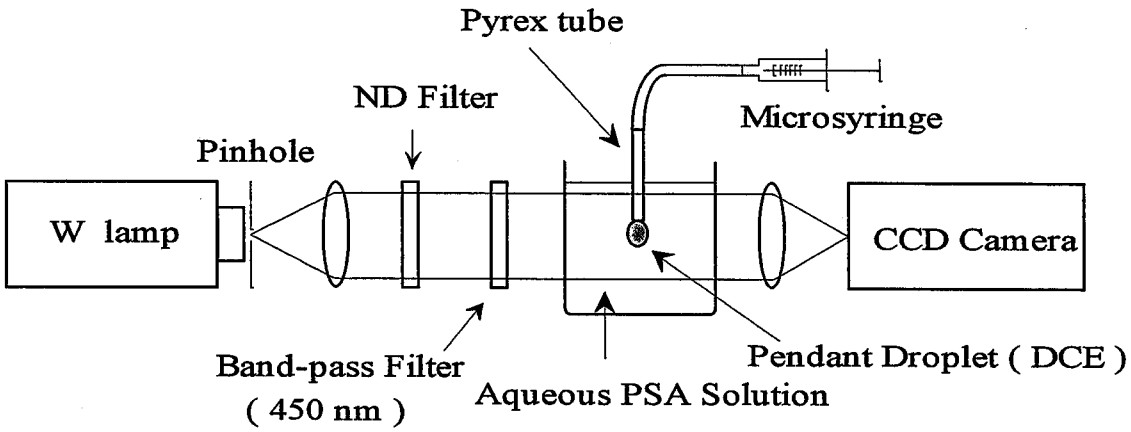

Figure 2-2 Apparatus for interfacial tension measurements by means of a pendant drop method

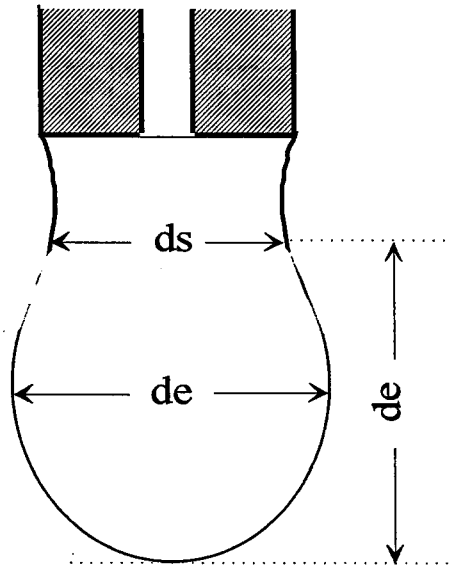

Figure 2-3 The shape of a pendant droplet

2.3 Results and Discussion

2.3.1 *Ground-state Dimer Formation of PSA in Water*

It is well known that pyrene and its derivatives are typical compounds that form excimer, produced by a collisional interaction of an excited molecule ($^1M^*$) and the relevant ground-state molecule (^1M).[1-6] However, PSA in water has been known to form an association complex in the ground state.[13] Fig. 2-4 shows fluorescence spectra of PSA (5.0 mM in water) measured by using a thin-layer optical cell (~5 μm width). The spectra excited at various wavelengths exhibited monomer and structureless bands at around 370 – 430 and 420 – 600 nm, respectively. The ratio of the fluorescence intensity of the structureless band (I_D) to that of the monomer band (I_M), excited at 366 nm, was larger than that excited at 347 nm. Figure 2-5 shows excitation spectra of PSA (5.0 mM in water),

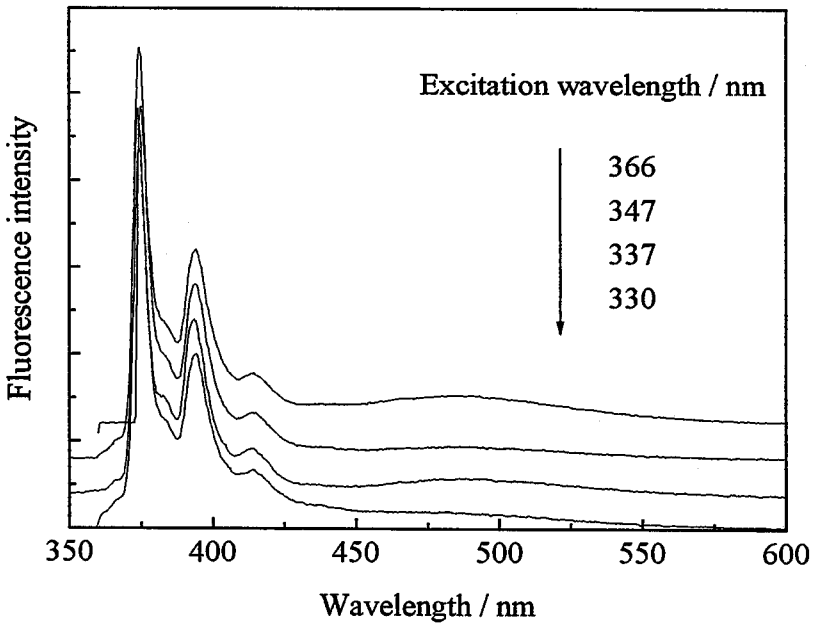

Figure 2-4 Fluorescence spectra of an aqueous PSA (5.0 mM) solution at various excitation wavelengths.

monitored at 395 (the monomer band) and 490 nm (the structureless band). Although no significant peak-shift was observed, the excitation spectrum monitored at 490 nm (Figure 2-5 (b)) was very broad compared with that at 395 nm (Figure 2-5 (a)).

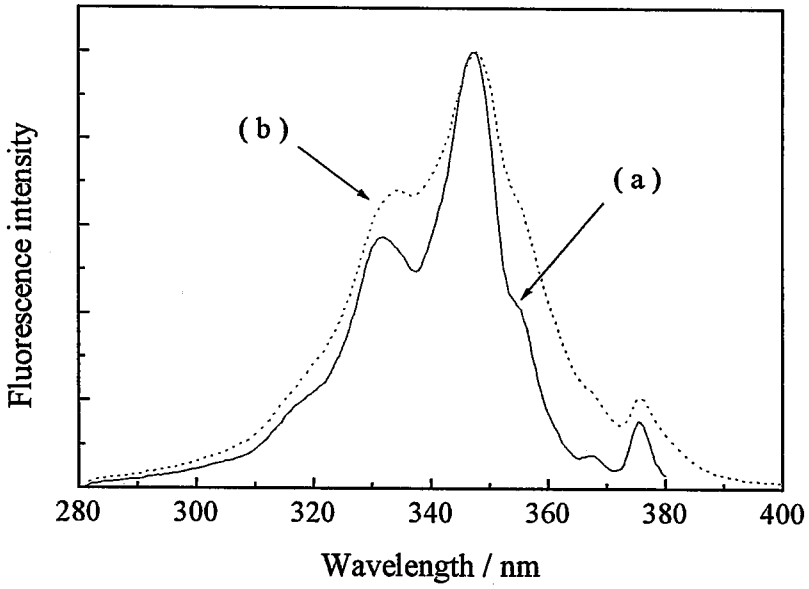

Figure 2-5 Fluorescence excitation spectra of an aqueous PSA (5.0 mM) solution. The spectra were obtained by monitoring the fluorescence at 395 (a) and 490 nm (b) corresponding to the monomer and structureless bands, respectively.

These results suggested that the structureless fluorescence originated from ground-state association of PSA. Figure 2-6 shows absorption spectra of dilute aqueous PSA solutions ($0.6 \sim 3.0 \times 10^{-5}$ M). The vibrational bands appeared at 375, 310-360 and 260-280 nm are assigned to the ^1L_b, ^1L_a and ^1B_b states, respectively.[1] Absorbance at 365 nm was proportional to the concentration of PSA as shown in Figure 2-7, and the molar extinction coefficient calculated from its slope was 1310 $cm^{-1}M^{-1}$. For concentrated PSA solutions (1.0 ~ 5.0 mM in

water), on the other hand, the absorption spectra measured by using a thin-layer optical cell (~100 μm width) exhibited different features compared to those in dilute solutions. Namely, a plot of absorbance at 365 nm vs. the concentration of PSA (Figure 2-8 (a)) deviated from linearity (Figure 2-8 (b)) above [PSA] ~ 1 mM, which was calculated from the molar extinction coefficient (ε_{365} = 1310 $cm^{-1}M^{-1}$) obtained for the dilute aqueous PSA solution. This is because the absorption spectrum of the associated complex of PSA overlaps with that of the monomer as shown in Figure 2-9. Actually, the absorption spectrum of the concentrated aqueous PSA solution (Figure 2-9 (b)) was very broad compared with that of the dilute solution (Figure 2-9 (a)), and new absorption appeared at 365 nm. These results also support that the structureless fluorescence originates from ground-state association of PSA. It has been reported that 1-pyrene sulfonic acid produces a stable ground-state dimer in water.[13] Therefore, the broad fluorescence band seen in the water phase is best characterized as the dimer fluorescence of PSA.

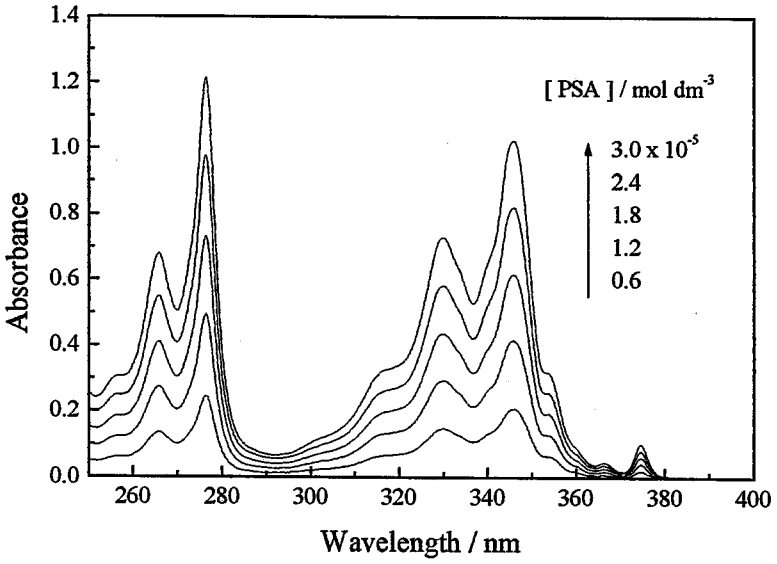

Figure 2-6 Absorption spectra of dilute aqueous PSA solutions (0.6 ~ 3.0 × 10^{-5} M)

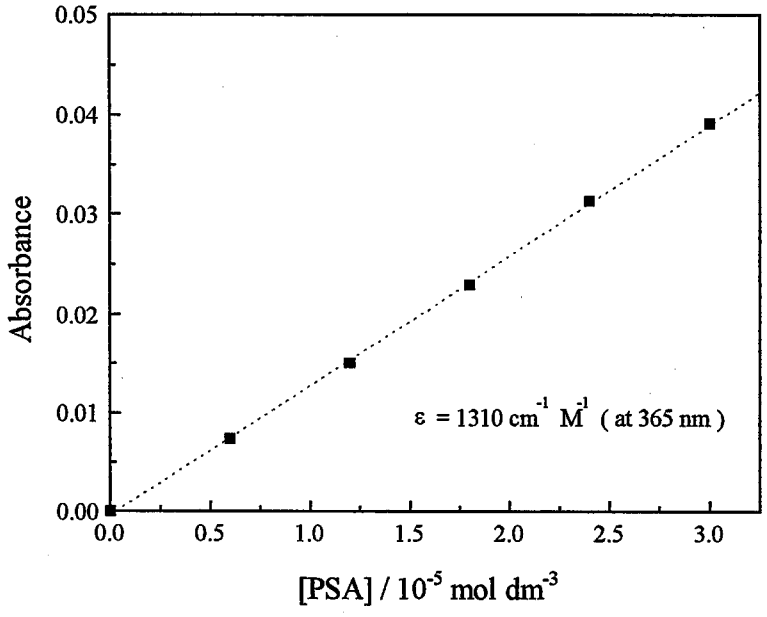

Figure 2-7 A plot of absorbance at 365 nm(Fig. 2-6) vs. the PSA concentration.

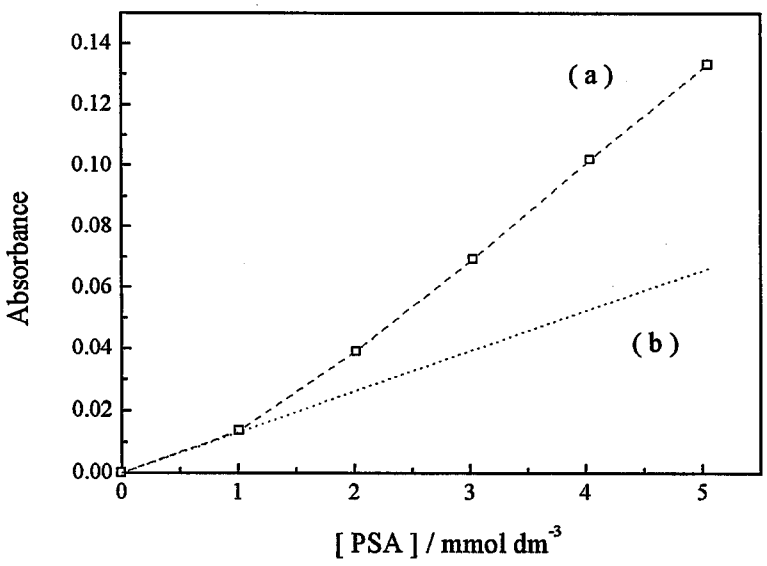

Figure 2-8 A plot of absorbance of an aqueous PSA solution at 365 nm vs. the PSA concentration. Experimental data (a) and those predicted from the Beer's law and the molar extinction coefficient determined for dilute aqueous PSA solutions (b).

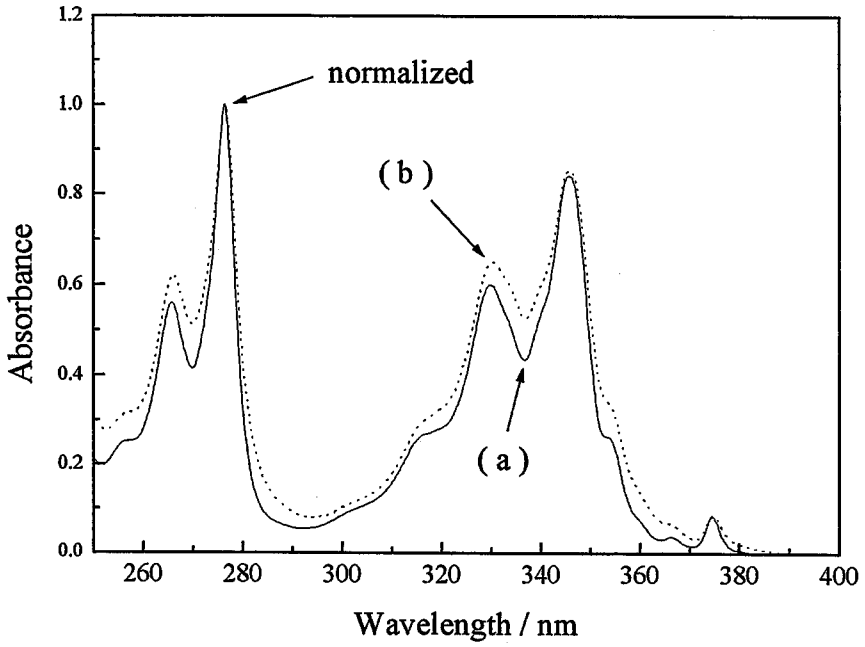

Figure 2-9 Absorption spectra of dilute ((a), 3.0×10^{-5} M) and concentrated ((b), 5.0×10^{-3} M) aqueous PSA solutions.

2.3.2 *General Features of the Fluorescence Spectrum and Dynamics of PSA in a Water/DCE System*

The fluorescence from PSA (3.0 mM) in the water phase, observed under normal conditions (Figure 2-1 (a)), exhibited the monomer and structureless bands at around 370–430 and 420–600 nm, respectively (Figure 2-10 (b)), while almost no fluorescence was observed from the DCE phase. At [PSA] = 1.0 mM (Figure 2-10 (a)), the structureless band was much weaker than the monomer fluorescence. Under the TIR conditions, on the other hand, although an analogous spectrum with that in the water phase was observed, the I_D/I_M value was much larger than that in the water phase. Also, it is worth noting that the I_D/I_M value is

smaller at 3.0 mM compared with that at 1.0 mM (discussed again in Section 2.3.4). PSA produces a stable ground-state dimer in water (detailed discussion in Section 2.3.1). Therefore, the broad fluorescence band seen in the water phase as well as at the interface is best characterized as the dimer fluorescence of PSA.

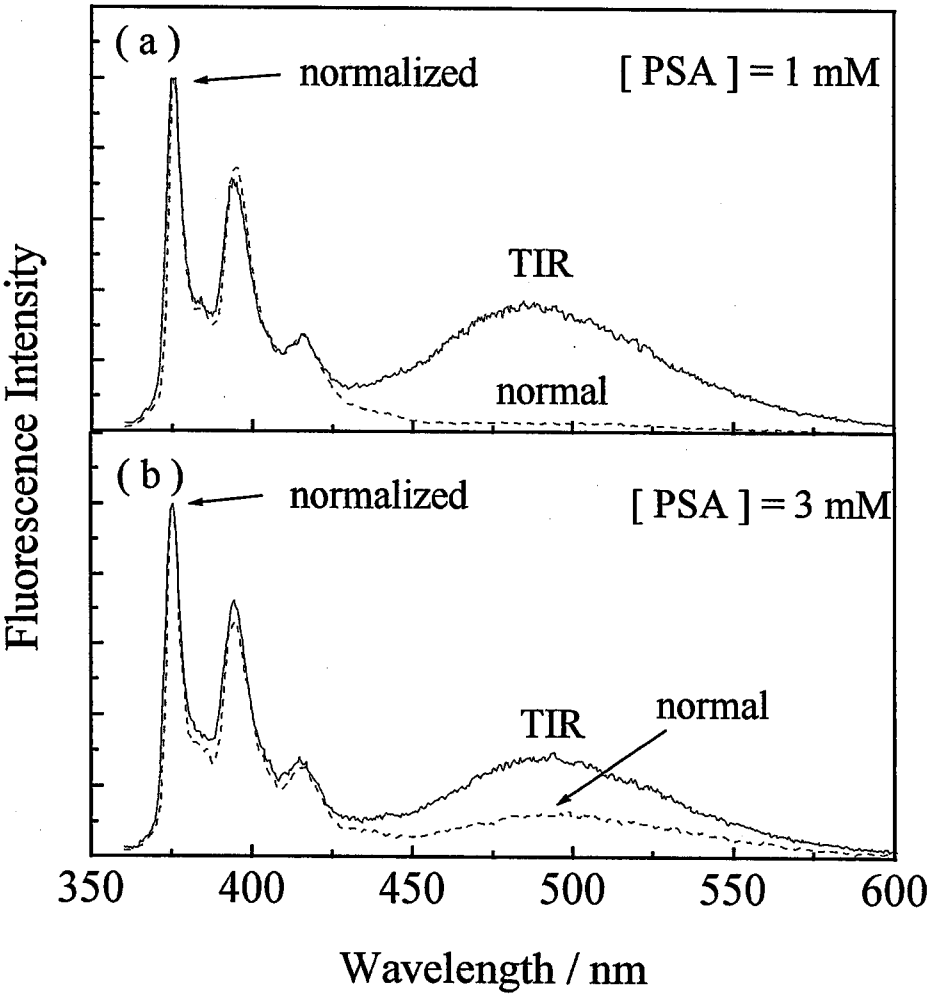

Figure 2-10 Fluorescence spectra of PSA observed under the normal and TIR conditions at [PSA] = 1.0 mM (a) and 3.0 mM (b).

Further information concerning the differences in the fluorescence characteristics between the interface and the water phase was collected on the basis of time-resolved measurements. In the water phase, the time responses of I_M (I_M(t) at 360 - 380 nm) and I_D (I_D(t) at 450 - 600 nm) showed almost single-exponential decays with time constants of 30 and 27 ns ([PSA] = 3.0 mM), respectively (Figure 2-11). In a homogeneous solution, pyrene derivatives undergo excimer formation and the time response of the fluorescence intensity for the monomer or excimer can be fitted by a double-exponential function.[1] Therefore, the present results in Figure 2-11 are in marked contrast to the dynamical behavior of pyrene excimer formation. As a rough approximation, the rate constant of the diffusion-limited excimer formation (k_{diff}) of PSA in water is calculated to be 2×10^7 s^{-1} by $k_{diff} = 8RT / 3000\eta$, where η, R and T are the viscosity of water (1.002×10^{-3} Pa s),[9] the gas constant, and the absolute temperature (296 K), respectively. Since the inverse of k_{diff} (50 ns) is comparable to the fluorescence decay time of PSA (45.3 ns) determined in a dilute aqueous solution (0.3 mM) without dimer and excimer formation, the contribution of the excimer fluorescence to I_D is concluded to be negligibly small compared to that of the dimer fluorescence. This also supports the ground-state dimer formation of PSA in the water phase, as discussed in the previous section.

On the other hand, I_M(t) or I_D(t) observed under the TIR conditions could not be analyzed by a single-exponential function, and was best fitted by a double-exponential function: fast and slow decay components (TIR in Figure 2-11). It is noteworthy that, since the fast decay components of I_M(t) and I_D(t) are not observed for those in the water phase (as described above), the fast decay components are attributed to the PSA fluorescence from the water/DCE interface.

The absence of a rise component in $I_D(t)$ also excludes excimer formation of PSA at the interface. Therefore, the characteristic fluorescence dynamics in Figure 2-11 under the TIR conditions are attributed to dimer formation at the interface.

The time-resolved fluorescence spectra of PSA (3.0 mM) were observed under the normal or TIR conditions, as shown in Figure 2-12. The I_D/I_M values of the spectra monitored under the TIR conditions (Figure 2-12(b)) were much larger than those under the normal conditions (Figure 2-12(a)) as well as those in the steady-state fluorescence spectra (Figure 2-10). Also, the dimer fluorescence

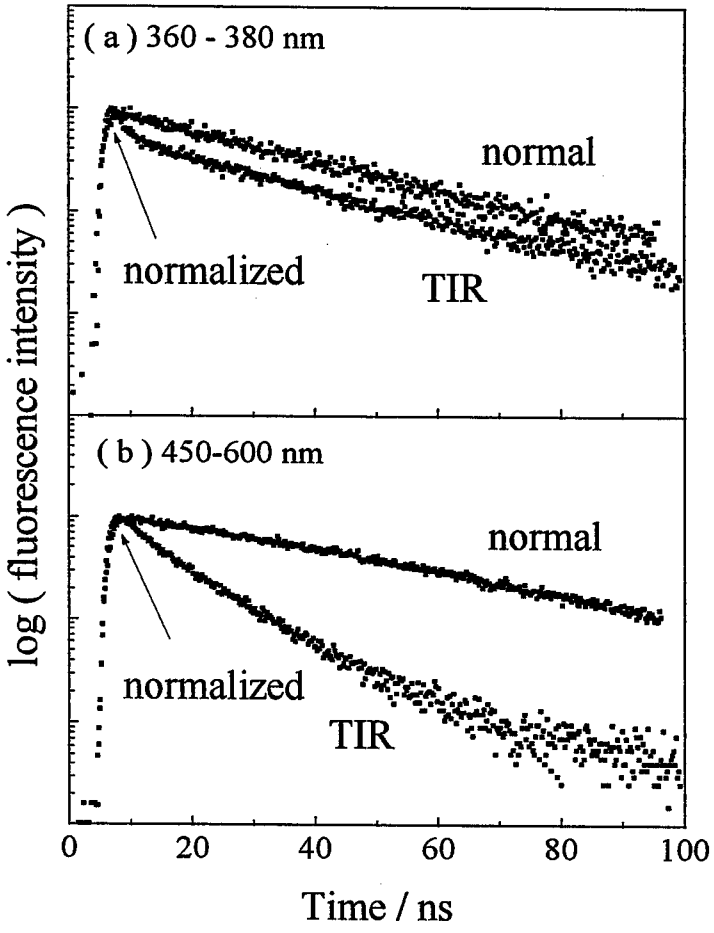

Figure 2-11 Fluorescence decay of PSA (3.0 mM) observed under the normal and TIR conditions. Monitored at 360 - 380 nm (a) and 450 - 600 nm (b).

band monitored under the TIR conditions disappeared (about 40 ns after the excitation pulse) much faster than that under the normal conditions. This result corresponds to that of the fluorescence decay measurements. Although it has been reported that the peak position of the time-resolved fluorescence spectrum for the ground-state dimer of pyrene derivatives in LB films shifts in the picoseconds to the nanoseconds time region, [14] such a shift has not been observed in the present experimental time resolution.

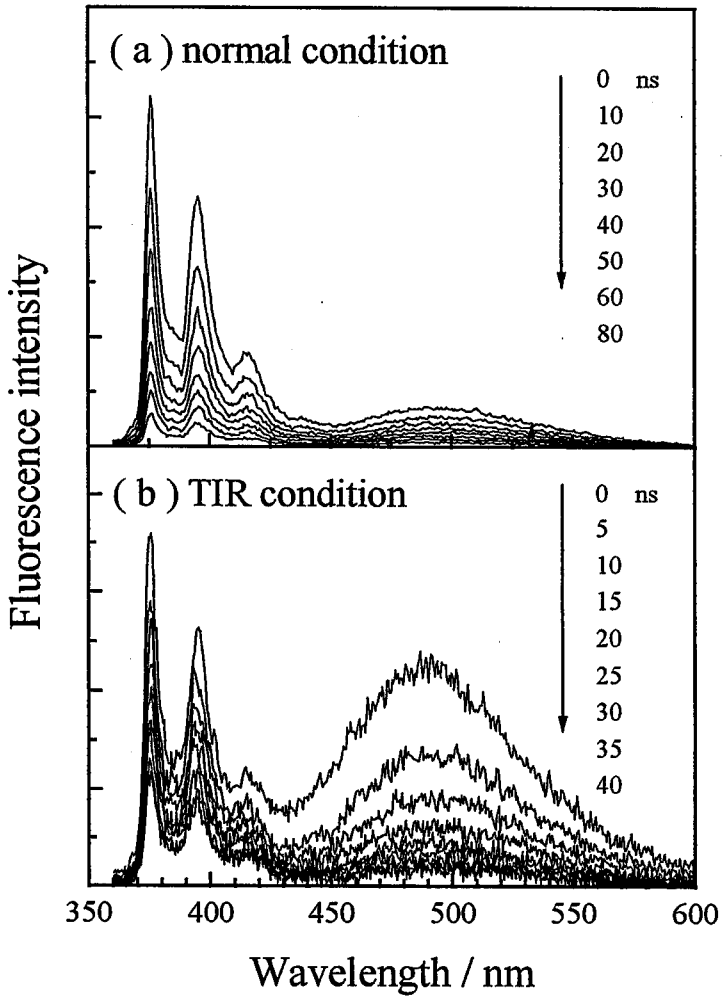

Figure 2-12 Time-resolved fluorescence spectra of PSA (3.0 mM) observed under the normal (a) and TIR (b) conditions.

2.3.3 *Adsorption of PSA on the Water/DCE Interface*

The dimer formation of PSA is facilitated at the water/DCE interface, as demonstrated by the large I_D/I_M value at the interface relative to that in water, suggesting adsorption of PSA on the water/DCE interface. In order to confirm this, water-DCE interfacial tension (γ) measurements were conducted on the basis of a pendant drop method. The relationship between γ and [PSA] thus obtained is shown in Figure 2-13. The γ value decreased with increasing [PSA] and saturated at [PSA] > ~1 mM. This behavior is quite analogous to that of an aqueous sodium dodecylsulfate (SDS) solution, known as a typical surfactant, as shown in Figure 2-14. This clearly demonstrates adsorption of PSA on a water/DCE interface. The amount of adsorbed PSA on the interface (Γ) is given by the Gibbs equation: $\Gamma = -(1/RT)\mathrm{d}\gamma / \mathrm{d}\ln[\mathrm{PSA}]$. [10] The plot of γ vs. log([PSA]) is shown in Figure 2-13(b). Since PSA molecules in the water phase form a ground-state dimer instead of producing micelles, no sharp bend corresponding to a critical micelle concentration similar to the data in Figure 2-14(b) is appeared in the plot (Figure 2-13(b)). [13] The saturated Γ value was then calculated to be 0.50×10^{-10} mol cm^{-2} for PSA. This value is comparable to that of SDS (0.64×10^{-10} mol cm^{-2}) in a water/DCE system. The PSA compound is thus concluded to act as a surfactant, and adsorption of PSA on the interface facilitates dimer formation in the ground-state. These results are in good agreement with those demonstrated by the TIR measurements.

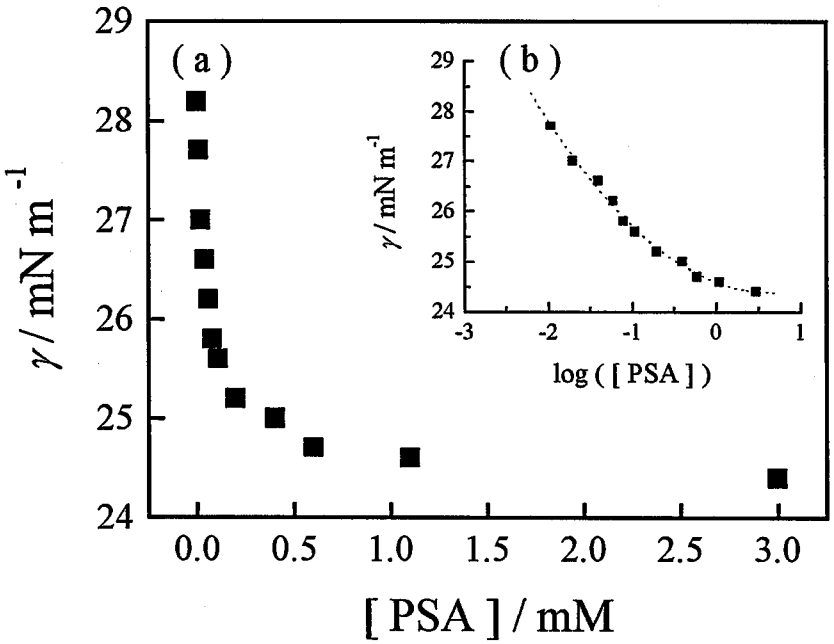

Figure 2-13 A relationship between the interfacial tension at a water/DCE interface and the concentration of PSA (a) and its logarithm plot (b).

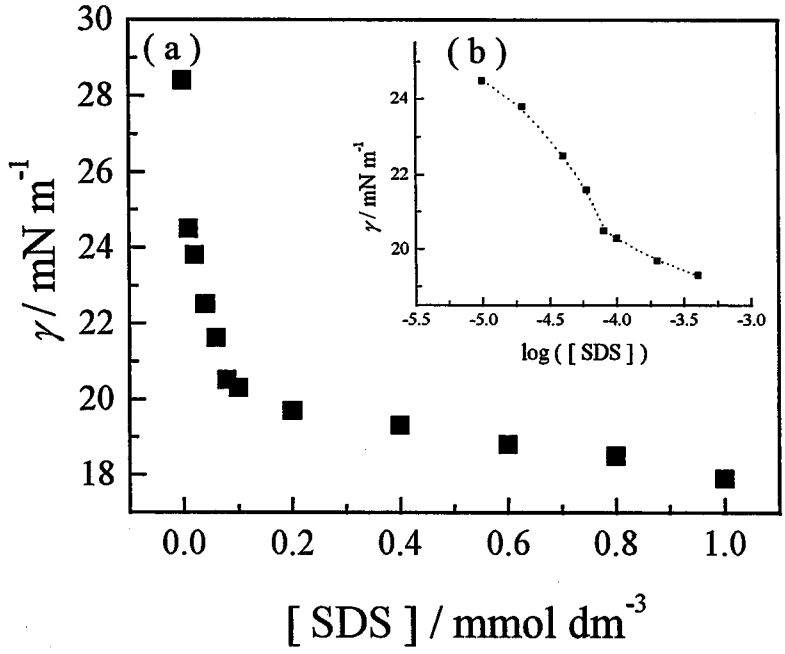

Figure 2-14 A relationship between the interfacial tension at a water/DCE interface and the concentration of SDS (a) and its logarithm plot (b).

2.3.4 *Fluorescence Characteristics at the Interface: Analyses of Fluorescence Dynamics*

Figure 2-13 indicates that the amount of PSA adsorbed on the water/DCE interface is saturated at [PSA] > ~1 mM, so that the I_D/I_M ratio is expected to be independent of [PSA] (>1 mM). However, the I_D/I_M value at [PSA] = 1.0 mM was larger than that at [PSA] = 3.0 mM, as shown in Figure 2-15. This is because the TIR spectra do not represent the fluorescence characteristics at the interface alone, since the penetration depth of the incident N_2-laser beam is ~50 nm.

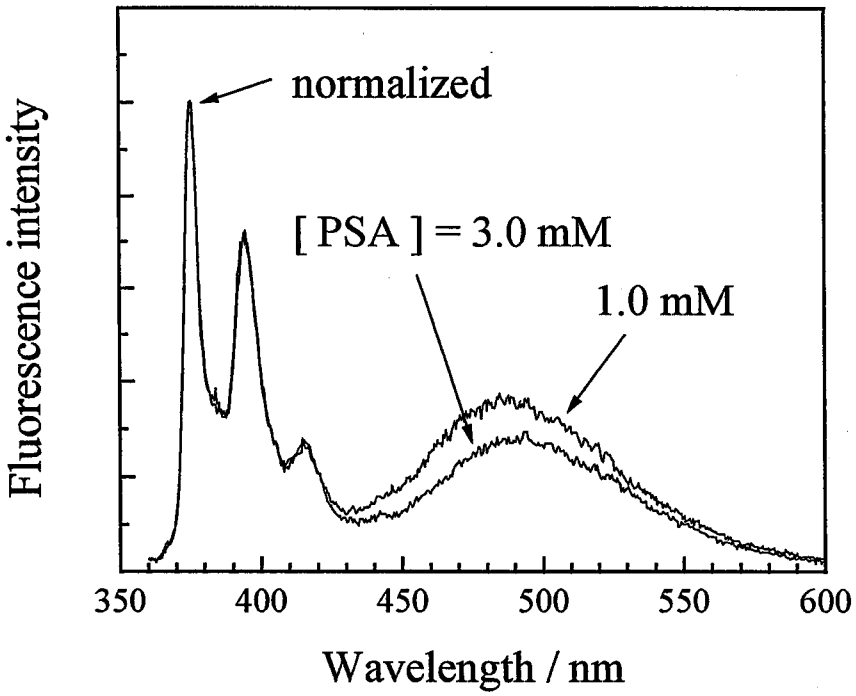

Figure 2-15 TIR fluorescence spectra of PSA (Figure 2-10). The intensity is normalized to that at 375 nm

On the water/DCE interface, PSA is supposed to be adsorbed with the hydrophobic pyrene ring being solubilized in the DCE phase while the hydrophilic sulfonate group being toward the water phase as shown in Figure 2-16. The molecular size of PSA is ~0.7 nm[15], so that the penetration depth of ~50 nm is too large to monitor the interfacial phenomena alone. Indeed, the slow decay component of $I_M(t)$ or $I_D(t)$, observed under the TIR conditions, almost agrees with that determined in the water phase (Figure 2-11), demonstrating that the bulk fluorescence characteristics contribute to the TIR data.

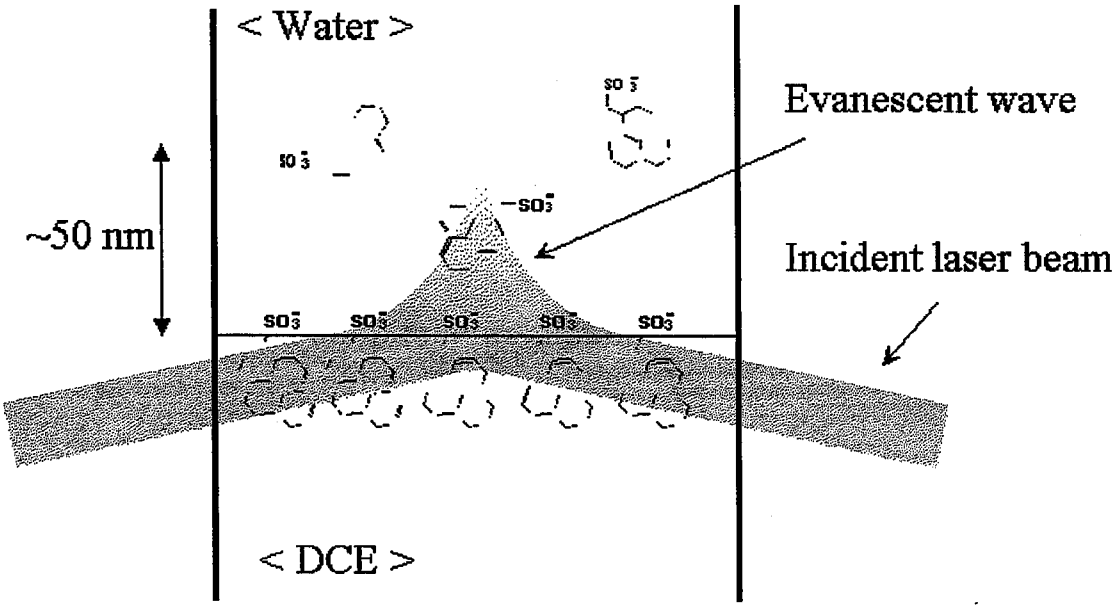

Figure 2-16 Schematic presentation of adsorption of PSA on the water/DCE interface and penetration of the evanescent wave

Table 2-1 Kinetic parameters of I_M(t) and I_D(t) observed under the TIR conditions

[PSA]/m	I_M(t)			I_D(t)		
M	A_2/A_1	τ_1/ ns	τ_2/ ns[a]	A_4/A_3	τ_3/ ns	τ_4/ ns[a]
1.0	0.15	1.3	39	0.034	10	34
3.0	0.20	0.8	30	0.085	8.8	27

a. Fixed constant at the relevant value observed in the water phase.

In order to discriminate the bulk component from the TIR data, the following analyses were performed. The TIR $I_M(t)$ or $I_D(t)$ curve can be analyzed by the following double-exponential function (as discussed in the preceding section),

$$I_M(t) = A_1 \exp(-t/\tau_1) + A_2 \exp(-t/\tau_2) \quad (2.3)$$

$$I_D(t) = A_3 \exp(-t/\tau_3) + A_4 \exp(-t/\tau_4) \quad (2.4)$$

where A_i and τ_i are the pre-exponential factor and the fluorescence decay time of a component i (i = 1, 2, 3, or 4), respectively. The fast and slow decay components observed under the TIR conditions are assumed to be ascribed to PSA adsorbed on the water/DCE interface (τ_1 or τ_3) and the molecules distributed in the water phase (τ_2 or τ_4), respectively. For decay analyses, τ_2 or τ_4 was fixed to be constant at the fluorescence decay time observed for the water phase: under normal conditions. The kinetic parameters thus obtained are summarized in Table 2-1. The τ_2 and τ_4 values at [PSA] = 1.0 mM were determined to be 39 and 34 ns, respectively, while they decreased to τ_2 = 30 and τ_4 = 27 ns at [PSA] = 3.0 mM. Although the [PSA] dependence of τ_2 or τ_4 cannot be discussed in detail, the decrease of τ_2 or τ_4 with increasing [PSA] will be explained due to excimer formation in the water phase (as mentioned briefly in the preceding section). On

the other hand, the τ_1 (~1 ns) and τ_3 (~10 ns) values at [PSA] = 1.0 mM were almost the same as the relevant ones at [PSA] = 3.0 mM, indicating that the amount of PSA adsorbed on the water/DCE interface was saturated at [PSA] > ~1 mM. The shorter decay time of PSA at the interface (τ_1 or τ_3) relative to that in the water phase (τ_2 or τ_4) will be ascribed to energy transfer and successive trapping of the excited-state at the ground-state dimer and/or higher aggregated species, as reported for pyrene derivative in a Langmuir-Blodgette film system.[14]

Since the fast decay components of $I_M(t)$ and $I_D(t)$ observed under the TIR conditions are ascribed to PSA adsorbed on the interface, the relevant fluorescence spectrum (Figure 2-15) can now be separated into those of the interface and the bulk water phase. The following procedures were employed to separate the spectrum. An aqueous dilute PSA solution (0.3 mM) exhibited monomer fluorescence alone. Thus, by using the spectrum in a dilute solution, the relative contributions of the monomer and dimer fluorescence to the observed TIR spectrum can be estimated. On the other hand, the fluorescence intensities of the monomer ($I_M = A_1\tau_1 + A_2\tau_2$) and the dimer ($I_D = A_3\tau_3 + A_4\tau_4$) are obtained by integrating $I_M(t)$ and $I_D(t)$ from $t = 0$ to ∞, respectively. Using the data in Table 2-1, the I_M and I_D values at the interface are obtained as $I_M A_1\tau_1 / (A_1\tau_1 + A_2\tau_2)$ and $I_D A_3\tau_3 / (A_3\tau_3 + A_4\tau_4)$, respectively. The fluorescence spectra at the interface and in the water phase were thus determined and are shown in Figure 2-17, together with the observed TIR spectrum.

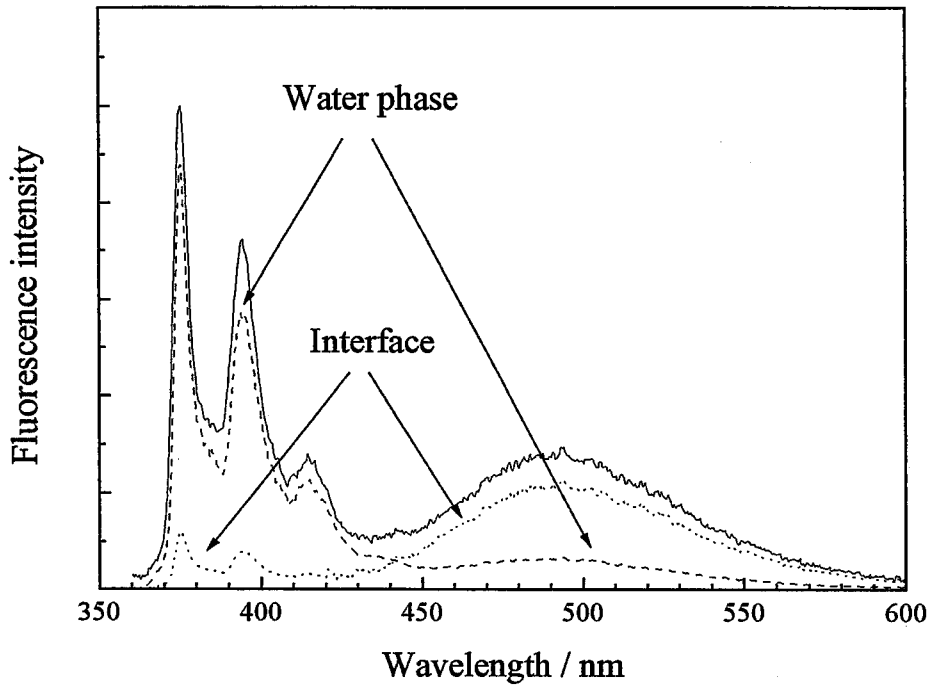

Figure 2-17 Fluorescence spectra of PSA (3.0 mM) at the water/DCE interface and in the water phase, separated by the observed TIR spectrum and the kinetic parameters in Table 2-1.

At the water/DCE interface, the fluorescence intensity of the dimer is more intense compared to that of the monomer, proving the facilitation of dimer formation due to the interfacial adsorption of PSA. The spectrum in the water phase is characterized by intense monomer fluorescence with a minor contribution of the dimer and/or excimer fluorescence at around 490 nm. The observed TIR spectrum thus comprises these spectra, leading to the marginal fluorescence intensity of the dimer relative to that of the monomer. The calculated fluorescence spectra at the water/DCE interface at [PSA] = 1.0 and 3.0 mM are shown in Figure 2-18, where the intensities are normalized to that at 375 nm. Although the I_D/I_M value observed under the TIR conditions is larger at [PSA]

= 1.0 mM compared to that at [PSA] = 3.0 mM (Figure 2-15), the spectra in Figure 2-18 agree very well with each other, demonstrating that the adsorption of PSA on the interface is saturated at [PSA] > ~1 mM, as predicted by γ measurements. The results clearly indicate that the bulk fluorescence characteristics are superimposed on the TIR spectrum and, therefore, that the TIR spectrum does not necessarily represent only the interfacial characteristics. Furthermore, the curious [PSA] dependence of I_D/I_M in Figure 2-15 can also be explained along the same context as that described above.

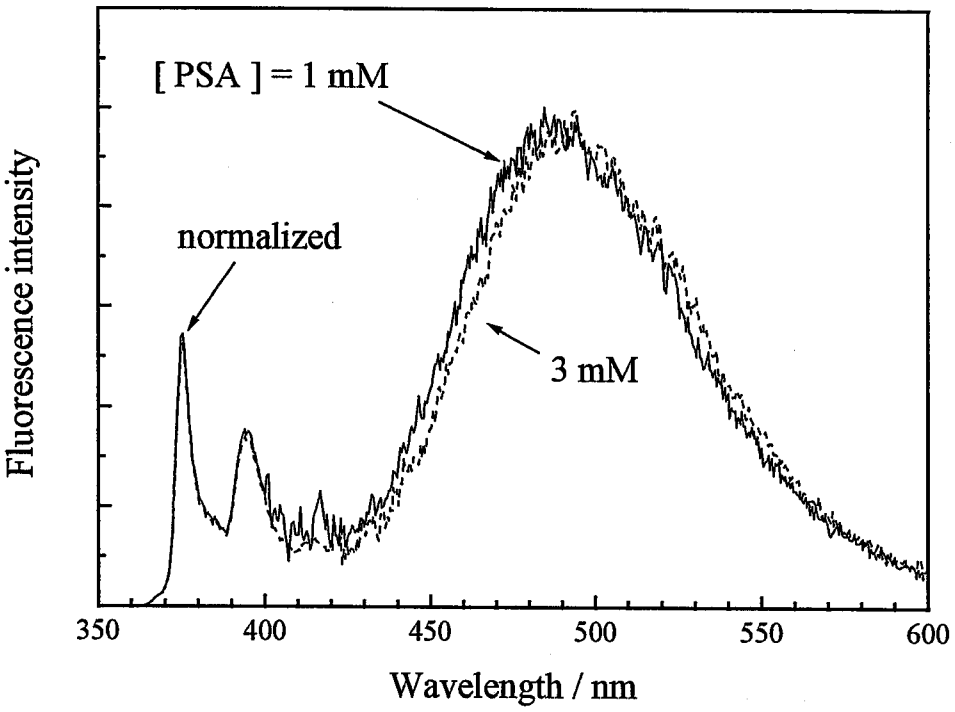

Figure 2-18 Calculated fluorescence spectra of PSA (1.0 and 3.0 mM) at the water/DCE interface.

2.4 Conclusion

PSA has been frequently used in the studies of micelles[16-18], since pyrene and its derivatives are typical compounds that form excimer. In such studies, the ratio of the fluorescence intensity of the structureless band to that of the monomer band has been discussed in terms of excimer formation. The PSA molecule, however, produces a stable ground-state dimer in water and, therefore, is very suitable for studying adsorption characteristics at a liquid/liquid interface.

Actually, adsorption of PSA on a water/DCE interface was successfully discussed in the present study. Although TIR fluorometry is potential to analyze chemical processes at liquid/liquid interfaces, detailed information is obtained only by a time- resolved study combined with TIR fluorometry. Since analogous experiments can be extended to solid/liquid and gas/liquid interfaces, understanding the chemical reactions and processes characteristic of an interface will be further advanced through such approaches.

2.5 References and Notes

(1) Birks, J.B.; " *Photophysics of Aromatic Molecules* ", Wiley-Interscience, New York, 1970.

(2) Turro, N. J.; " *Modern Molecular Photochemistry* ", University Science Books, 1991.

(3) Masuhara, H.; De Schryver, F.C.; Kitamura, N.; Tamai, N.; "*Microchemistry; Spectroscopy and Chemistry in Small Domains*", North-Holland, Amsterdam, 1994.

(4) Koshioka, M.; Misawa, H.; Sasaki, K.; Kitamura, N.; Masuhara, H. *J. Phys. Chem.* **1992**, *96*, 2909.

(5) Nakatani, K.; Misawa, H.; Sasaki, K.; Kitamura, N.; Masuhara, H. *J. Phys. Chem.* **1993**, *97*, 1701-1706.

(6) Loughran, T.; Hatlee, M.D.; Patterson, L.K.; Kozak, J.J. *J. Chem. Phys.* **1980**, *72*, 5791-5797.

(7) Nakatani, K.; Ishizaka, S.; Kitamura, N. *Anal. Sci.* **1996**, *12*, 701-705.

(8) Wendlandt, W. WM.; Hecht, H. G. "*Reflectance Spectroscopy*", John Wiley and Sons, New York, 1966

(9) Riddick, J. A.; Bunger, W. B. *Techniques of Chemistry: Organic Solvents*, Vol. II, Wiley-Interscience, New York, 1970.

(10) Adamson, W.; " *Physical Chemistry of Surfaces* ", John Wiley and Sons, New York, 1990.

(11) Kakiuch, T.; Nakanisi, M.; Senda, M. *Bull. Chem. Soc. Jpn.* **1988**, *61*, 1845.

(12) Andreas, J.M.; Hauser, E.A.; Tucker, W.B. *J. Phys. Chem.***1938**, *42*, 1001-1019.

(13) Menger, F.M.; Whitesell L.G. *J. Org. Chem.* **1987**, *52*, 3793.

(14) Yamazaki, I.; Tamai, N.; Yamazaki, T. *J. Phys. Chem.* **1987**, *91*, 3572.

(15) Gustav, V.K.; Seydenschwanz, C. *Z. Phys. Chem.* **1990**, *271*, 731.

(16) U. K. A. Klein, D. J. Miller and M. Hauser, *Spectrochim. Acta*, **1975**, *32A*, 379.

(17) A. Vbrbeeck and F. C. De Schryver, *Langmuir*, **1987**, *3*, 494.

(18) N. J. Turro and Ping-Lin Kuo, *Langmuir*, **1987**, *3*, 773 .

Chapter 3

Total-Internal-Reflection Fluorescence Dynamic Anisotropy of Sulforhodamine 101 at Liquid/Liquid interface: Rotational Reorientation Times and Interfacial Structures

3.1 Introduction

Phthalate esters (PE) represented by *o*-dibutyl phthalate are widely used in solvent extraction owing to their high solubilities towards various compounds.[1, 2] It is obvious that solvent extraction proceeds across a water/oil interface, so that the interfacial structures including solute adsorption govern the extraction efficiency, extraction kinetics, and so forth.[3-15] In analytical chemistry, therefore, the water/PE interface is a very interesting target of the study. As an another point of the study, a fluorescence dynamic anisotropy technique was employed to study dynamic aspects of molecules at water/PE interfaces. It is worth noting, furthermore, that dynamic anisotropy of a solute molecule is dependent strongly on a medium viscosity.[16-25] As an advantage of the use of PE, a variation of the alkyl chain length in the ester groups brings about a large change in the viscosity, [26, 27] so that a viscosity effect on the reorientational motions of a probe molecule would be studied in detail. Through such experiments, chemical and physical characteristics of both a probe molecule and water/PE interfaces would be elucidated. In this chapter, fluorescence dynamic anisotropy of Sulforhodamine 101 (SR101) at water/PE interfaces was described and the structures of the interface were discussed in detail on the basis of the rotational reorientation times of SR101.[28]

3.2 Experimental

Chemicals and Sample Preparation

Water was purified by distillation and deionization (GSR-200, Advantec Toyo Co., Ltd.). The structures and abbreviations of PE used in this study are shown in Scheme 3-1. Bis(2-ethyhexyl) phthalate (DEHP; 99.5%, Kanto Chemical Co., Inc.), di-*n*-heptyl phthalate (DHP; 98%, Wako Pure Chemical Industries, Ltd.), di-*n*-butyl phthalate (DBP; 99.5%, Kanto Chemical Co., Inc.) and di-*n*-ethyl phthalate (DEP; 99%, Kanto Chemical Co., Inc.) were purified by vacuum distillation after washing successively with 0.1 M NaOH, 0.1 M Na_2CO_3, and water. Glycerol (MERCK, Uvasol) and Sulforhodamine 101 (SR101; ACROS ORGANICS, Laser grade) were used without further purification.

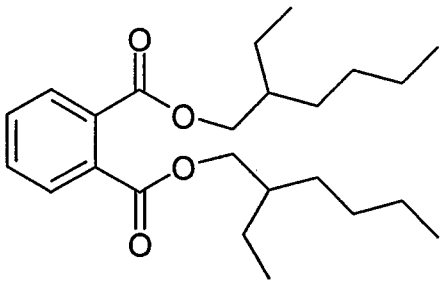

bis(2-ethylhexyl) phthalate (DEHP), 61.6 cP

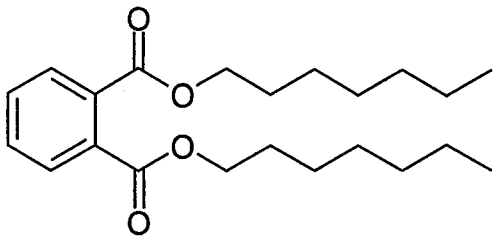

di-*n*-heptyl phthalate (DHP), 34.5 cP

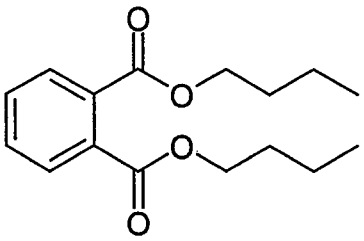

di-*n*-butyl phthalate (DBP), 16.9 cP

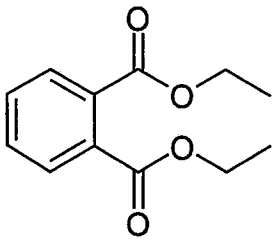

di-ethyl phthalate (DEP), 11.0 cP

Scheme 3-1 The structures and abbreviations of the phthalate esters used in this study.

As a sample solution for TIR experiments, a water-saturated phthalate ester was poured onto an aqueous SR101 solution (concentration [SR101]=1.0×10^{-7} M, saturated with a phthalate ester) in a Pyrex cell (inner diameter = 40 mm). The upper inside of the cell was treated with dichlorodimethylsilane to construct a flat water/oil interface. The cell was washed thoroughly with a phthalate ester and then with water prior to a sample preparation. Spectroscopic measurements were carried out after the sample solution in the cell being kept standing over 100 min.

Measurements

Fluorescence dynamic anisotropy measurements under normal (bulk) or TIR conditions were conducted as described below. The fundamental laser pulses from a mode-locked Ti:Sapphire laser (Coherent, Mira model 900-F), pumped by a diode laser (Verdi), were amplified by a regenerative amplifier (RegA model 9000) pumped by an Ar^+ ion laser (INNOVA 300). Optical parametric amplification (Coherent, Model 9400) of the output gave 580 nm pulses as an excitation light source (repetition rate; 100 kHz, FWHM; 200fs-autocorrelation trace). The excitation laser beam, polarized perpendicular to the plane of incidence (s-polarized) by using a Glan-laser prism, was irradiated to a water/PE interface through the oil phase, as illustrated in Figure 3-1. In the present experiments, the incident angle of the laser beam (θ_i) was set (80°) larger than the critical total-reflection angle at the water/PE interface ($\theta_i = 62 \sim 64°$). The fluorescence from the sample was collected along surface normal and its polarization was selected with a polarizer (Polaroid, HNP'B). The polarized fluorescence was detected by a microchannel-plate photomultiplier (Hamamatsu, R3809U-50) equipped with a monochromator (Jobin

Ybon, H-20) and analyzed by a single-photon counting module (Edinburgh Instruments, SPC-300). The monitoring wavelength of the fluorescence was set 615 nm throughout the study. Dynamic anisotropy measurements of SR101 in a series of water-glycerol mixtures were conducted in a quartz cuvette. A fluorescence spectrum of SR101 under the normal or TIR conditions was recorded on a multichannel photodetector (Hamamatsu, PMA11). All experiments were conducted at room temperature (~23 °C).

The viscosities of the phthalates and water-glycerol mixtures were determined by an Ostwald viscometer at 23 °C. The interfacial tension (γ) at the water/PE interface was measured by a pendant drop method as described in Chapter 2.[29-31]

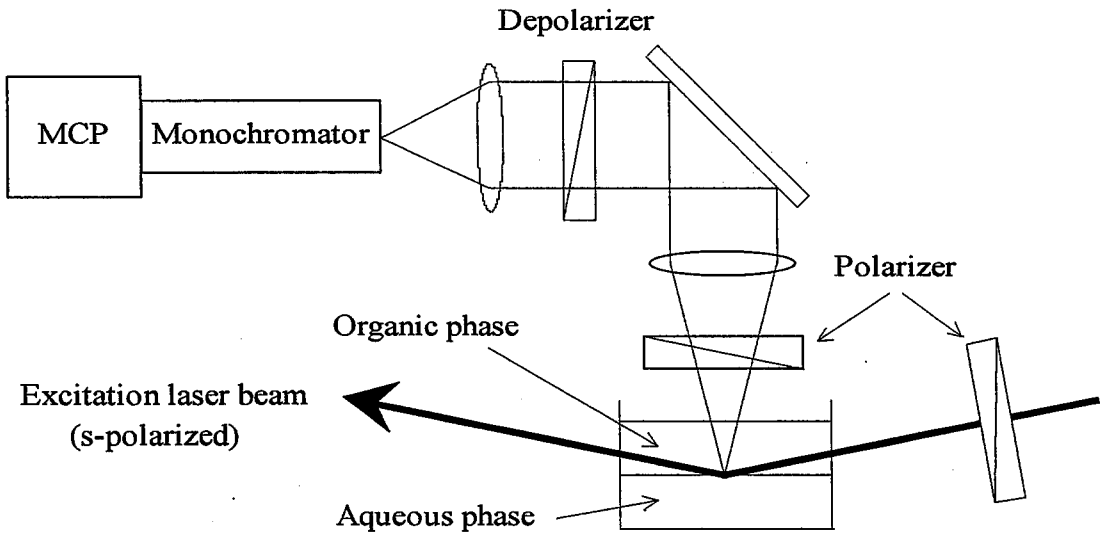

Figure 3-1 A schematic illustration of a system for total-internal-reflection fluorescence dynamic anisotropy measurements at a liquid/liquid interface.

3.3 Model of Fluorescence Dynamic Anisotropy at Liquid/Liquid Interface

The laboratory coordinate system chosen for TIR fluorescence anisotropy measurements is illustrated in Figure 3-2. SR101 molecules located at a water/PE interface (in the X-Y plane) are excited by an s-polarized laser beam along the X axis. The TIR fluorescence is then detected along the Z-axis and its polarization is selected by a polarizer. The fluorescence decay profile observed under such a configuration is analyzed by two limiting cases, depending on the structure of a water/PE interface: two-dimension or three-dimension.

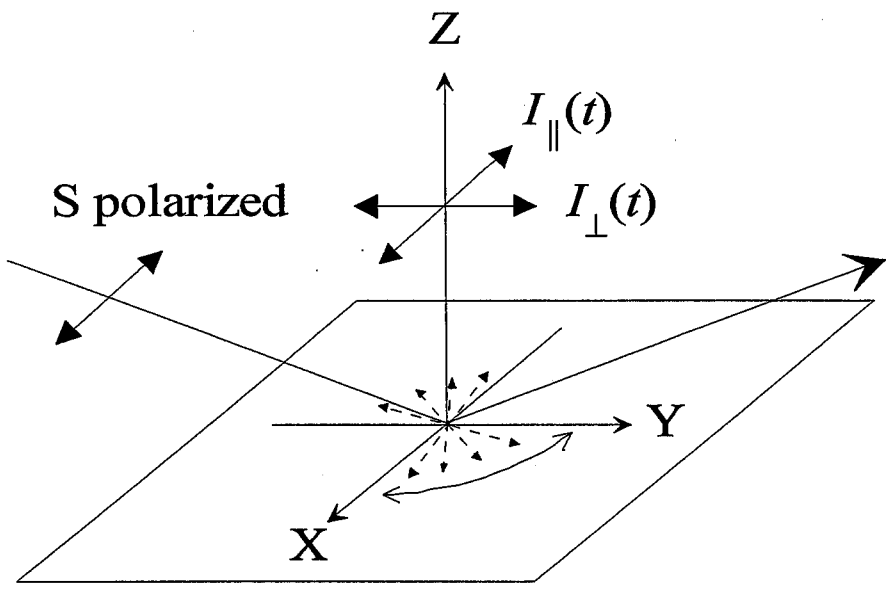

Figure 3-2 A coordinate system defined in the experiment. The X-Y plane is the plane of the interface.

Case I: Two-dimensional Model

If the thickness of a water/PE interface is comparable to the molecular size of SR101 and the dye molecules located at the interface are strongly oriented, the rotational motions of SR101 will be strongly restricted in the interfacial layer (X-Y plane of the interface, two-dimension), and the emission dipole moment of SR101 (direction of the long axis of the xanthene ring) directs within the X-Y plane. In such a case, the time profile of the total fluorescence intensity of SR101 observed from the interface should be proportional to $I_{\parallel}(t) + I_{\perp}(t)$, where $I_{\parallel}(t)$ and $I_{\perp}(t)$ represent the fluorescence decay profiles observed with emission polarization parallel and perpendicular to the direction of excitation polarization, respectively. When the angle of the emission polarizer is set 45° respect to the X axis (magic angle), fluorescence anisotropy is canceled, so that the TIR fluorescence decay curve should be analyzed by a single-exponential function. If a water/PE interface is very sharp, therefore, fluorescence dynamic anisotropy $r(t)$ obeys with eq 3.1,

$$r(t) = \frac{I_{\parallel}(t) - I_{\perp}(t)}{I_{\parallel}(t) + I_{\perp}(t)} = r(0)\exp\left(-t/\tau^{rot}\right) \qquad (3.1)$$

where $r(0)$ and τ^{rot} are initial anisotropy (t =0) and the reorientation correlation time, respectively. In the *Case I*, $r(0)$ should be equal to 0.5.[32]

Case II: Three-dimensional Model

On the other hand, if the interfacial layer is thick enough compared to the molecular size of SR101 and SR101 molecules adsorbed on the interface are weakly oriented, the rotational motions of SR101 take place in three dimension, similar to those in a bulk phase. If this is the case, the contribution of the fluorescence with the excited dipole moment of SR101 being directed along the Z axis cannot be neglected, so that the time profile of the total fluorescence intensity must be proportional to $I_{\parallel}(t) + 2I_{\perp}(t)$. Thus,

fluorescence dynamic anisotropy is given by eq 3.2, as well known for that in a macroscopically isotropic system,[33]

$$r(t) = \frac{I_{||}(t) - I_{\perp}(t)}{I_{||}(t) + 2I_{\perp}(t)} = r(0)\exp\left(-t/\tau^{rot}\right) \qquad (3.2)$$

and $r(0)$ and the magic angle are calculated to be 0.4 and 54.7°, respectively.

The thickness of a water/PE interfacial layer would be thus evaluated through TIR fluorescence anisotropy measurements and the τ^{rot} value(s) provides information about characteristic features of a water/PE interface.

3.4 Results and Discussion

3.4.1 Adsorption of SR101 at Water/PE Interface

For TIR fluorescence spectroscopy on liquid/liquid interfaces, a choice of a probe molecule is of primary importance. In the present case, the penetration depth (d_p) of an incident evanescent wave at a DEHP (refractive index (n); $n_1 = 1.48$) / water ($n_2 = 1.33$)[34] interface is calculated to be ~80 nm on the basis of the equation; $d_p = \lambda / \{4\pi(n_1^2 \sin^2\theta_i - n_2^2)^{1/2}\}$ where λ is the wavelength (580 nm) of an excitation laser beam and $\theta_i = 80°$.[35, 36] It has been reported that the thickness of a sharp liquid/liquid interface represented by a water/1,2-dichloroethane interface is ~ 1 nm,[37-42] so that d_p of the incident evanescent wave is thicker than the thickness of the interfacial layer, and the fluorescence characteristics of a probe molecule in the bulk phase is superimposed, more or less, on that at the interface.[43] Therefore, a probe molecule should be highly surface active and adsorb on the interface, so as to exclude fluorescence of the probe molecule from the bulk phase. In the present experiments, SR101 was employed as a fluorescence probe throughout the study, since SR101 is highly surface active and adsorbs strongly on a water/PE interface. This has been confirmed by interfacial tension (γ) measurements. As a typical example, a relationship between γ and log[SR101] determined for the water/DEHP system by a pendant drop method is shown in Figure 3-3. The γ value decreased sharply with increasing [SR101] (> 10^{-5} M). The result clearly demonstrates adsorption of SR101 on the water/DEHP interface. The amount of adsorbed SR101 on the interface (Γ) is given by the Gibbs equation: $\Gamma = -(1/\ 2.3RT)\ d\gamma / d\log[\text{SR101}]$. The Γ value was then calculated to be 3.0×10^{-12} mol cm^{-2} ([SR101] = 1.0×10^{-7} M). When the interfacial area is assumed to be 1 cm^2 for simplicity, the number of SR101 molecules

adsorbed on the interface (3.0×10^{-12} mol) is 3000 times higher than that expected to be involved in the excited volume by the evanescent wave (1.0×10^{-15} mol) without adsorption. Almost the same results with those for DEHP were obtained for other water/PE systems. At [SR101] = 1×10^{-7} M, therefore, the fluorescence response observed under the TIR conditions is limited to that from the interface alone.

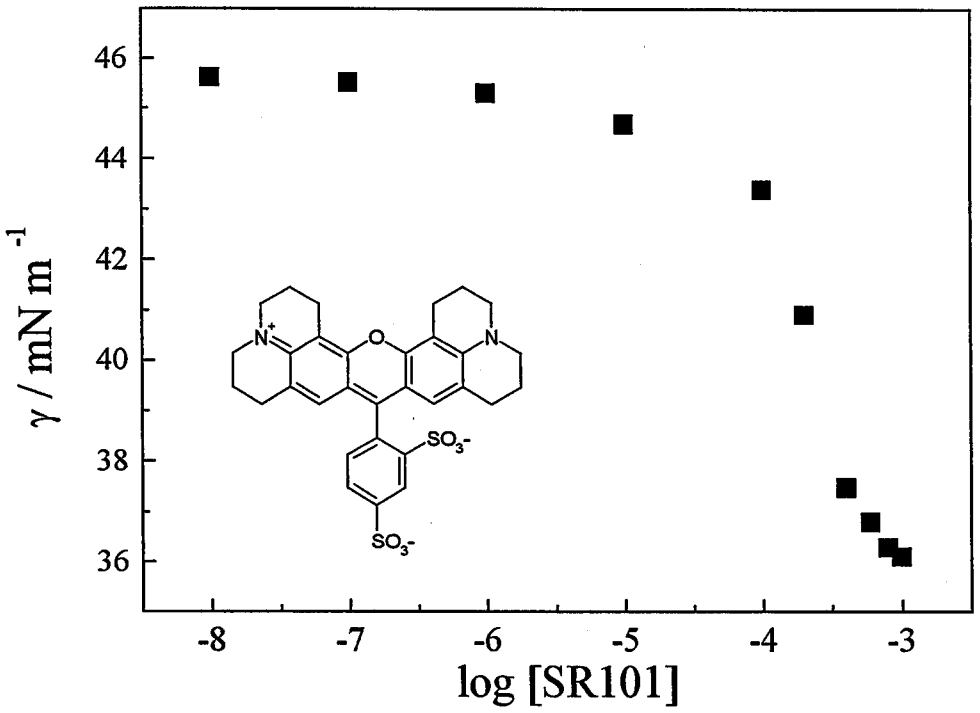

Figure 3-3 An SR101 concentration dependence of the interfacial tension in a water/DEHP system.

3.4.2 *TIR Fluorescence Decay of SR101 at Water/PE Interface*

Figure 3-4 shows a fluorescence decay profile of SR101 at a water/DEHP interface observed with emission polarization being set parallel ($I_{\parallel}(t)$) or perpendicular ($I_{\perp}(t)$) to the direction of excitation polarization. The difference in the profile between $I_{\parallel}(t)$ and $I_{\perp}(t)$ in the initial stage of excitation (< 10 ns) clearly demonstrates that rotational reorientation of the excited SR101 is restricted at the water/DEHP interface, while that is randomized with time. Since $I_{\parallel}(t)$ and $I_{\perp}(t)$ under the TIR conditions have been obtained with good signal-to-noise ratios, the structure of the water/DEHP interface can be discussed on the basis of $r(t)$ and the relevant models (eqs 3.1 and 3.2). Thus, a magic angle dependence of the fluorescence decay profile of SR101 was studied at a water/PE interface.

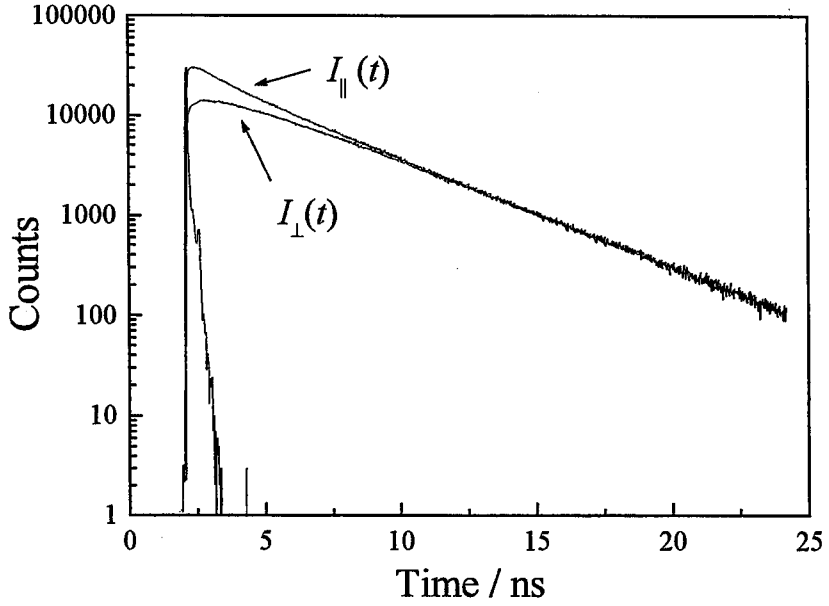

Figure 3-4 Fluorescence anisotropy decays of SR101 at a water/DEHP interface determined under the TIR conditions (θ_i = 80°). $I_{\parallel}(t)$ and $I_{\perp}(t)$ represent the parallel and perpendicular components of the fluorescence, respectively.

Figure 3-5, 3-6, 3-7 and 3-8 show fluorescence decay profiles of SR101 observed for a water/DEP, DBP, DHP and DEHP interfaces at an emission polarization angle of 45° ((a); *Case I*) or 54.7° ((b); *Case II*), together with the relevant weighted residuals (*Re*) and autocorelation trace (*Cr*) for a single exponential fit, respectively. The fittings of the data obtained at the angles of 45° and 54.7° gave the decay times (τ) of 4.06 ~ 4.18 and 4.20 ~ 4.31 ns, respectively, while τ in an aqueous solution was 4.12 ns (Table 3-1).

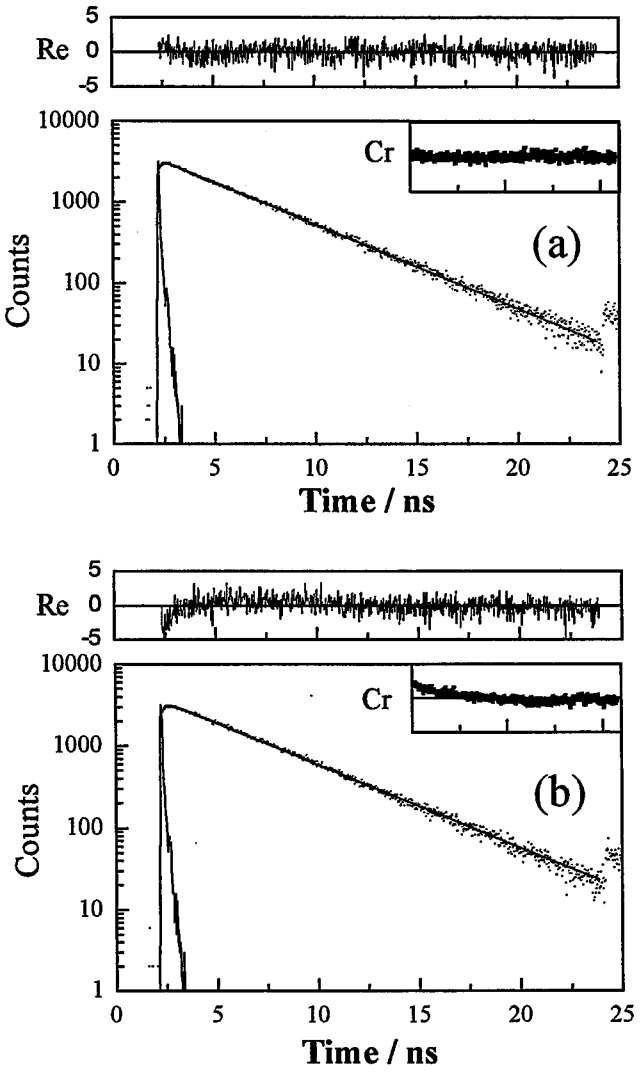

Figure 3-5 TIR fluorescence decay curves of SR101 at a water/DEP interface observed at the direction of the emission polarizer, 45° (a) or 54.7° (b). The upper and inner panels of each figure represent the plots of the weighted residuals (*Re*) and the autocorelation trace for a single-exponential fitting, respectively.

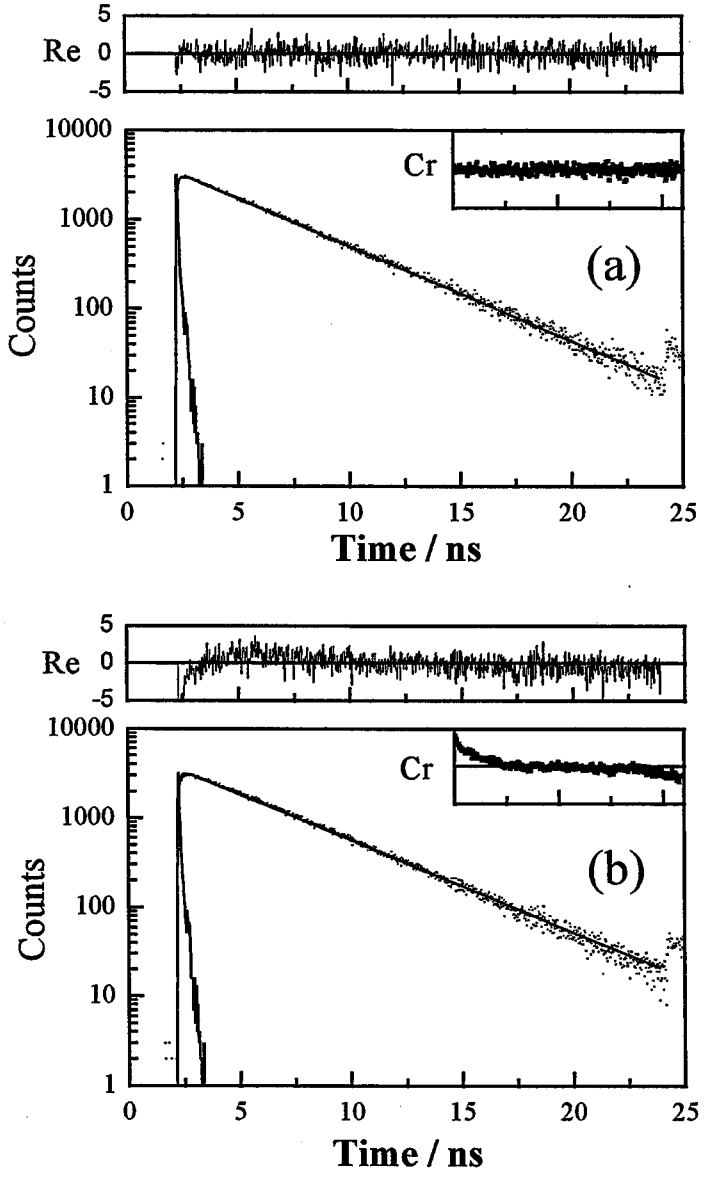

Figure 3-6 TIR fluorescence decay curves of SR101 at a water/DBP interface observed at the direction of the emission polarizer, 45° (a) or 54.7° (b). The upper and inner panels of each figure represent the plots of the weighted residuals (*Re*) and the autocorelation trace for a single-exponential fitting, respectively.

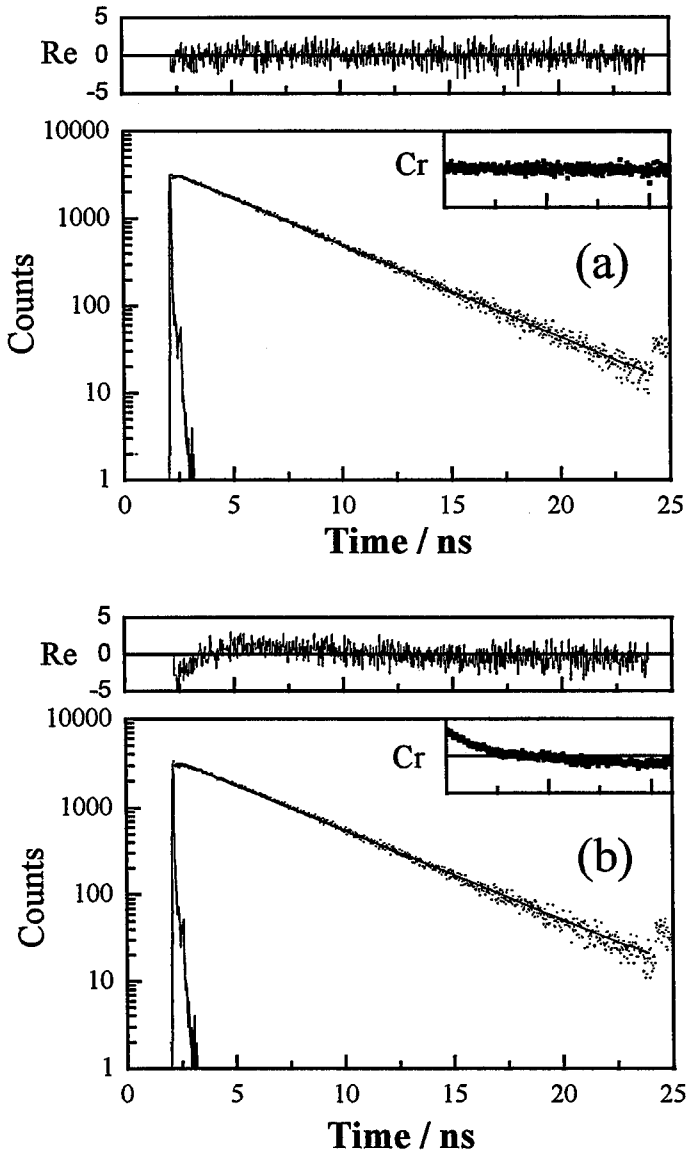

Figure 3-7 TIR fluorescence decay curves of SR101 at a water/DHP interface observed at the direction of the emission polarizer, 45° (a) or 54.7° (b). The upper and inner panels of each figure represent the plots of the weighted residuals (*Re*) and the autocorelation trace for a single-exponential fitting, respectively.

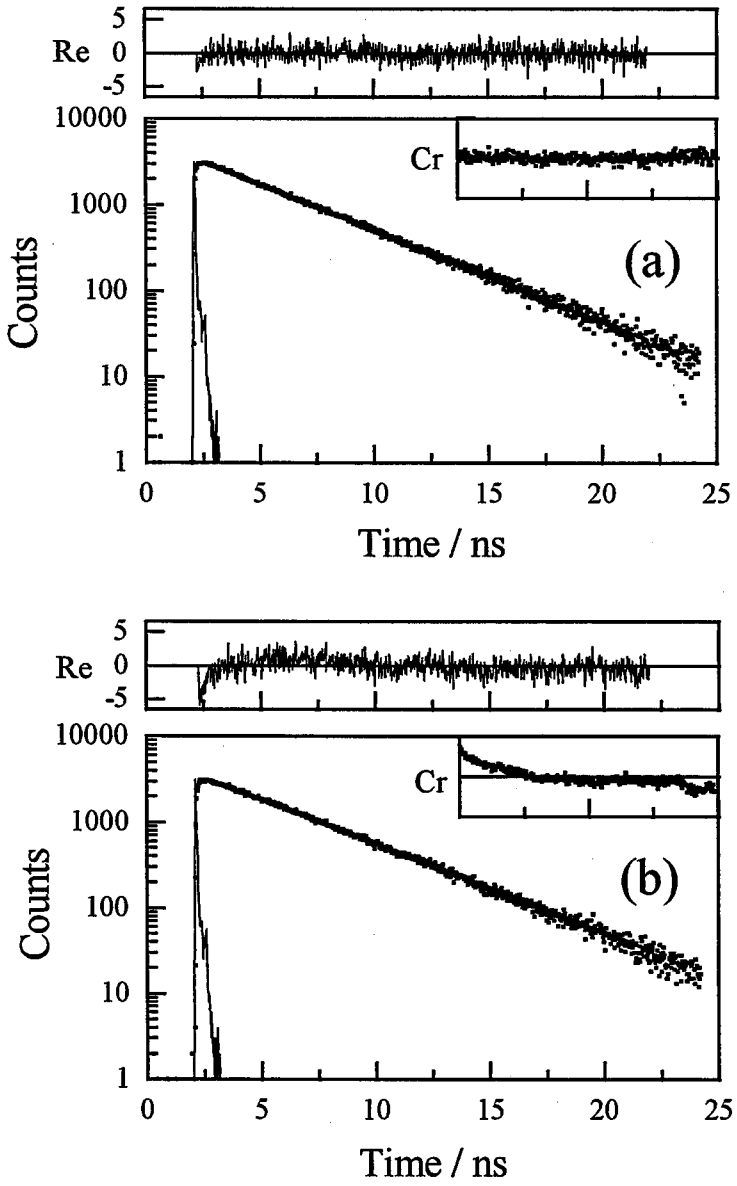

Figure 3-8 TIR fluorescence decay curves of SR101 at a water/DEHP interface observed at the direction of the emission polarizer, 45° (a) or 54.7° (b). The upper and inner panels of each figure represent the plots of the weighted residuals (*Re*) and the autocorelation trace for a single-exponential fitting, respectively.

Table 3-1: Fluorescence decay parameters of SR101 adsorbed on a water/PE interfaces observed under the TIR conditions and in an aqueous solution.

PE		τ_1 / ns	$\chi^{2\,a)}$	D.W. [a)]
DEP	45° [b)]	4.18	1.02	1.96
	54.7° [b)]	4.31	1.31	1.53
DBP	45° [b)]	4.08	1.02	1.89
	54.7° [b)]	4.22	1.92	1.11
DHP	45° [b)]	4.08	1.04	1.97
	54.7° [b)]	4.21	1.54	1.29
DEHP	45° [b)]	4.06	1.08	1.94
	54.7° [b)]	4.20	1.62	1.26
aq. [c)]		4.12	1.16	1.94

a) χ^2 and D.W. represent the χ^2 and Darbin-Watson parameters for the fitting, respectively.

b) The angle of the emission polarizer in respect to the X-axis.

c) Determined in an aqueous solution ([SR101] = 1.7×10^{-7} M).

The decay times almost agreed with each other. Furthermore, the fluorescence spectrum of SR101 observed under the TIR conditions coincided very well with that in an aqueous solution, so that there is no indication of a change in the electronic properties of the dye upon adsorption. On the other hand, *Re* and *Cr* of the data at 54.7° exhibited non-random distributions from those predicted by the best fit (b), particularly, in the initial stage of excitation (< 10 ns). The χ^2 and Durbin-Watson (D.W.) parameters also support that the best fit by a single exponential function can be attained by setting emission polarization at the magic angle, 45° (Table 3-1).[44] Analogous results were obtained for other water/PE systems. Therefore, it can be concluded that the water/phthalate ester interface is sharp in respect to the molecular size of SR101 and three-dimensional rotations of SR101 are

inhibited at the interface. The two-dimensional rotational reorientation model in eq 3.1 is valid for the present system. Recently, Wirth and Burbage reported roughness of a water/oil interface on the basis of the $r(0)$ value for the out-of-plane rotational reorientation time of Acridine Orange determined by a frequency-domain technique.[45] A direct comparison between these two results is very difficult, since both oil and probe molecule studied are different : n-hexadecane, cyclohexane, or cis/trans-decalins as an oil in their case. Compared to a frequency-domain technique, nonetheless, the magic angle dependence study on the fluorescence decay based on the dimensionality models (eqs 3.1 and 3.2) and a single-photon counting method would be a more direct approach to study rotational reorientation of a molecule at a water/oil interface.

3.4.3 Viscosity Dependence of Rotational Reorientation Time of SR101 in Bulk Solutions

In order to discuss characteristics of the water/PE interfacial structures, factors governing the rotational motions of SR101 should be clarified. In bulk solutions, it is well known that the rotational reorientation time (τ^{rot}) of an excited molecule is highly dependent on the viscosity of a medium. A comparison of τ^{rot} of SR101 in the interfacial system with that in a bulk solution is one possible approach of the study along the line. Before describing results on τ^{rot} at the water/PE interfaces, therefore, a viscosity (η) dependence of τ^{rot} of SR101 in bulk solutions is discussed.

Anisotropy decay profiles ($r(t)$) of SR101 determined in a series of water-glycerol mixtures and the relevant fits by the three-dimensional model in eq 3.2 (solid lines) are

summarized in Figure 3-9. As seen clearly in the figure, all of the decays were fitted satisfactorily by single-exponential functions irrespective of a wide variation of η (1 ~ 70 cP). The τ^{rot} and $r(0)$ values determined for each medium are listed in Table 3-2. The $r(0)$ value was almost constant at 0.38 - 0.39 regardless of η as expected, while τ^{rot} increased with increasing in η. If τ^{rot} is governed by rotational reorientation of SR101, a relationship between τ^{rot} and η should obey with the Debye-Stokes-Einstein (DSE) hydrodynamic theory (eq 3.3),[46]

$$\tau^{rot} = \frac{4\pi\eta R^3}{3kT} = \frac{\eta V}{kT} \tag{3.3}$$

where k and T are the Boltzmann constant and the absolute temperature, respectively. R and V are the hydrodynamic radius and volume of a probe molecule, respectively. Equation 3.3 predicts a linear increase in τ^{rot} with η and, the slope of the plot should give the hydrodynamic radius of SR101. Indeed, a linear relationship between τ^{rot} and η was obtained as shown in Figure 3-10 (correlation coefficient = 1.00). Although the value at η = 70.7 seems to deviate slightly from the linear relation, this will be explained by a saturation effect as reported for an η dependence of τ^{rot} for Rhodamine 6G.[47] The hydrodynamic diameter of SR101 thus calculated from the slope of the plot was ~ 11Å, which was in good agreement with that estimated by a molecular orbital simulation (10 ~ 14 Å). Thus, dynamic anisotropy of SR101 in bulk solutions is explained satisfactorily by the DSE theory.

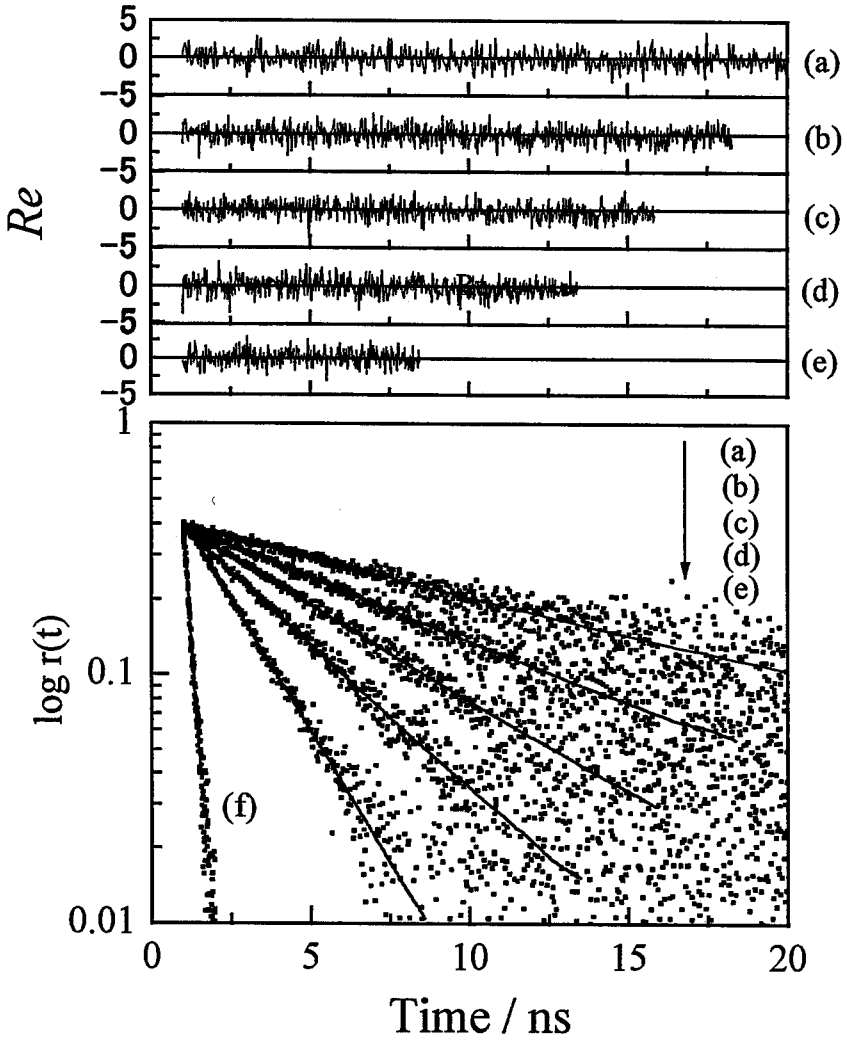

Figure 3-9 Fluorescence anisotropy decay curves of SR101 in glycerol/water mixtures. The weight percentage of glycerol in water is 83 (a), 80 (b), 75 (c), 70 (d), 60 (e), and 0 (f).

Table 3-2: Anisotropy decay parameters of SR101 in glycerol/water mixtures at 23 °C.

Glycerol/ Water wt %	η (23 °C) [a)] cP	τ^{rot} ns	$r(0)$	χ^2
0	0.93	0.21	0.38	1.17
60	9.74	2.04	0.39	1.00
70	18.9	3.71	0.38	1.03
75	28.4	5.57	0.38	0.98
80	43.4	8.44	0.39	0.93
83	70.7	12.9	0.39	1.05

a) The viscosity was determined by an Ostwald viscometer at 23 °C.

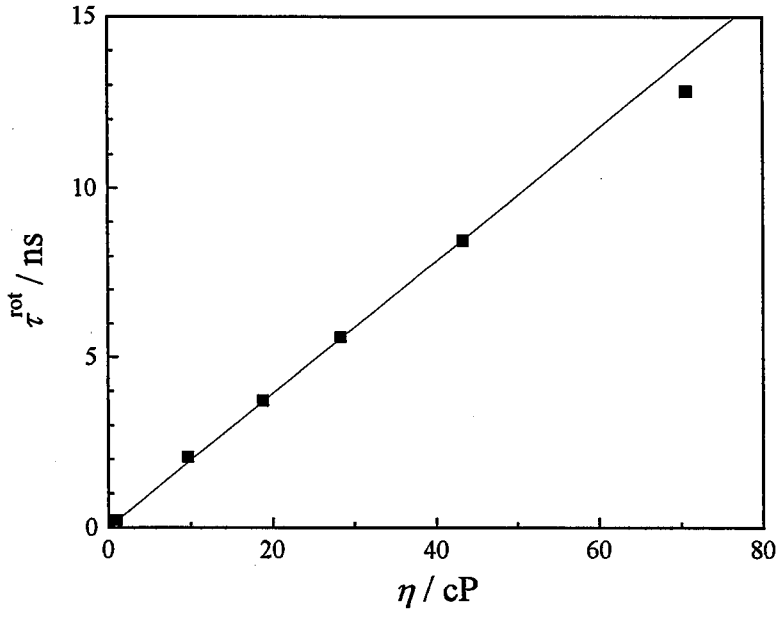

Figure 3-10 A relationship between the reorientational reorientation time of SR101 and the viscosity of the glycerol/water mixture. The solid line represents the best fit by eq (3.3).

3.4.4 *Rotational Reorientation Times of SR101 at Water/PE Interface*

A water/PE interface is expected to be very sharp similar to a water/1,2-dichloroethane or water/nitrobenzene interface (thickness ~ 1 nm),[37,48] since the solubility of water in the phthalate ester is very low (0.2 ~ 0.5 wt %).[34] As discussed in the previous section, actually, the fluorescence dynamics at the water/PE interface was best analyzed by eq 3.1 (two-dimensional model). Therefore, the thickness of the interfacial layer is comparable to the molecular size of SR101 (10 ~ 14 Å). Since the dye molecule sits on the interface, the chemical and physical structures of the water/PE interface should reflect on τ^{rot}. Fluorescence dynamic anisotropy measurements under the TIR conditions were thus performed for the water/PE interfacial systems with the viscosity of the oil phase being varied from 11 (DEP) to 62 cP (DEHP). The results are summarized in Figure 3-11 and Table 3-3, in which $r(t)$ was analyzed by eq 3.1 as discussed before. Note that the anisotropy decay of the dye at the water/DEP interface was very similar to that at the water/DBP interface, so that the results are not shown in Figure 3-11.

Table 3-3: Anisotropy decay parameters of SR101 at the water/phthalate ester interfaces.

oil	η / cP [a)]	γ / mNm^{-1} [b)]	r_1	τ_1^{rot} / ns	r_2	τ_2^{rot} / ns	$r(0)$	χ^2
DEP	11.0	15.3	0.14	0.27	0.40	1.38	0.54	1.07
DBP	16.9	21.5	0.18	0.28	0.32	1.54	0.50	1.04
DHP	34.5	41.1	0.12	0.32	0.39	2.00	0.51	1.17
DEHP	61.6	45.8	0.15	0.89	0.31	3.30	0.46	1.06

a) The viscosity was determined by an Ostwald viscometer at 23 °C.

b) The interfacial tension was determined by a pendant drop method.

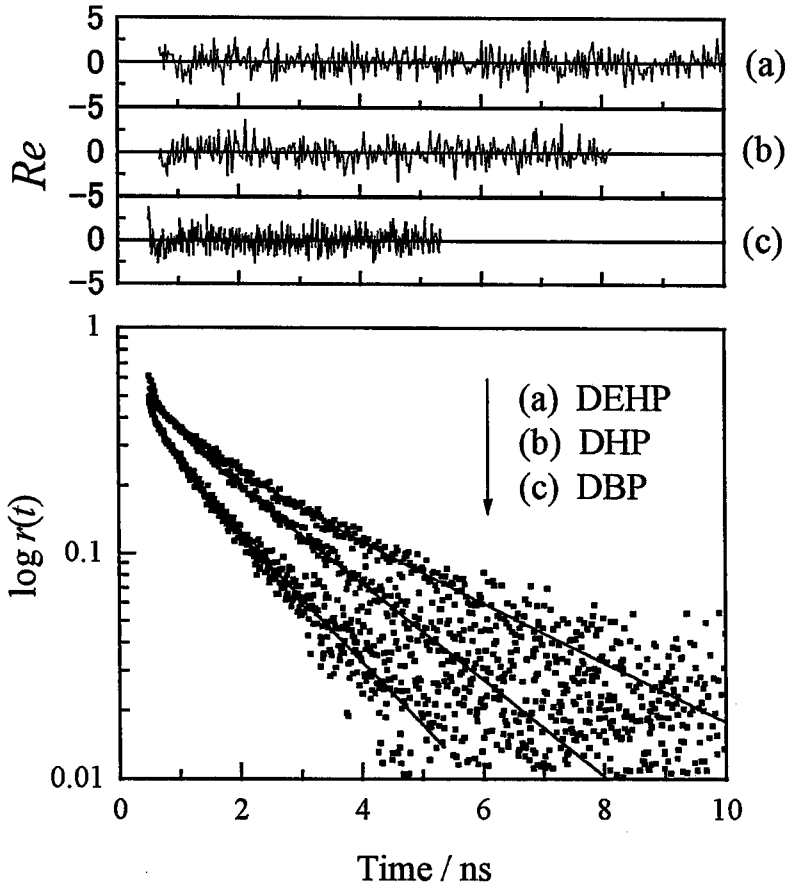

Figure 3-11 Anisotropy decay curves of SR101 at the water/phthalate ester interfaces observed under the TIR conditions : DEHP (a), DHP (b), or DBP (c). The result on DEP was very similar to that on DBP, so that the data were not shown here.

Although the initial anisotropy values ($r(0)$) obtained for DEP and DEHP deviated slightly from 0.5, the best fit of $r(t)$ was attained by a double-exponential function, in marked contrast to that in a macroscopically isotropic bulk solution:

$$r(t) = \sum_i r_i \exp\left(-t/\tau_i^{rot}\right) \qquad (i = 1,2) \qquad (3.4)$$

Knowing the rotational reorientation time of SR101 in water to be 0.21 ns (Table 3-2), it is concluded that the time constants (τ_i^{rot}) are influenced by the presence of the oil phase and, the fast (τ_1^{rot}) and slow decay times (τ_2^{rot}) ranged 0.3 ~ 0.9 ns and 1.4 ~ 3.3 ns, respectively, with τ_2^{rot} being the major component contributed to $r(t)$ as judged by the pre-exponential factor of the decay component (r_i in Table 3-3).

The appearance of the two rotational reorientation times is characteristic to the water/PE interface. In Figure 3-12, τ_1^{rot} and τ_2^{rot} were plotted against η of PE. Although the variation of τ_1^{rot} with η is small, τ_1^{rot} tends to converge to that in water with decreasing η. On the other hand, τ_2^{rot} was affected by η stronger than τ_1^{rot}. However, the η dependence of τ_2^{rot} was much weaker than that predicted from the rotational reorientation time of SR101 in a bulk solution (DSE theory in eq 3.3; solid line in Figure 3-12). The deviation between the observed (τ_2^{rot}) and calculated rotational reorientation times for a given η (solid line) increases with increasing η. This is also characteristic behavior of τ^{rot} at the water/PE interface. All of these results should be discussed to clarify characteristics of the water/PE interface.

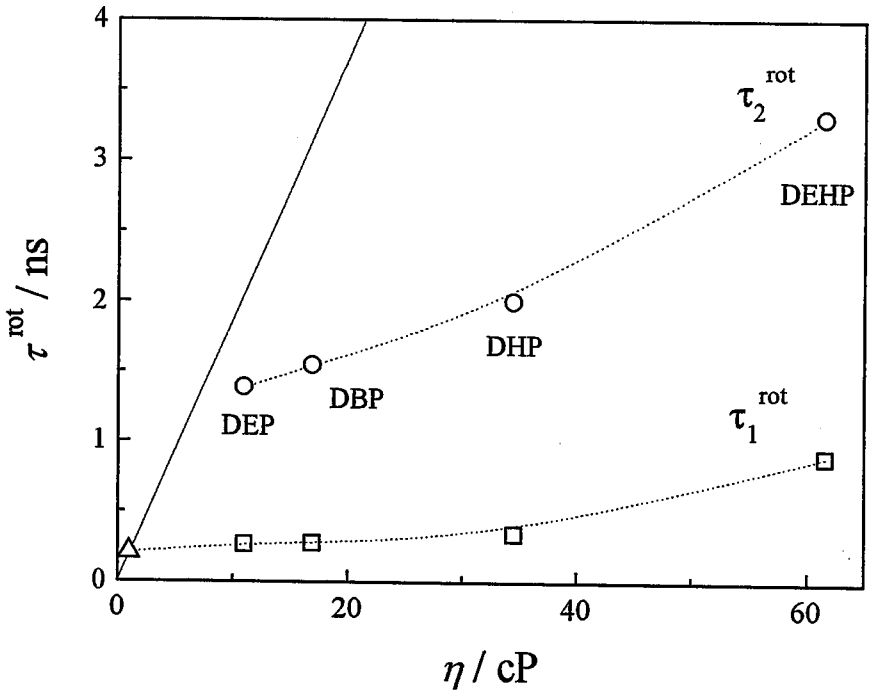

Figure 3-12 Relationships between the rotational reorientation times of SR101 at the water/phthalate ester interfaces and the viscosity of PE. The data point shown by the triangle represents the result determined in water.

One possible explanation for the origin of the double exponential decay of $r(t)$ might be to assume excitation energy migration between SR101 at the interface. However, the concentration of SR101 was set as low as possible (1.0×10^{-7} M) and the mean distance between adsorbed SR101 on the interface is 75 Å as estimated from the interfacial area and the Γ value. The mean distance is larger than the critical energy transfer distance reported for that between rhodamine 6G (58 Å).[49] Furthermore, the TIR fluorescence decay curve observed at the magic angle (45 °) was analyzed successfully by a single-exponential function, and the fluorescence lifetime agreed satisfactorily with that in a dilute aqueous solution. Therefore, energy migration between SR101 at the water/PE interface is not the origin of the double exponential decay of $r(t)$.

Another explanation might be an effect of thermal capillary waves at the interface, since the variation of the oil phase accompanies that of the interfacial tension (Table 3.3) and, both frequency and amplitude of a thermal capillary wave generated at the interface are related to the interfacial tension.[50-53] If the capillary wave contributes significantly to rotational reorientation of SR101, only high frequency capillary waves, whose wavelengthes are comparable to the molecular size of SR101, would influence τ_i^{rot}. When one assumes that the wavelength of the capillary wave is as short as the thickness of the interfacial layer (~ 1 nm), the frequency of the wave is calculated to be several hundreds of GHz on the basis of the Lamb's equation.[54] This frequency corresponds to the time scale of the thermal fluctuation of several ps. Since the observed rotational reorientation times at the interface are 0.3 ~ 3 ns, it is concluded that the thermal fluctuations at the interface are not reflected on τ_1^{rot} and/or τ_2^{rot}. Thus, the thermal capillary waves at the interface cannot explain the present results.

The τ_1^{rot} value is rather similar to that in water except for the data at the water/DEHP interface, while τ_2^{rot} increases with increasing η of PE. Thus, an adsorption equilibrium of SR101 between the interface (τ_2^{rot}) and water phase (τ_1^{rot}; not far from the interface) might explain the double exponential decay. If this is the case, the adsorption equilibrium should reflect on the r_1/r_2 ratio and the value is expected to decrease with increasing γ. However, such a tendency cannot be seen from the data in Table 3-3. Furthermore, when SR101 locates in the water phase much deeper than the thickness of the interfacial layer or molecular size of SR101, the dynamic anisotropy data cannot be analyzed by the two-dimensional model in eq 3.1. Thus, the emissive species responsible for τ_1^{rot} and τ_2^{rot} should locate close vicinity of the interface, whose thickness allows the two-dimensional analysis (~1 nm).

3.4.5 Adsorption of SR101 on the Water/PE Interface and Its Implication to Rotational Reorientation Times

Above discussions lead to the conclusion that the double exponential decay of $r(t)$ is intrinsic nature of dynamic anisotropy at the water/PE interface and is caused by the microscopic structure of the interface itself. It is noteworthy that τ_2^{rot} should be slower than the value expected from the three-dimensional rotation model, since the out-of-plane rotational motion is restricted at the water/PE interface; the freedom of the molecular motion is reduced at the interface. Nevertheless, τ_2^{rot} was faster than that predicted by DSE at a given η (solid line in Figure 3-12) and the deviation between the observed (τ_2^{rot}) and predicted values increased with increasing η. The results would indicate that rotational reorientation of SR101 at the interface is not governed by the bulk viscosity of the oil itself, but determined by microscopic friction between the dye and solvent molecules. Therefore, it is supposed that the two rotational reorientation times of SR101 (τ_1^{rot} and τ_2^{rot}) are originated from two different adsorption modes (mode-1 and -2, respectively) as schematically illustrated in Scheme 3-2. A simple molecular orbital calculation indicates that the phenyl ring of SR101 rotates almost perpendicularly to the plane of the xanthene ring owing to steric hindrance of the sulfonate group. Such a conformation is also favorable for electrostatic attraction between the sulfonate group and the cationic charge on the xanthene chromophore. Furthermore, the xanthene ring is planer and rigid. As one mode, therefore, SR101 will adsorb on a water/PE interface with the molecular plane of the xanthene chromophore being almost faced to the interface while the $-SO_3^-$ group on the phenyl ring directs to the water phase: mode-1. Under such a condition, the rotational and/or tumbling motions of SR101 are restricted in the X-Y plane, and expected to be insensitive to the viscosity of the oil phase: τ_1^{rot} = 0.27 ns (η =

11.0 cP) ~ 0.32 ns (η = 34.5 cP). In the water/DEHP system, the oil is very viscous (61.6 cP) so that the molecular motion of SR101 at the interface is influenced by η : τ_1^{rot} = 0.89 ns. The adsorption mode-1, however, would be unstable (r_1/r_2 = 0.3 ~ 0.5, Table 3), since the hydrophobic part of SR101 (i.e., aza-tetraline part of the xanthene chromophore) will be likely to bury in the oil phase with the hydrophilic parts ($-SO_3^-$ and the quinoid structure) being toward the water phase; thus, the long axis of the xanthene chromophore corresponding to the direction of the emission dipole bisects the water/PE interface (mode-2). In such an adsorption mode, a contribution of the Z-axis component of the TIR fluorescence to the total fluorescence intensity will not be neglected and, therefore, the

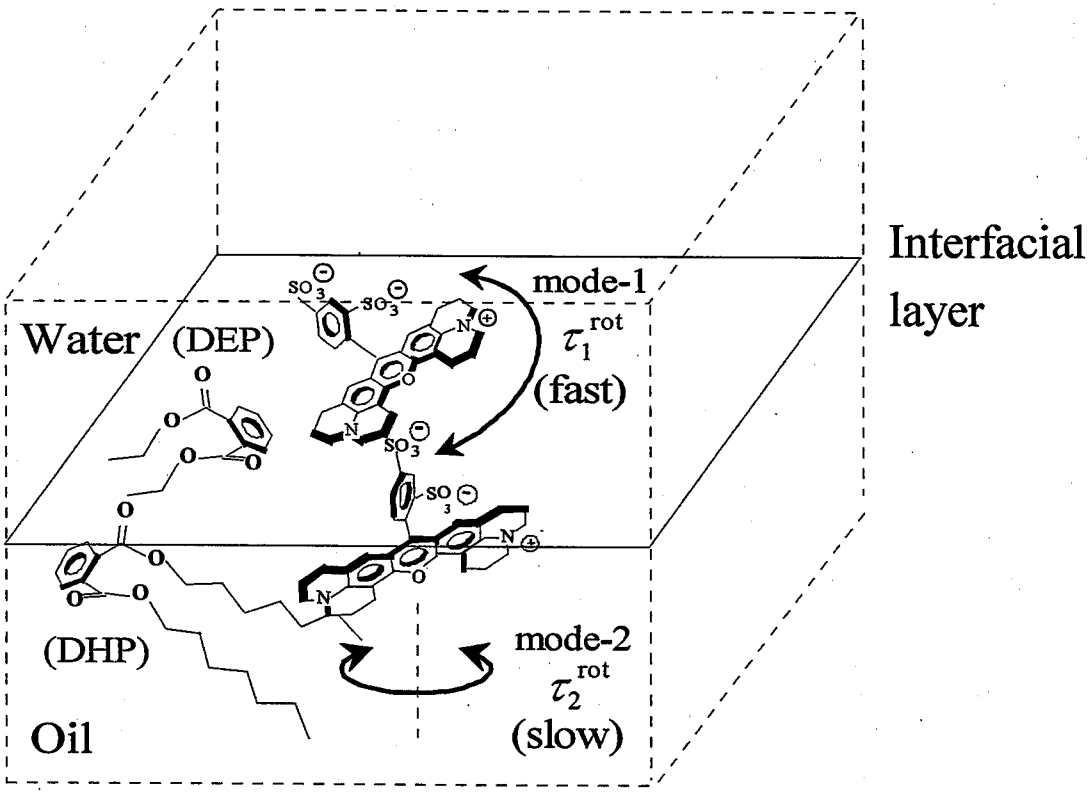

Scheme 3-2 A proposed model for the interfacial structure and adsorption of SR101.

observed decay curve should be fitted by the three-dimensional model. Nonetheless, the TIR fluorescence decay curve observed at an emission polarization angle of 54.7° could not be fitted by a single-exponential function as described before, indicating a minor contribution of the Z-axis component (out-of-plane) of the fluorescence to the TIR fluorescence. This might be explained by a small tilt angle of SR101 at the interface as shown in Scheme 3-2. Recently, Uchida et al. reported that Rhodamine derivatives (Rhodamine B, Sulforhodamine B, and Rhodamine 110) were adsorbed on a water/heptane interface with the long axis of the xanthene ring being tilted about 70° to surface normal as revealed by a second harmonic generation technique.[55] Their results would support the present adsorption mode: mode-2. It is supposed that wobbling-cone like rotation and/or tumbling motions of SR101 around the axis shown in Scheme 3-2 take place within the thin interfacial layer. Such the adsorption model is favored for the explanation, since the τ_2^{rot} value is dependent on the viscosity of PE (Figure 3-12) as discussed below.

The characteristics of the water/PE interface are reflected on the η dependence of τ_2^{rot}. The first layer of the PE phase at the interface is expected to possess, more or less, an ordered structure, with the ester -COOR groups as a relatively hydrophilic part facing to the water phase while the phenyl ring and the alkyl chains as hydrophobic parts direct toward the PE phase (Scheme 3-2). For such a structure, the bulk viscosity of PE will not determine τ_2^{rot}. Even in bulk solutions, Kim and Jonas reported that the macroscopic and microscopic viscosities of the phthalate esters are governed strongly by the length of the alkyl chain as well as by the presence or absence of a branching group in the alkyl chain, and demonstrated important roles of the mobility of the alkyl chain in the medium viscosity.[26, 27] The mobility of the alkyl carbons increases as one moves away from the phenyl group of the molecule to the end of the chain, and the absence of the branching

group also increases the mobility. Therefore, the rotational reorientation time of SR101 (τ_2^{rot}) adsorbed on the water/PE interface is not governed by the bulk viscosity, but is influenced by the length of the alkyl chains of PE. When the alkyl chains of PE is long as in the case of DHP, the flexible alkyl chains of PE result in a faster rotational reorientation time relative to that predicted by the macroscopic viscosity. On the other hand, when the alkyl chains of the phthalate are short (i.e., DEP), the alkyl carbons are not flexible compared to the terminal alkyl groups in DHP, so that the rotational reorientation of SR101 at the interface is determined mainly by the macroscopic viscosity. If the motional flexibility of the alkyl chains of PE is important for determining τ_2^{rot}, the deviation between the observed τ_2^{rot} and that predicted from the bulk viscosity (solid line in Figure 3-12) increases with increasing the length of the alkyl chain and, thus, with increasing η. Phenomenologically, this is what is observed in Figure 3-12. In preliminary experiments, fluorescence dynamic anisotropy of perylene in bulk PE solutions was shown to be governed by the bulk viscosity. For discussion on fluorescence anisotropy data, the chemical structure of a probe molecule is important, so that a comparison of the present results with those on the perylene/bulk PE solution data might be difficult. Also, the models in Scheme 3-2 are speculative and needed a more detailed study including a molecular dynamic simulation. Nonetheless, the appearance of the two rotational reorientation times of SR101 and faster τ_2^{rot} at the interface compared to the prediction from the DSE theory would indicate the characteristic structure of the water/PE interface.

Conclusions

A study on a magic angle dependence of the TIR fluorescence decay profile of SR101 adsorbed on the water/PE interface was shown to be a potential means to discuss the thickness of the interfacial layer, and the two-dimensional interfacial model explained very well the present results. Thus, the water/PE interface was concluded to be very sharp in respect to molecular dimension of SR101: 10 - 14 Å. Furthermore, the observed rotational reorientation times (τ_1^{rot} and τ_2^{rot}) provided molecular-level information about both adsorption mode of SR101 on the interface and the structure of the interface (Scheme 3-2). So far, characteristics of a water/oil interface has been discussed in terms of the polarity, the density, and thermal capillary waves.[56-59] However, the interfacial viscosity at a water/oil interface has been rarely discussed except for the report by Wirth and Burbage.[45] In the present experiments, clear evidence for the η dependence of the rotational reorientation time at the water/PE interfaces was demonstrated. A further study including a molecular dynamic simulation will reveal detailed characteristics of a water/oil interface and its roles in separation sciences.

References and Notes

(1) Okumura, R.; Hinoue, T.; Watarai, H. *Anal. Sci.* **1996**, *12*, 393-397.

(2) Petrovic, M.; Barcelo, D. *Anal Chem.* **2000**, *72*, 4560-4567.

(3) Surakitbanharn, Y.; Muralidharan, S.; Freiser, H.; *Anal. Chem.* **1991**, *63*, 2642.

(4) Chen, F.; Ma, H.; Freiser, H.; Muralidharan, S. *Langmuir* **1995**, *11*, 3235.

(5) Starks, C.M.; Liotta, C.; *Phase Transfer Catalysis*; Academic Press: London, 1978.

(6) Demlow, E.V. and Demlov, S.S., *Phase Transfer Catalysis: 2nd revised edition*, Verlag Chemie, Weinheim, 1983.

(7) Cunnane, V.J.; Schiffrin, D.J.; Beltran, C.; Geblewicz, G.; Solomon, T. *J Electroanal. Chem.*, **1988**, *247*, 203

(8) Carter, S.P.; Freiser, H. *Anal. Chem.* **1979**, *51*, 1100.

(9) Watarai, H.; Cunningham, L.; Freiser, H. *Anal. Chem.* **1982**, *54*, 2390.

(10) Watarai, H.; Takahashi, M.; Shibata, K. *Bull. Chem. Soc. Jpn.* **1986**, *59*, 3469.

(11) Watarai, H. *Bunseki Kagaku* **1996**, *45*, 725-744.

(12) Watarai, H. *J. Chromatography* **1997**, *780*, 93-102.

(13) Shi, C.; Anson, F. C. *Anal. Chem.* **1998**, *70*, 3114–3118.

(14) Shao, Y.; Mirkin, M.V. *Anal. Chem.* **1998**, *70*, 3155–3161.

(15) Ma, M.; Cantwell, F.F. *Anal. Chem.* **1999**, *71*, 388–393.

(16) Rice, S.A.; Kenney-Wallace, G.A. *Chem. Phys.* **1980**, *47*, 161-170.

(17) Barkley, M.D.; Kowalczyk, A.A.; Brand, L. *J. Chem. Phys.* **1981**, *75*, 3581-3593.

(18) Waldeck, D.H.; Fleming, G.R. *J. Phys. Chem.* **1981**, *85*, 2614-2617.

(19) Dote, J.L.; Schwartz, R.N. *J. Phys. Chem.* **1981**, *85*, 3756-3758.

(20) Moog, R.S.; Ediger, M.D.; Boxer, S.G.; Fayer, M.D. *J. Phys. Chem.* **1982**, *86*, 4694-4700.

(21) Phillips, L.A.; Webb, S.P.; Yeh, S.W.; Clark, J.H. *J. Phys. Chem.* **1985**, *89*, 17-19.

(22) Christensen, R.L.; Drake, R.C; Phillips, D. *J. Phys. Chem.* **1986**, *90*, 5960-5967.

(23) Visser, A.J.W.G.; Arie van Hoek, K.V.; Santema, J.S. *J. Phys. Chem.* **1988**, *92*, 759-765.

(24) Flom, S.R.; Fendler, J.H. *J. Phys. Chem.* **1988**, *92*, 5908-5913.

(25) Jiang, Y.; Blanchard, G. J. *J. Phys. Chem.* **1994**, *98*, 6436-6440.

(26) Kim, Y. J.; Jonas, J. *J. Phys. Chem. A* **1998**, *102*, 2767.

(27) Kim, Y. J.; Jonas, J. *J. Phys. Chem. A* **1998**, *102*, 2778.

(28) Ishizaka, S.; Nakatani, K.; Habuchi, S.; Kitamura, N. *Anal. Chem.* **1999**, *71*, 419–426.

(29) Adamson, W.; " *Physical Chemistry of Surfaces* ", John Wiley and Sons, New York, 1990.

(30) Kakiuch, T.; Nakanisi, M.; Senda, M. *Bull. Chem. Soc. Jpn.* **1988**, *61*, 1845.

(31) Andreas, J.M.; Hauser, E.A.; Tucker, W.B. *J. Phys. Chem.***1938**, *42*, 1001-1019.

(32) Wirth, M.J.; Burbage, J.D, *Anal. Chem.* **1991**, *63*, 1311.

(33) Christensen, R.L.; Drake, R.C.; Phillips, D. *J. Phys. Chem.***1986**, *90*, 5960.

(34) Riddick, J. A.; Bunger, W. B. *Techniques of Chemistry: Organic Solvents*, Vol. II, Wiley-Interscience, New York, 1970.

(35) Wendlandt, W. WM.; Hecht, H.G. "*Reflectance Spectroscopy*", John Wiley and Sons, New York, 1966

(36) Masuhara, H.; De Schryver, F.C.; Kitamura, N.; Tamai, N.; "*Microchemistry; Spectroscopy and Chemistry in Small Domains*", North-Holland, Amsterdam, 1994.

(37) Benjamin, I. *J. Chem. Phys.* **1992**, *97*, 1432–1445.

(38) Benjamin, I. *Science* **1993**, *261*, 1558–1560.

(39) Michael, D.; Benjamin, I. *J. Phys. Chem.* **1995**, *99*, 1530–1536.

(40) Schweighofer, K. J.; Benjamin, I. *J. Phys. Chem.* **1995**, *99*, 9974–9985.

(41) Michael, D.; Benjamin, I. *J. Phys. Chem.* **1995**, *99*, 16810–16813.

(42) Michael, D.; Benjamin, I. *J. Chem. Phys.* **1997**, *107*, 5684–5693.

(43) Nakatani, K.; Ishizaka, S.; Kitamura, N. *Anal. Sci.* **1996**, *12*, 701-705.

(44) O'Connor, D.V.; Phillips, D. "*Time-Correlated Single Photon Counting*"; Academic Press: New York, 1986.

(45) Wirth, M.J.; Burbage, J.D, *J. Phys. Chem.* **1992**, *96*, 9022.

(46) Moog, R. S.; Ediger, M. D.; Boxer, S. G.; Fayer, M. D. *J. Phys. Chem.* **1982**, *86*, 4694.

(47) Rice, S. A.; Kenney-Wallace, G. A. *Chem. Phys.* **1980**, *47*, 161.

(48) Volkov, A.G.; Deamer, D.W., Eds. *Liquid-Liquid interfaces*; CRC Press: Boca Raton, FL, 1996.

(49) Scully, A. D.; Matsumoto, A.; Hirayama, S. *Chem. Phys.* **1991**, *157*, 253.

(50) Buff, F.P.; Lovett, R.A.; Stillinger, Jr. F.H. *Phys. Rev. Lett.* **1965**, *15*, 621-623.

(51) Braslau, A.; Pershan, P.S.; Swislow, G.; Ocko, B.M.; Als-Nielsen, J. *Phys. Rev. A* **1988**, 38, 2457-.2470

(52) Pershan, P.S. *Faraday Discuss. Chem. Soc.* **1990**, *89*, 231-245.

(53) Simpson, G. J.; Rowlen, K. L. *Chem. Phys. Lett.* **1999**, *309*, 117-122.

(54) Lamb, H. *Hydrodynamics*, 6th ed.; Dover: New York, 1945.

(55) Uchida, T.; Yamaguchi, A.; Ina, T.; Teramae, N. *Annual Meeting of the Japan Society for Analytical Chemistry, Abstract 2A02*, **1998**, 10.6 - 10.8, Gifu University.

(56) Perera, J. M.; Stevens, G. W.; Grieser, F. *Colloids Surf. A* **1995**, *95*, 185–192.

(57) Bessho, K.; Uchida, T.; Yamauchi, A.; Shioya, T.; Teramae, N. *Chem. Phys. Lett.* **1997**, *264*, 381–386.

(58) Wang, H.; Borguet, E.; Eisenthal, K. B. *J. Phys. Chem. B* **1998**, *102*, 4927–4932.

(59) Tsuyumoto, I; Noguchi, N.; Kitamori, T.; Sawada, T. *J. Phys. Chem. B* **1998**, *102*, 2684.

Chapter 4

Excitation Energy Transfer from Sulforhodamine 101 to Acid Blue 1 at a Liquid/Liquid Interface: Experimental Approach to Estimate Interfacial Roughness.

4.1 Introduction

In the previous chapters, dimer formations of PSA and fluorescence dynamic anisotropy of SR101 under TIR conditions were shown to be highly potential to study characteristics of water/oil interfaces.[1, 2] These approaches are certainly sensitive to the microstructures and the dynamic motions of a solute at the interface. Nonetheless, chemical and physical properties at a liquid/liquid interface would be governed by various factors, another experimental approaches other than those described in Chapter 2 and 3 should be also explored. In this study, therefore, dipole-dipole (Förster-type) excitation energy transfer between an energy donor (D) and an acceptor (A) both adsorbed on a liquid/liquid interface was introduced to study a water/oil interface.[3] An idea of the experiments is as follows.

When diffusional motions of D and A are inhibited as in the case for strong binding of the molecules to the surface by adsorption, excitation energy transfer quenching dynamics of D by A reflects structural dimension around D and A through spatial distributions of the components.[4, 5] In such a case, fluorescence dynamics of D ($I_D(t)$) should obey the following equation as reported by Klafter and Blumen,[4, 5]

$$I_D(t) = A\exp\left(-(t/\tau_D) - P(t/\tau_D)^{\bar{d}/6}\right) \tag{4.1}$$

where A is a pre-exponential factor and τ_D is the excited state lifetime of D without A. P is a parameter proportional to the probability that A resides within the critical energy transfer distance (R_0) of the excited donor. $\bar{d}$ is called fractal dimension and reflects a spatial distribution of the acceptor around the donor. Therefore, a study on excitation energy transfer dynamics provides invaluable information about the characteristics at a

liquid/liquid interface, along with a complementary study on the same system by fluorescence dynamic anisotropy.

In this study, experiments are focused on water/carbon tetrachloride (CCl_4) and water/1,2-dichloroethane (DCE) interfaces. So far, water/CCl_4 and water/DCE interfaces have been studied by various techniques, and it has been reported that the water/CCl_4 and water/DCE interfaces are very thin: the thickness ~1 nm.[6-12] Furthermore, molecular dynamics simulations reported by Michael and Benjamin indicate that the water/DCE interface is thick and rough compared to the water/CCl_4 interface.[11] Molecular dynamics simulations give molecular-level insight about a liquid/liquid interface and are the indispensable basis for understanding the characteristics at the interface. Nonetheless, complementary studies by experiments are absolutely necessary. Therefore, the present idea was tested to elucidate the structures of water/CCl_4 and water/DCE interfaces, and explored to compare the results with those predicted by molecular dynamics simulations. In the following, fluorescence dynamic anisotropy and excitation energy transfer quenching of Sulforhodamine 101 (SR101) at water/CCl_4 and water/DCE interfaces are discussed, with special references to elucidating thickness and/or roughness of the interface.[13]

4.2 Experimental

Chemicals and Sample Preparation

Carbon tetrachloride (Kanto Chemical Co., Inc.) was purified by distillation after washing successively with an aqueous potassium hydroxide solution and water. 1,2-Dichloroethane (DCE; MERCK, Uvasol) and Sulforhodamine 101 (SR101; ACROS ORGANICS, Laser grade) were used without further purification. Acid Blue 1 (AB1; Tokyo Kasei Kogyo Co., Inc) was purified by recrystallizations from an acetone-water mixture. The chemical structures of SR101 and AB1 are inserted in Figure 4-2.

For dynamic anisotropy experiments, an aqueous SR101 solution (concentration [SR101]=1.0 × 10^{-9} M) saturated with CCl_4 or DCE was poured carefully onto water-saturated carbon tetrachloride or DCE in a Pyrex cell (inner diameter = 40 mm). As a sample for excitatin energy transfer measurements, a mixture of SR101 (1.0 × 10^{-9} M) and AB1 (1.9 ~ 5.7 × 10^{-9} M) was used as a water phase and a water/oil interface was constructed by the analogous procedures with those mentioned above. Spectroscopic measurements were carried out after the sample solution in the cell being kept standing over 100 min.

Measurements

TIR fluorescence decay profiles of SR101 were measured by the system described in Chapter 3. The steady-state absorption and fluorescence spectra were measured by using Hitachi U-3300 and Hitachi F-4500 spectrometers, respectively. All experiments were conducted at room temperature (~23 ˚C).

4.3 Results and Discussion

4.3.1 A Magic-Angle Dependence of the TIR Fluorescence Decay Profiles of SR101 at the Water/Oil Interfaces

Before describing the results on excitation energy transfer quenching of SR101 by AB1 at water/CCl_4 and water/DCE interfaces, a magic angle dependence of the total-internal reflection (TIR) fluorescence decay profile of SR101 at the interface is worth discussing. The studies are quite important to compare the results with those by excitation energy transfer quenching, as discussed later in detail.

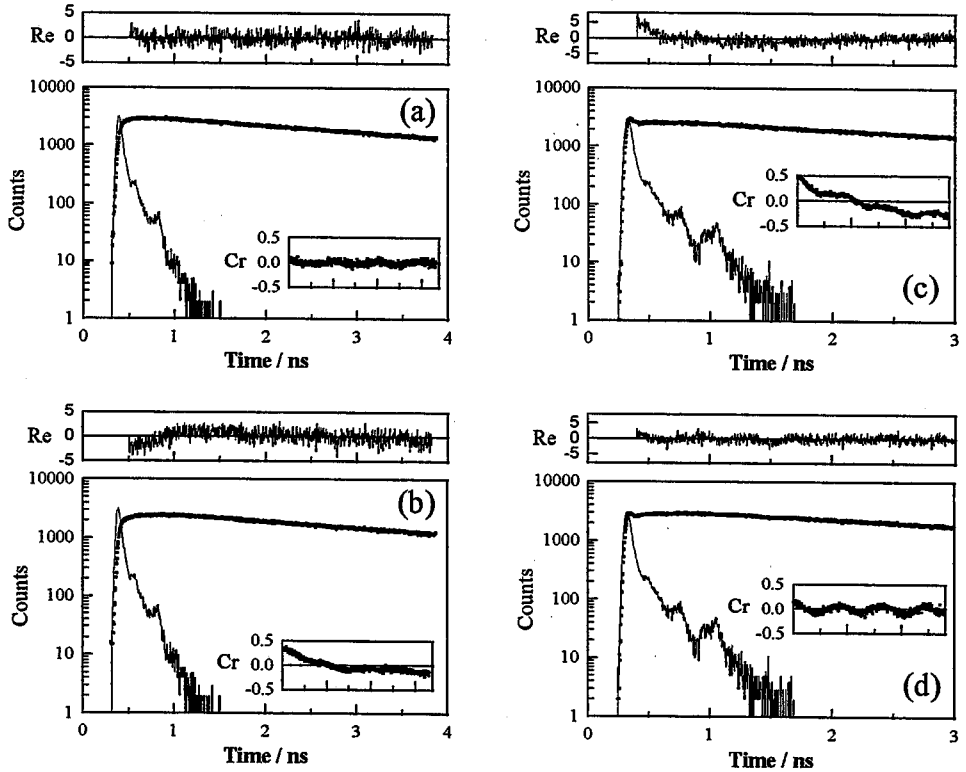

Figure 4-1 TIR fluorescence decay curves of SR101 at water/CCl_4 ((a) and (b)) and water/DCE ((c) and (d)) interfaces. The angle of the emission polarizer was set at 45° ((a) and (c)) or 54.7° ((b) and (d)) in respect to the direction of excitation polarization. The upper trace and the inner panel of each figure represent the plots of the weighted residuals (*Re*) and the autocorelation trace (*Cr*) for a single-exponential fitting, respectively.

Table 4-1. Fluorescence Decay Parameters of SR101 Adsorbed on Water/Oil Interfaces Observed under the TIR Conditions and in an Aqueous Solution.

		τ / ns	$\chi^{2\,a}$	DW[a]
water/CCl_4	45° [b]	4.06 ± 0.02	1.11	1.88
	54.7° [b]	4.21 ± 0.03	1.61	1.37
water/DCE	45° [b]	3.62 ± 0.02	2.28	0.90
	54.7° [b]	4.12 ± 0.03	1.09	1.73
aq[c]		4.12 ± 0.01	1.16	1.94

a) χ^2 and DW represent the χ^2 and Darbin-Watson parameters for the fitting, respectively.

b) The angle of the emission polarizer in respect to that of the excitation laser beam.

c) Determined in an aqueous SR101 solution ([SR101] = 1.7×10^{-7} M).

Figure 4-1 shows fluorescence decay profiles of SR101 observed from water/CCl_4 and water/DCE interfaces at an emission polarization angle of 45° ((a) and (c)) or 54.7° ((b) and (d)), together with the relevant weighted residuals (*Re*) and autocorelation trace (*Cr*) for each single-exponential fit. In the case of the water/CCl_4 interface ((a) and (b)), *Re* and *Cr* of the data observed at 54.7° exhibited nonrandom distributions compared to those predicted by the best fit (b), particularly, those in the initial stage of excitation (<1 ns).

Contrary, the profile observed at the magic angle 45° was reasonably fitted by a single exponential function as judged by the relevant *Re* and *Cr* (a).[14] The χ^2 and Durbin-Watson (DW) parameters for the fitting also support that the best fit of the observed data by a single-exponential function is attained by setting an emission polarizer at the magic angle, 45° (Table 4-1). Therefore, it is concluded that the water/CCl_4 interface was sharp with respect to the molecular size of SR101 and, three-dimensional rotational motions of SR101 were inhibited at the water/CCl_4 interface.

In the case of a water/DCE interface ((c) and (d)), on the other hand, a fitting of the data by a single exponential function cannot be attained by setting an emission polarizer at 45° as confirmed by deviations of *Re* and *Cr* from the optimum values (c). When the

fluorescence decay profile is measured by setting an emission polarizer at 54.7° (d), fluorescence anisotropy can be reasonably fitted by a single exponential function including the time response in the initial stage of excitation (see also χ^2 and DW in Table 4-1). Therefore, the interfacial layer of the water/DCE interface is thick compared to the molecular size of SR101, and the dye molecules adsorbed on the interface are weakly oriented. Otherwise, the interface is spatially rough at the molecular size of SR101. An orientational distribution of SR101 at the interface might also influence the fluorescence dynamics. Irrespective of the reason, however, SR101 molecules at the water/DCE interface behave similar to those in an isotropic medium in contrasting to the results at the water/CCl_4 interface.

4.3.2 Excitation Energy Transfer and Its Dynamics at the Interface.

Although both water/CCl_4 and water/DCE interfaces are believed to be sharp, the fluorescence dynamic anisotropy study suggested that the structure of the interface was different with each other. In order to obtain more detailed information, therefore, excitation energy transfer quenching of SR101 by AB1 at the interface was explored.

Figure 4-2 shows the fluorescence and absorption spectra of SR101 (donor) and AB1 (acceptor) in water, respectively. As seen in Figure 4-2, since the fluorescence spectrum of SR101 overlaps with the absorption spectrum of AB1, effective excitation energy transfer from SR101 to AB1 is expected. In the present case, energy transfer between the excited singlet state of SR101 and AB1 proceeds via a Förster-type mechanism,[3] so that the energy transfer efficiency can be estimated by the following equation.

$$R_0^{\,6} = \frac{9000\ln(10)\kappa^2\phi_0}{128\pi^5 n^4 N_A}\int_0^{\infty}\frac{F_D(\upsilon)\varepsilon_A(\upsilon)}{\upsilon^4}\mathrm{d}\upsilon \qquad (4.2)$$

In eq 4.2, R_0 is the critical energy transfer distance and κ^2 is an orientational factor for energy transfer (usually assumed to be 2/3). ϕ_0 is the fluorescence quantum yield of the donor in the absence of an acceptor and n is the refractive index of the medium. N_A, $F_D(\nu)$ and $\varepsilon_A(\nu)$ are the Avogadro's number, the spectral distribution of the fluorescence in quanta normalized to unity, and the molar absorptivity of AB1 at each wavenumber ν, respectively. According to eq 4.2, R_0 in water is calculated to be 71 Å,[15] indicating that efficient excitation energy transfer from SR101 to AB1 should occur. Therefore, on the basis of analysis of fluorescence decay curves of SR101 at the water/oil interface in the presence of AB1, the structure of the water/oil interface could be estimated with the spatial resolution being in the order of R_0.

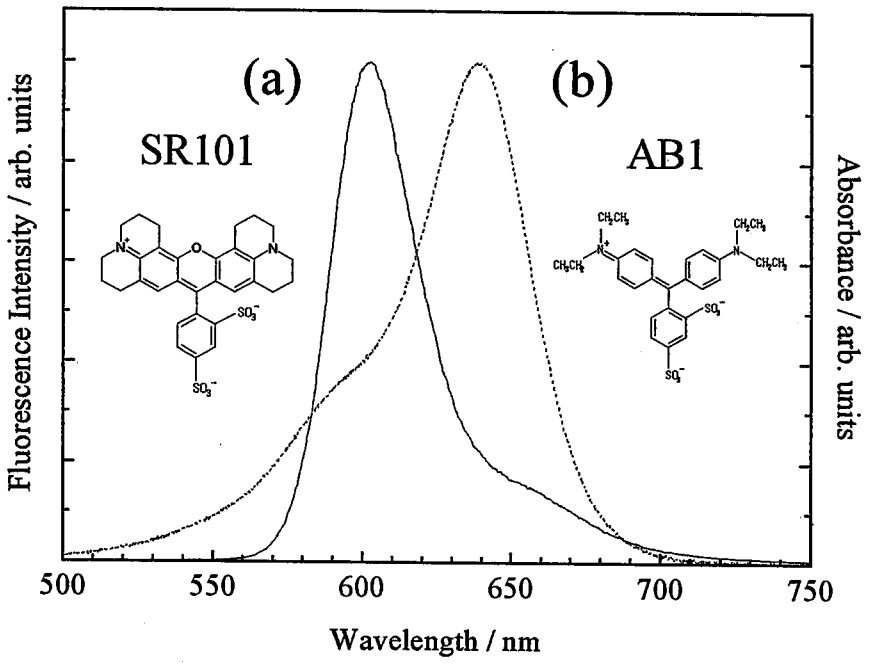

Figure 4-2 Fluorescence spectrum of SR101 (a) and absorption spectrum of AB1 (b) in water.

Figure 4-3 shows the fluorescence decay curves of SR101 at a water/CCl_4 interface in the absence ((a)) and presence of AB1 (1.91, 3.82, and 5.73 × 10^{-9} M for (b), (c) and (d), respectively). Analogous results were obtained for the water/DCE system and, data are shown in Figure 4-4. In the absence of AB1, the fluorescence decay of SR101 was fitted satisfactorily by a single-exponential function with the decay time of 4.06 ns. In the presence of the acceptor, on the other hand, the fluorescence exhibited a non-single exponential decay.

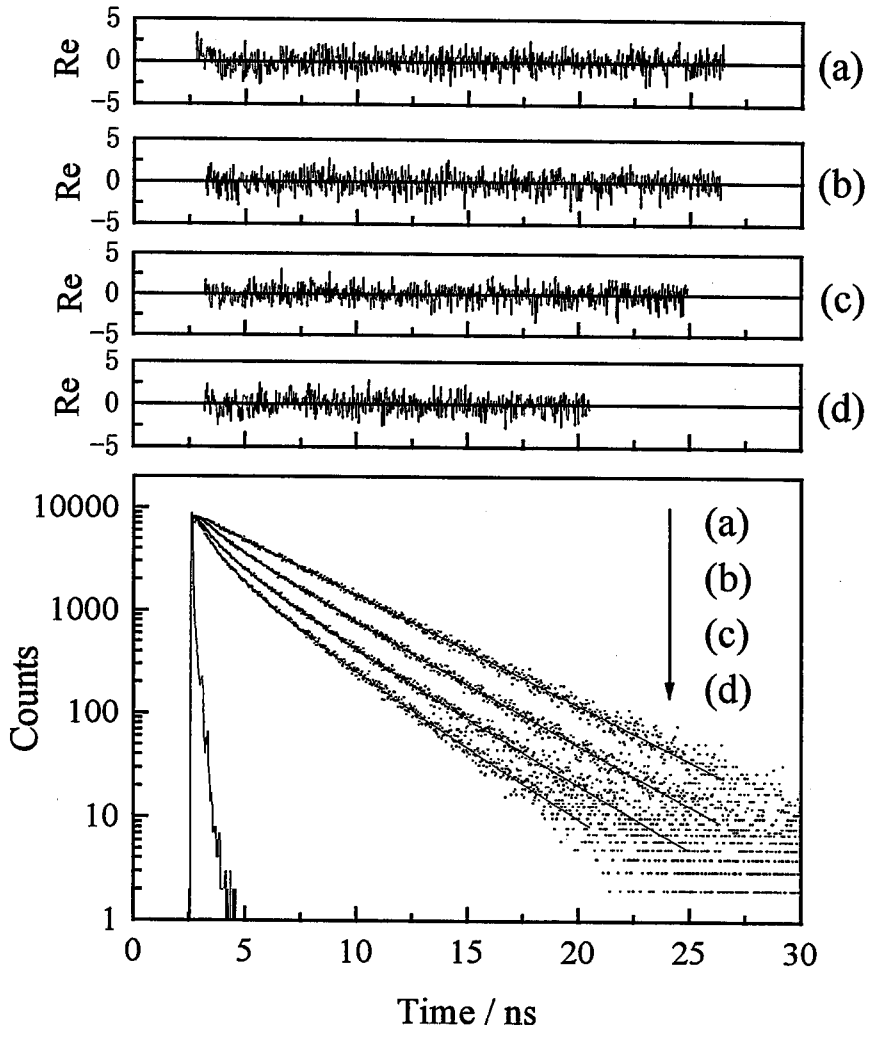

Figure 4-3 Fluorescence decay profiles of SR101 at a water/CCl_4 interface in the absence and presence of AB1: (a) [AB1] = 0, (b) 1.91 × 10^{-9}, (c) 3.82 × 10^{-9}, (d) 5.73 × 10^{-9} M. The solid curve shows the best fit by eq 4.3, and the fitting parameters are listed in Table 4.2.

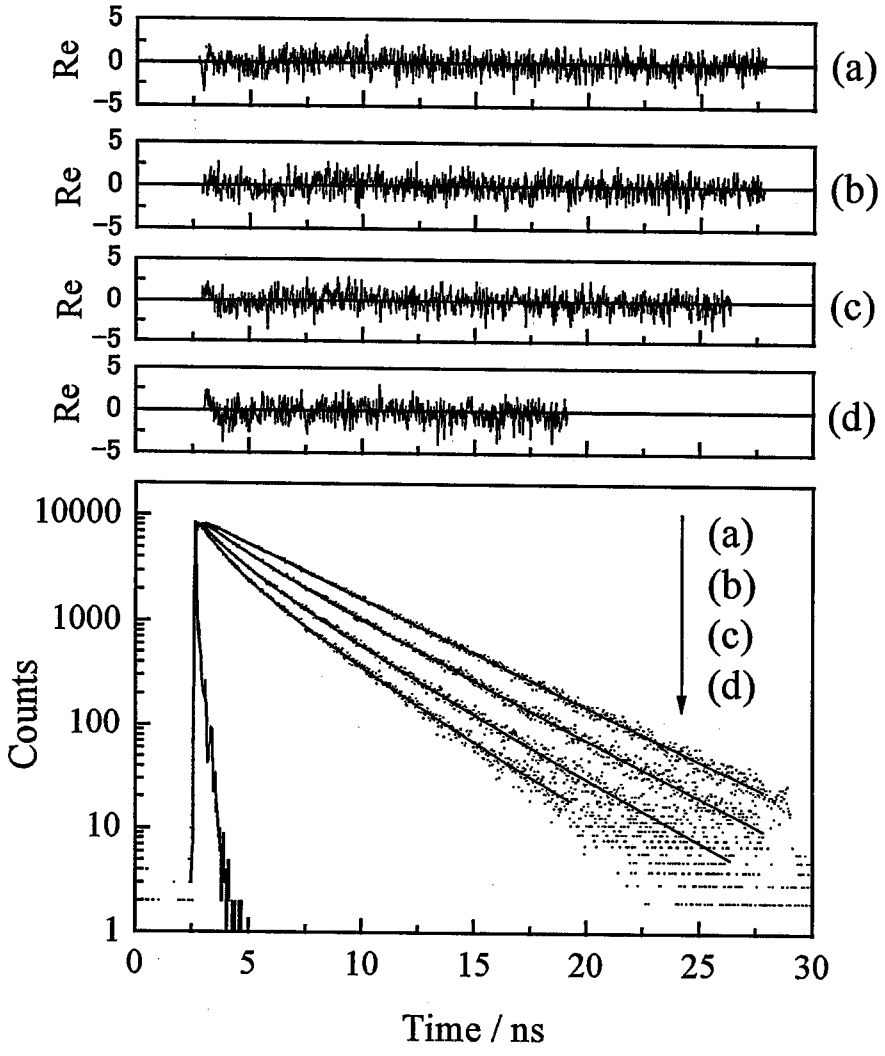

Figure 4-4 Fluorescence decay profiles of SR101 at a water/DCE interface in the absence and presence of AB1: (a) [AB1] = 0, (b) 1.91×10^{-9}, (c) 3.82×10^{-9}, (d) 5.73×10^{-9} M. The solid curve shows the best fit by eq 4.3, and the fitting parameters are listed in Table 4.2.

For energy transfer dynamics in fixed geometries of both energy donor and acceptor, the fluorescence decay profile of the donor cannot be expressed by a single exponential function, but should be analyzed by a Klafter-Blumen equation (eq 4.1) as demonstrated for that in various inhomogeneous systems.[4, 5, 18-27] In eq 1, $\bar{d}$ is the structural (fractal)

dimension as described before and, in the present case, this reflects the spatial distribution of AB1 around SR101 at a water/CCl_4 or water/DCE interface. P is the term related to the AB1 concentration at the water/oil interface, which is defined by eq 4.3.

$$P = \theta_A (d/\bar{d}) \Gamma (1 - \bar{d}/6)(R_0/a)^{\bar{d}} \tag{4.3}$$

In eq 4.3, θ_A is the degree of interfacial coverage of AB1 and d is an Euclidean dimension (2, in the case of surface adsorption). a is the effective radius of SR101 (7 Å). Simulations of the observed decay profiles in Figures 4-3 and 4-4 were then performed on the basis of eq 4.1 with τ_D being fixed at 4.06 and 4.21 ns, respectively. The parameters obtained by the simulation, P and $\bar{d}$, are summarized in Table 4-2, together with the χ^2 parameters of the fittings. The χ^2 parameters and the weighted residuals (*Re*) of the fittings, shown in the upper traces of Figures 4-3 and 4-4, indicate that the fluorescence decay profiles of SR101 are well fitted by eq 4.1.

Although statistical validity of the fitting can be judged by χ^2 and *Re*, the application of the Klafter-Blumen equation to the decay profile analysis is not necessarily warranted and worth checking in detail. First, the Klafter-Blumen model requires that the fluorescence decay profiles observed at different AB1 concentrations should be fitted by a common $\bar{d}$ value. As shown in Table 4-2, this requirement is safely satisfied; the $\bar{d}$ value for the water/CCl_4 or water/DCE system was 1.86-2.00 or 2.45-2.53, respectively, which were within the experimental errors.

Table 4-2. Structural Dimension Analysis of Excitation Energy Transfer Quenching of SR101 by AB1 at the Water/Oil Interfaces.

	[AB1] / 10^{-9} M	P	$\bar{d}$	χ^2
Water/CCl_4	1.91	0.82	1.86	1.06
	3.82	1.46	1.94	1.00
	5.73	1.97	2.00	1.01
Water/DCE	1.91	0.50	2.47	1.05
	3.82	1.06	2.45	1.05
	5.73	1.40	2.53	1.15

According to eq 4.3, second, the P value obtained by the fitting should increase linearly with an increase in the degree of interfacial coverage (θ_A) of AB1 on the water/oil interface. In order to estimate θ_A, therefore, interfacial tension (γ) measurements were conducted. The relationship between γ and log [AB1] determined for a water/CCl_4 or water/DCE system is shown in Figure 4-5. It is clear from Figure 4-5 that the γ value decreases with increasing [AB1] in the range of 10^{-7} ~ 10^{-6} M. This behavior is quite analogous to a concentration dependence of γ for a typical surfactant. The [AB1] dependence of γ was thus analyzed by the Gibbs equation and the Langmuir isotherm. The interfacial excess (Γ_i) of a solute (AB1) is defined by the Gibbs equation,

$$\Gamma_i = -\frac{1}{RT}\frac{\partial\gamma}{\partial \ln[\mathrm{AB1}]} \tag{4.4}$$

where R and T have their usual meanings. According to the Langmuir isotherm, on the other hand, the interfacial concentration of AB1 (C_i) is given by,

$$C_i = \frac{a'K'[\mathrm{AB1}]}{a'+K'[\mathrm{AB1}]} \tag{4.5}$$

where a' and K' are the saturated amount of adsorbed AB1 on the interface and the adsorption equilibrium constant of AB1 between the interface and the water phase at infinite dilution, respectively. Under the approximation of $\Gamma_i = C_i$, eqs 4.4 and 4.5 afford eq 4.6,[28]

$$\gamma = \gamma_0 - a'RT\ln\left(1+\frac{K'[\mathrm{AB1}]}{a'}\right) \tag{4.6}$$

where γ_0 is the interfacial tension at [AB1] = 0. A simulation of the data in Figure 4-5 was then performed by using eq 4.6 with a' and K' as variable parameters. The results of the fits are shown by the solid curves in Figure 4-5 and, the parameters, a' and K', are

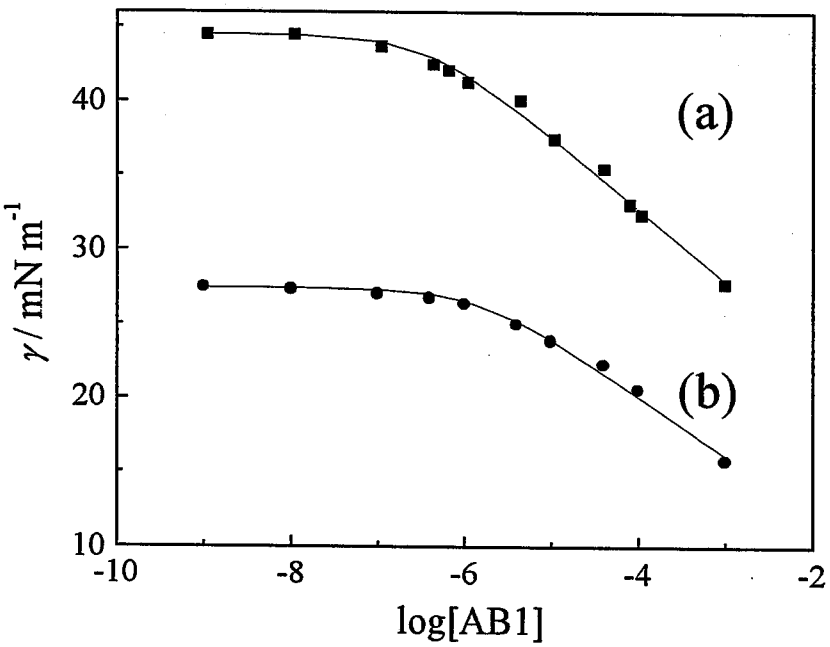

Figure 4-5 AB1 concentration dependence of the interfacial tension in water/CCl_4 (a) and water/DCE (b) systems.

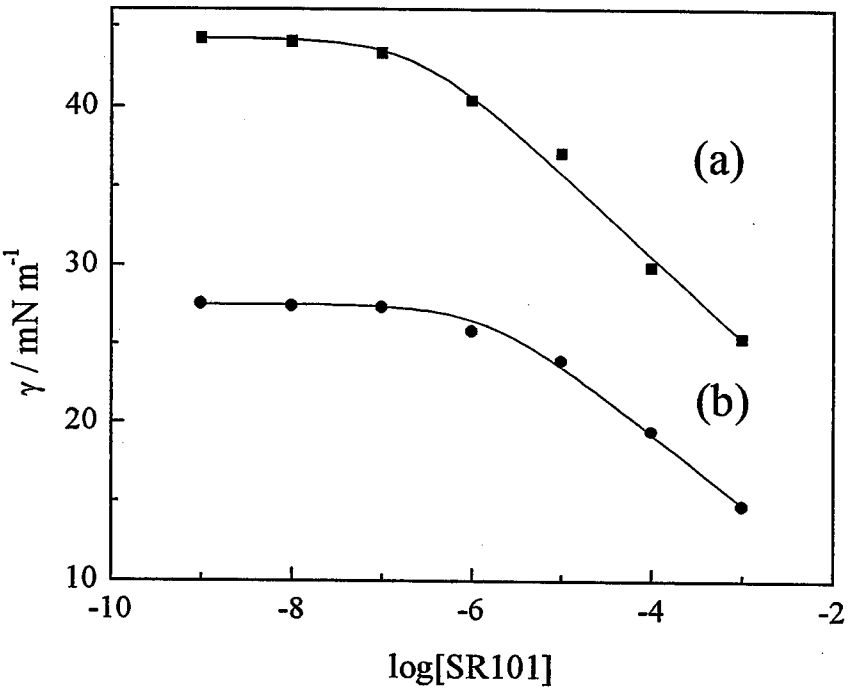

Figure 4-6 SR101 concentration dependence of the interfacial tension in water/CCl_4 (a) and water/DCE (b) systems.

Table 4-3. Parameters for Interfacial Adsorption of AB1

	a' / mol cm^{-2}	K' / m
Water/CCl_4	8.6×10^{-11}	2.3×10^{-3}
Water/DCE	7.2×10^{-11}	4.5×10^{-4}

Table 4-4. Parameters for Interfacial Adsorption of SR101

	a' / mol cm^{-2}	K' / m
Water/CCl_4	9.6×10^{-11}	2.9×10^{-3}
Water/DCE	7.6×10^{-11}	5.3×10^{-4}

summarized in Table 4-3. On the basis of these parameters and eq 4.6, C_i and θ_A at each AB1 concentration were calculated, as the results were included in Table 4-5. The relationship between P and θ_A thus obtained is shown in Figure 4-7. It is worth noting that the P value increases linearly with an increase in θ_A for both cases. The results demonstrate explicitly that the Klafter-Blumen model in eqs 4.1 and 4.3 is applicable to the present system. Furthermore, the dye concentration adsorbed on the interface is very low (interfacial coverage of AB1: 0.12 ~ 1.51% shown in Table 4-4, SR101: 0.06 ~ 0.29% data are shown in Figure 4-6 and the fitting parameters are summarized in Table 4-4) so that the interfacial structure is not influenced appreciably by the dye adsorption. Therefore, the variation of the $\bar{d}$ value with the nature of the oil (Table 4-2) is meaningful and worth discussing in detail.

The results in Figure 4-7 also provide information about the critical energy transfer distance between SR101 and AB1 at the water/oil interface. Knowing d, $\bar{d}$, and a, one can calculate the R_0 value on the basis of the slope value of the plot in Figure 4-7 and eq 4.3. Actually, the R_0 value at the water/CCl_4 or water/DCE interface was calculated to be 75 or 74 Å, respectively. These R_0 values are comparable to that (71 Å) estimated from eq 4.2. This also supports validity of the present analysis of the dynamic data by the Klafter-Blumen model in eq 4.1.

Table 4-5. Interfacial Coverage θ_A of AB1 on the Water/Oil Interfaces and P Parameters

	C / M [a]	C_i / mol cm^{-2}	θ_A [b]	P
Water/CCl_4	1.91×10^{-9}	4.4×10^{-13}	5.1×10^{-3}	0.82
	3.82×10^{-9}	8.7×10^{-13}	1.0×10^{-2}	1.46
	5.73×10^{-9}	1.3×10^{-12}	1.5×10^{-2}	1.97
Water/DCE	1.91×10^{-9}	8.6×10^{-14}	1.2×10^{-3}	0.50
	3.82×10^{-9}	1.7×10^{-13}	2.4×10^{-3}	1.06
	5.73×10^{-9}	2.6×10^{-13}	3.6×10^{-3}	1.45

a) The concentration of AB1 in an aqueous phase.

b) Interfacial coverage defined by $\theta_A = C_i / a'$ (saturated concentration on the interface; see also Table 4-3).

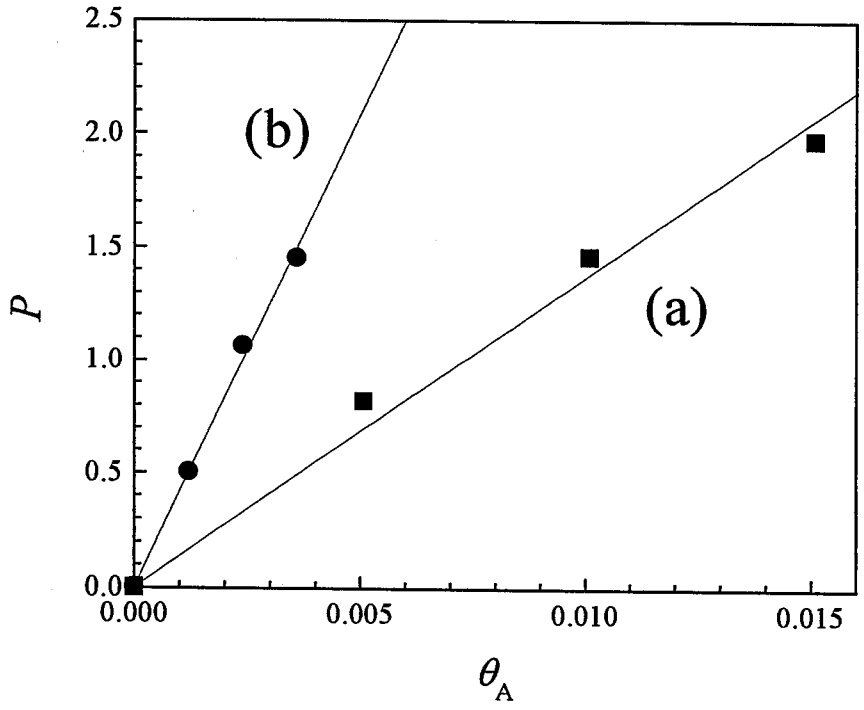

Figure 4-7 Relationship between P and θ_t, for water/CCl_4 (a) and water/DCE systems (b). The solid curve represents the best fit by using eq 4.3.

4.3.3 *Structural Dimension of Energy Transfer at the Water/Oil Interface*

The structural dimension for energy transfer at the water/CCl_4 or water/DCE interface (Table 4-2) was 1.86 ~ 2.00 (average, 1.93) or 2.45 ~ 2.53 (2.48), respectively. The present Klafter-Blumen analysis of the data is very meaningful as described above, so that structural characteristics of the interface should be reflected on the $\bar{d}$ value. The $\bar{d}$ value for the water/CCl_4 interface (1.93) indicates that the interface is sharp and regarded as two-dimension, as long as the spatial resolution by the energy transfer quenching method (~ 70 Å or ~ 7 nm). Phenomenologically, the result agrees well with that derived from fluorescence dynamic anisotropy measurements; the interface is thin enough to inhibit three-dimensional rotational motions of SR101. If the interface is thin enough and modeled strictly by two-dimension, however, the structural dimension should be equal to 2.0 since energy transfer quenching is restricted in the X-Y plane of the interface. A $\bar{d}$ value smaller than 2.0 has been frequently reported for the interfacial systems such as vesicles and Langmuir-Blodgett films, and $\bar{d} < 2.0$ in these systems has been discussed in terms of a non-uniform distribution of an energy acceptor at the interface: fractal structure.[15, 16] Therefore, a fractal-like distribution of AB1 at the water/CCl_4 interface might play a role in deciding the $\bar{d}$ value.

On the other hand, the structural dimension determined for the water/DCE interface was larger than 2.0: 2.48. This suggests that the water/DCE interface is thicker than the water/CCl_4 interface. The fluorescence dynamic anisotropy measurements also gave analogous results; the interface is thick enough to allow three-dimensional rotational motions of SR101. It should be noted that these results do not necessarily imply that the water/DCE interface is characterized by a three-dimensional space. Taking the results obtained by molecular dynamics simulations into account, it is supposed that the

water/DCE interface is thin, but is rough in respect to the spatial resolution by the energy transfer quenching method as discussed in the following section.

4.3.4 Structures of the Water/CCl_4 and Water/DCE Interfaces

A water/CCl_4 or water/DCE interface is a representative system studied by various techniques and, so far, invaluable information about the structure of the interface has been accumulated.[6-12]. As an example, Benjamin and his co-workers have reported the structures of water/CCl_4 and water/DCE interfaces on the basis of molecular dynamics computer simulations, and demonstrated that a water/DCE interface is molecularly sharp; there is no-mixed solvent layer between the two phases.[6, 7, 9, 11] However, they have also pointed out that the physical property of the interface is characterized by thermally capillary waves generated at the sharp interface and, the interface is quite rough at a short time scale.[7, 29] According to their calculations, namely, the capillaries with the amplitude as short as 0.8 nm are constantly moving at the interface and these protrude into the DCE phase on the time scale of tens of picoseconds. However, the long time average (hundreds of picoseconds) of the interface results in a relatively smooth density profile that gives rise to the interface thickness of about 1 nm. Molecular dynamics simulations and interfacial tension measurements have also demonstrated that the water/CCl_4 interface is thinner than the water/DCE interface and, the thickness of the water/CCl_4 interface has been reported to be <1 nm.[11]

In the present study, both fluorescence dynamic anisotropy and excitation energy transfer methods were successful to provide information about the structures and thickness/roughness of the water/CCl_4 and water/DCE interfaces. Therefore, the present

results are worth comparing with the available information described above. However, it should be noted that, although the results obtained by the present two methods are complementary to discuss the structures of the interfaces, these cannot be compared directly with each other, since fluorescence dynamic anisotropy provides information about molecular level structures of the interface (i.e., dimension of the molecular size of SR101 ~ 1 nm) while the excitation energy transfer method affords relatively long-range interfacial structures (i.e., dimension of the critical energy transfer distance ~ 7 nm). On the basis of such experimental backgrounds, following discussions could be made.

The thickness of the water/DCE interface (1 nm) is comparable to the molecular size of SR101 (1.0 ~ 1.4 nm).[2] Furthermore, SR101 molecules adsorbed on the water/DCE interface are supposed to be restricted within the two-dimensional plane, with the hydrophilic SO_3^- group being towards to the water phase while the hydrophobic xanthene ring being directed to the DCE phase.[2] Therefore, when the water/DCE interface is very sharp, three-dimensional-like rotational reorientation of SR101 would not be observed, in contrast to our experimental observation. One possible reason for this is thermal fluctuations of the interface, by which SR101 molecules behave similar to those in an isotropic medium: SR101 sit on the interface is tumbled by thermal fluctuations. Similar situations are also expected for SR101 at the water/CCl_4 interface, while the dynamic anisotropy experiments suggest that the interface is a two-dimensional-like. It has been reported that thermal capillary waves at an interface are related to the interfacial tension of the system.[30-33] In the present systems, the lower interfacial tension of the water/DCE system compared to that at the water/CCl_4 interface (infinite dilution limit of the data in Fig 4-4) indicates that the amplitude(s) of the surface wave(s) is larger for the water/DCE system relative to that for the water/CCl_4 interface. This prediction agrees with the results by the computer simulations as described above; the thickness of the

water/DCE or water/CCl_4 interface is 1 nm or < 1 nm, respectively. Thus, the contribution of the thermal capillary waves to the rotational motions of SR101 would be smaller at the water/CCl_4 interface, leading to a two-dimensional-like anisotropy decay of the dye at the interface. Furthermore, the adsorption equilibrium constant (K') of SR101 measured at the water/CCl_4 interface ($K' = 2.93 \times 10^{-3}$ m) is larger than that at the water/DCE interface ($K' = 5.27 \times 10^{-4}$ m). Therefore, relatively strong adsorption of SR101 on the water/CCl_4 interface also makes the rotational motions of the dye two-dimensional-like.

Short-range (~1 nm) structural information about the interface obtained by fluorescence dynamic anisotropy experiments is not contradicted from the results by the excitation energy transfer method: $\bar{d}$ (water/CCl_4) = 1.93 and $\bar{d}$ (water/DCE) = 2.48. Energy transfer at a liquid/liquid interface is schematically shown in Scheme 4-1. For simplicity, it is assumed here that an SR101 molecule (closed circle) sits on the interface (X-Y plane). The molecular size of SR101 is 1.4 nm and the critical energy transfer

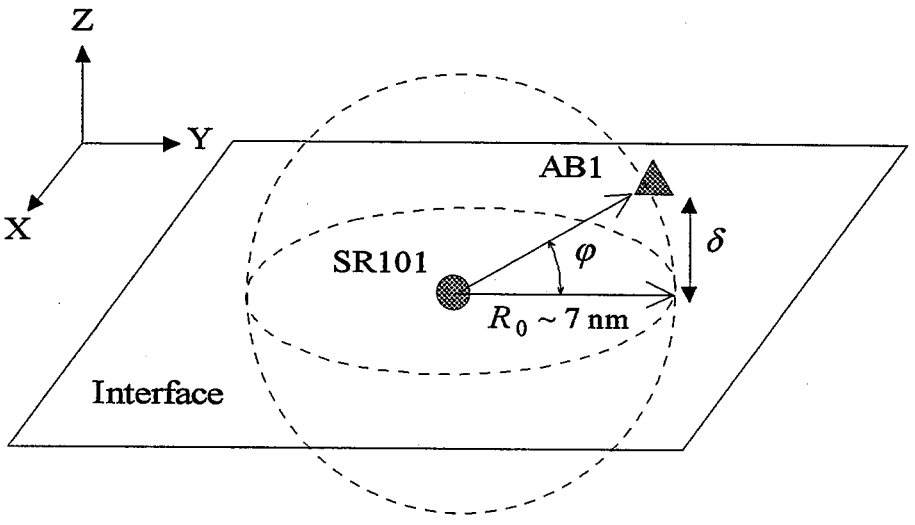

Scheme 4-1

distance is ~7 nm, so that energy transfer proceeds at a long distance. When both SR101 and AB1 are located at a flat interface, the structural dimension of energy transfer should be exactly 2.0. If the interface is rough and AB1 (closed triangle in Scheme 4-1) is displaced from the X-Y plane, on the other hand, the angle between the positions of the SR101 and AB1 molecules along the Z axis (φ in Scheme 4-1) determines the $\bar{d}$ value. Clearly, when the displacement along the Z axis (δ) is very small, $\bar{d}$ is 2.0. An increase in δ implies that the interface becomes more rough, and thus, $\bar{d}$ increases to 3.0. Since SR101 at the water/DCE interface exhibits three-dimensional-like motions and the interface has been suggested to be more rough compared to the water/CCl_4 interface. Therefore, the structural dimension of the water/DCE interface ($\bar{d}$ = 2.48) will be a reasonable consequence, reflecting the characteristic structure of the interface.

In the present experiments, the size of the probe molecule used (~1.4 nm) is comparable to the thickness of the water/CCl_4 or water/DCE interface (~1 nm), so that one cannot estimate the thickness of the interface. A smaller probe molecule should be employed for further discussion on this problem. Nonetheless, the present results indicate that the water/DCE interface is more rough compared to the water/CCl_4 interface. The results agree with those predicted by molecular dynamics simulations.

Although the structural difference between the water/CCl_4 and water/DCE interfaces is not so large, the chemical and/or physical nature of the organic phase itself is reflected on the photophysical properties of a probe molecule, indicating novelty of the present experimental approaches. The simplest way to understand the difference in the interfacial structure will be to consider the difference in the interfacial tension. In terms of thermodynamics, an interfacial tension in a water/oil system is closely related to miscibility of water in an oil (vide infra).[34] As shown in Figure 4-4, the interfacial tension (free energy) in the water/CCl_4 system (44.5 mN m^{-1} (mJ m^{-2})) is higher than that in the

water/DCE system (27.9 mN m^{-1} (mJ m^{-2})). The solubility of water in the oil (or that of the oil in water) is reported to be 0.07 (0.01) and 0.81 (0.15) wt% for CCl_4 and DCE, respectively.[17] These values indicate that the solubility of water in CCl_4 is almost ten times smaller than that in the DCE. Because of the immiscible nature of water in CCl_4, the water/CCl_4 interface is likely to construct a molecularly sharp interface as compared to the water/DCE interface. Beside this, the molecular shape of CCl_4 or DCE might also play an important role in determining the interfacial structure.

The present approaches have a high potential to elucidate experimentally the structure and properties of a liquid/liquid interface and, complementary studies by both experiments and computer simulations are fruitful for further progresses in chemistry at liquid/liquid interfaces.

Conclusions

A study on structural dimension analysis of excitation energy transfer dynamics between the dye molecules adsorbed on water/oil interfaces was shown to be a potential means to discuss thickness and roughness of the interfacial layer and, structural dimension of the water/CCl_4 or water/DCE interface was determined to 1.93 or 2.48, respectively. The magic-angle dependence of the TIR fluorescence decay profile of SR101 adsorbed on the interface also supported the results derived from the present structural dimension analysis. Thus, the water/CCl_4 interface was concluded to be very sharp with respect to molecular dimension of SR101: 1.0 ~ 1.4 nm. On the other hand, the water/DCE interface was demonstrated to be more rough than the water/CCl_4 interface. It is worth noting that the spatial resolution of the present approaches is 1 (anisotropy) ~ 7 nm (energy transfer), so that other techniques having smaller spatial resolution might afford different aspect on the interfacial structures. Also, the results obtained by the present study are limited to water/CCl_4 and water/DCE interfaces, and analogous study should be extended to other systems. Nonetheless, the present study is very meaningful in respect to comparative discussion on the same systems by both experiments and available computer simulation data.

References and Notes

(1) Nakatani, K.; Ishizaka, S.; Kitamura, N. *Anal. Sci.* **1996**, *12*, 701-705.

(2) Ishizaka, S.; Nakatani, K.; Habuchi, S.; Kitamura, N. *Anal. Chem.* **1999**, *71*, 419-426.

(3) Förster, Th. *Discuss. Faraday Soc.* **1959**, *27*, 7–17.

(4) Klafter, J.; Blumen, A. *J. Chem. Phys.* **1984**, *80*, 875–877.

(5) Klafter, J.; Blumen, A. *J. Lumin.* **1985**, *34*, 77–82.

(6) Benjamin, I. *J. Chem. Phys.* **1992**, *97*, 1432–1445.

(7) Benjamin, I. *Science* **1993**, *261*, 1558–1560.

(8) Michael, D.; Benjamin, I. *J. Phys. Chem.* **1995**, *99*, 1530–1536.

(9) Schweighofer, K. J.; Benjamin, I. *J. Phys. Chem.* **1995**, *99*, 9974–9985.

(10) Michael, D.; Benjamin, I. *J. Phys. Chem.* 1995, *99*, 16810–16813.

(11) Michael, D.; Benjamin, I. *J. Chem. Phys.* 1997, *107*, 5684–5693.

(12) Chang, T. -M.; Dang, L. X. *J. Chem. Phys.* 1998, *108*, 818–819.

(13) Ishizaka, S.; Habuchi, S.; Kim, H.-B.; Kitamura, N. *Anal. Chem.* **1999**, *71*, 3382–3389.

(14) O'Connor, D.V.; Phillips, D. "*Time-Correlated Single Photon Counting*"; Academic Press: New York, 1986.

(15) The following values were used to calculate the R_0 value: $\phi_0 = 1.00$,[16] n (water) = 1.33,[17] and $\int_0^\infty F_D(\nu)\varepsilon_A(\nu)/\nu^4 d\nu = 7.0 \times 10^{-13}$.

(16) Karstens, T.; Kobs, K. *J. Phys. Chem.* **1980**, *84*, 1871–1872.

(17) Riddick, J. A.; Bunger, W. B. *Techniques of Chemistry: Organic Solvents*, Vol. II, Wiley-Interscience, New York, 1970.

(18) Tamai, N.; Yamazaki, T.; Yamazaki, I. *Chem. Phys. Lett.* **1988**, *147*, 25–29.

(19) Yamazaki, I.; Tamai, N.; Yamazaki, T. *J. Phys. Chem.* **1990**, *94*, 516–525.

(20) Tamai, N.; Yamazaki, T.; Yamazaki, I.; Mizuma, A.; Mataga, N. *J. Phys. Chem.* **1987**, *91*, 3503–3508.

(21) Lin, Y.; Nelson, M. C.; Hanson, D. M. *J. Chem. Phys.* **1987**, *86*, 1586–1592.

(22) Tcherkasskaya, O.; Spiro, J. G.; Ni, S.; Winnik, M. A. *J. Phys. Chem.* **1996**, *100*, 7114–7121.

(23) Yekta, A.; Spiro, J. G.; Winnik, M. A. *J. Phys. Chem. B* **1998**, *102*, 7960–7970.

(24) Kim, H. -B.; Habuchi, S.; Kitamura, N. *Anal. Chem.* **1999**, *71*, 842–848.

(25) Rojanski, D.; Huppert, D.; Bale, H. D.; Dacai, X.; Schmidt, P. W.; Farin, D.; Seri-Levy, A.; Avnir, D. *Phys. Rev. Lett.* **1986**, *56*, 2505–2508.

(26) Levitz, P.; Drake, J. M. *Phys. Rev. Lett.* **1987**, *58*, 686–689.

(27) Rojanski, D.; Huppert, D.; Avnir, D. *Chem. Phys. Lett.* **1987**, *139*, 109–115.

(28) Watarai, H.; Horii, Y.; Fujishima, M. *Bull. Chem. Soc. Jpn.* **1988**, *61*, 1159–1162.

(29) Volkov, A. G.; Deamer, D. W., Eds. *Liquid-Liquid interfaces*; CRC Press: Boca Raton, FL, 1996.

(30) Buff, F.P.; Lovett, R.A.; Stillinger, Jr. F.H. *Phys. Rev. Lett.* **1965**, *15*, 621-623.

(31) Braslau, A.; Pershan, P.S.; Swislow, G.; Ocko, B.M.; Als-Nielsen, J. *Phys. Rev. A* **1988**, 38, 2457-.2470

(32) Pershan, P.S. *Faraday Discuss. Chem. Soc.* **1990**, *89*, 231-245.

(33) Simpson, G. J.; Rowlen, K. L. *Chem. Phys. Lett.* **1999**, *309*, 117-122.

(34) Israelachvili; J. N. *Intermolecular and Surface Forces*, Academic Press Ltd., 1992.

Chapter 5

Time-Resolved Total Internal Reflection Fluorometry Study on Polarity at Liquid/Liquid Interface

5.1 Introduction

The polarity of a liquid/liquid interface sometimes plays important roles in deciding heterogeneous reaction kinetics.[1-4] Such results suggest that solvent environments at the interface are different from those in bulk media. In practice, the polarity of interfacial regions such as in microemulsions[5] and micelles[6, 7] has been investigated by means of UV/vis absorption spectroscopy on a polarity indicator molecule: 2,6-diphenyl-4-(2,4,6-triphenyl-1-pyridino) phenoxide (DPP). However, these studies do not provide direct information about the interfacial polarity, since the experiments are conducted for bulk systems. Recently, surface selective spectroscopic techniques have been applied to studying the polarity of a liquid/liquid interface. As an example, Perera et al. reported the mean polarities at water/*n*-heptane, water/*n*-decane, and water/cyclohexane interfaces by using attenuated-total-internal reflectance (ATR) absorption spectroscopy and, demonstrated that the absorption peak of DPP at the interface was in the range of 600 ± 10 nm, corresponding to a solvent polarity parameter of $E_T(30)$ = 47.7 ± 0.8 kcal/mol.[4] Since the bulk polarity of the oil used was very similar with each other, the interfacial polarity was almost independent of the oil. On the other hand, Bessho et al. applied time-resolved total-internal-reflection (TIR) fluorescence spectroscopy to studying microenvironments around 8-anilino-1-naphthalenesulfonate (ANS) at a water/heptane interface,[8] and they suggested that the interfacial polarity was intermediate between that of heptane and water.

As an another approach, Wang et al. reported an SHG (second harmonic generation) spectroscopic study on the polarities of water/1,2-dichloroethane (DCE) and water/chlorobenzene (CB) interfaces by using a polarity indicator molecule: *N,N*-diethl-*p*-nitroaniline (DEPNA).[9] According to their study, the interfacial polarity ($P_{A/B}$) is equal to

the arithmetic average of the polarity of the adjoining bulk phase (P_A and P_B): eq 5.1.

$$P_{A/B} = \frac{P_A + P_B}{2} \tag{5.1}$$

They explained the results by dominance of long-range solute-solvent interactions in determining the difference in the excited- and ground-state solvation energies around DEPNA at the interface, but not by local interfacial interactions. The validity of this idea was checked experimentally by using a π^* scale polarity parameter, which was derived from the peak of the SHG spectrum of DEPNA at the water/DCE or water/CB interface. As discussed in their paper, an $E_T(30)$ scale parameter is more suitable to estimate the interfacial polarity compared to the use of the π^* scale parameter, since a relationship between the absorption maximum of a probe molecule and a dielectric constant has been checked for more than 30 solvents. In practice, the applicability of eq 5.1 was checked for water/*n*-heptane, water/*n*-decane, and water/cyclohexane systems on the basis of the $E_T(30)$ parameter. However, a variation of $E_T(30)$ by these three solvents was only 1.2 kcal/mol. On the other hand, Michael and Benjamin reported molecular dynamics computer simulations of an electronic spectrum of DEPNA at a water/DCE interface[10] and predicted that the interfacial polarity was influenced by both interfacial roughness and the position of the probe molecule at the interface.[11] In addition to the long-range solute-solvent interaction at the interface, they demonstrated that short-range solute-solvent interactions were also important in determining the difference in the excited- and ground-state solvation energies around the probe molecule at the interface. Both experimental and theoretical studies on the polarity at an water/oil interface are still limited as discussed above. In particular, the applicability of eq 5.1 should be checked in a wide range of $E_T(30)$ and, the role of interfacial roughness in determining the polarity

should be clarified experimentally.

In this study, Sulforhodamine B (SRB) was used as a probe molecule to investigate the interfacial polarity. Since SRB is surface active and possesses a high fluorescence quantum yield, the dye is very suitable for TIR fluorescence measurements at a liquid/liquid interface. Furthermore, it has been reported that the non-radiative decay rate constant (k_{nr}) of Rhodamine B (RB) is sensitive to a medium polarity and, $\ln(k_{nr})$ is linearly correlated to $E_T(30)$.[12, 13] On the basis of fluorescence dynamic measurements of SRB adsorbed on a water/oil interface, therefore, a relationship between interfacial thickness/roughness and the polarity at the interface was studied in detail, and the applicability of eq 5.1 was discussed.

5.2 Experimental

Chemicals and Sample preparation

Water was purified by distillation and deionization prior to use (GSR-200, Advantec Toyo Co., Ltd.). Carbon tetrachloride (Kanto Chemical Co., Inc.) was purified by distillation after washing successively with an aqueous hydroxide solution and water. Chlorobenzene (Kanto Chemical Co., Inc.) was purified by distillation after washing successively with an aqueous sodium hydrogencarbonate solution and water. Cyclohexane (Dojindo, Sp grade), toluene (Dojindo, Sp grade), *o*-dichlorobenzene (Wako Chemical Co., Inc.), 1,2-dichloroethane (MERCK, Uvasol) and 1,4-dioxane (Dojindo, Sp grade) were used without further purification. Sulforhodamine 101 (SR101; ACROS Organics, laser grade) and Sulforhodamine B (SRB; Tokyo Kasei Kogyo Co., Inc.) were

used as received. Acid Blue 1 (AB1; Tokyo Kasei Kogyo Co., Inc) was purified by recrystallizations from an acetone-water mixture.

For TIR experiments, an aqueous SRB solution (concentration [SRB] = 1.0×10^{-9} M) saturated with an organic solvent was poured carefully onto a water-saturated organic solvent in a Pyrex cell (inner diameter = 40 mm). The lower or upper inside of the cell was treated with dichlorodimethylsilane to construct a flat water/oil interface. The cell was washed thoroughly with each organic solvent and then with water prior to a sample preparation. Spectroscopic measurements were carried out after the sample solution in the cell being kept over 100 min at 25 °C.

Measurements

Steady-state absorption and fluorescence spectroscopy were conducted by using Hitachi U-3300 and Hitachi F-4500 spectrometers, respectively. Fluorescence measurements for bulk solutions were carried out at 25 ± 1 °C. Relative fluorescence quantum yields of SRB in several solvents were determined with that of SR101 in ethanol as a standard.[15] Corrected fluorescence spectra were obtained by accepted procedures.

Fluorescence dynamic spectroscopy was conducted with a time-correlated single photon-counting technique, as described in Chapter 3.[14, 16] TIR fluorescence spectra were measured by using a gated photon counter (STANFORD RESERCH SYSTEMS, SR400). The temperature of the sample cell for bulk and TIR fluorescence measurements was maintained at 25 ± 1 °C by using an electric temperature controller. Fluorescence decay curves were analyzed by a non-linear least-squares iterative convolution method based on the Marquardt algorithm.[17]

5.3 Results and Discussion

5.3.1 Estimation of Interfacial Roughness

As discussed in the previous chapter, fluorescence dynamic anisotropy of SR101 adsorbed on a liquid/liquid interface provides information about molecular-level structures of the interface (i.e., dimension of the molecular size of SR101 ~ 1nm).[14, 16] Figure 5-1 shows fluorescence decay profiles of SR101 observed at water/CCl_4, water/*o*-dichlorobenzene (DCB), and water/DCE interfaces with an emission polarization angle of 45° ((a), (b), (c)) or 54.7° ((d), (e), (f)), together with the relevant weighted residuals (Re) for each single-exponential fit. Fluorescence anisotropy at the water/CCl_4 interface ((a) and (d)) and water/DCE interfaces ((c) and (f)) was reasonably canceled by setting the emission polarizer at 45° ((a)) and 54.7° ((f)), respectively. This demonstrates that the water/CCl_4 interface is regarded as two dimension while thickness of the water/DCE interface is comparable to the molecular size of SR101, as described previously in detail.[14] For TIR fluorescence decay observed at the water/DCB interface ((b), and (e)), on the other hand, a single-exponential fit was failed by either the polarization angle of 45° or 54.7°, as revealed by Re in the initial stage of excitation. Therefore, it is considered that thickness of the water/DCB interface is intermediate between that of the water/CCl_4 and water/DCE interfaces. Analogous experiments were conducted for other water/oil systems and, the results of the magic angle of the TIR fluorescence decay profile of SR101 are summarized in Table 5-1, together with the $E_T(30)$ values of the oils. Phenomenologically, Table 5-1 demonstrates that rotational freedom of SR101 at the interface is two- dimensional-like (magic angle ~45°) for the system with a low $E_T(30)$ value, while rotational reorientation of the dye at the water/oil interface having a

relatively large $E_T(30)$ value (DCB and DCE) takes place in three-dimensional-like.

Another possible approach to estimate the interfacial structures is an application of an excitation energy transfer dynamics method as described in Chapter 4.[14] It has been well known that Förster-type excitation energy transfer takes place within the spatial range of several nanometers (i.e., critical energy transfer distance), so that an information about relatively long-range interfacial roughness can be studied if excitation energy transfer proceeds exclusively at a water/oil interface. Therefore, excitation energy transfer quenching of SR101 fluorescence by AB1 at the water/oil interfaces was explored (data are shown in Figure 5-2 ~ 5-5).[14]

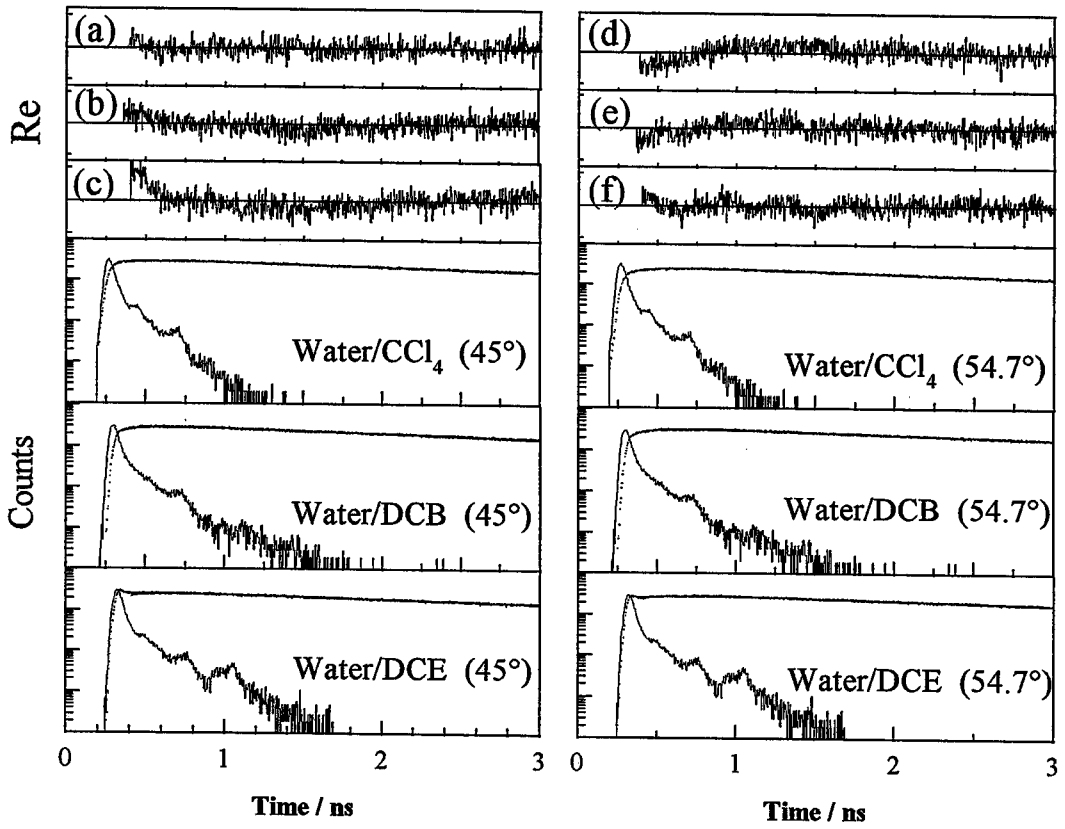

Figure 5-1 TIR fluorescence decay curves of SR101 at water/CCl_4 ((a) and (d)), water/DCB ((b) and (e)), and water/DCE ((c) and (f)) interfaces. The angle of the emission polarizer was set at 45° ((a), (b) and (c)) or 54.7° ((d), (e) and (f)) in respect to the direction of excitation polarization. The upper panel represents the plot of the weighted residuals (*Re*) for a single-exponential fit of each decay profile.

Table 5-1. Magic-Angles for the TIR Fluorescence Anisotropy Measurements and Structural Dimensions at the Interfaces.

Org. Phase	$E_T(30)$ [a] / kcal mol^{-1}	γ [b] /mN m^{-1}	Magic Angle [c]	$\bar{d}$ [d]
Cyclohexane	30.9	51[e]	45°	1.90
CCl_4	32.4	45	45°	1.93
Toluene	33.9	33	~45°	2.13
CB	36.8	37	~45°	2.20
DCB	38.0	39	45~54.7°	2.30
DCE	41.3	28	~54.7°	2.48

a) Taken from ref. (28)

b) Interfacial tension of the water/oil system, determined by a pendant drop method.

c) The angle of an emission polarizer, by which the fluorescence decay is best fitted by a single-exponential function.

d) The structural dimension determined by excitation energy transfer quenching of SR101 fluorescence by AB1 (see main text).

e) Ref. (29)

The structural dimension ($\bar{d}$) of the interface was then estimated by fitting the TIR fluorescence decay curve in the presence of AB1 (data are not shown) by using the Klafter-Blumen equation.[18] The results are included in Table 5-1. The structural dimension increased with increasing the polarity ($E_T(30)$) of the organic solvent. It has been reported that thermal capillary waves at the interface are related to interfacial tension of the system.[19-22] However, any clear relationship between interfacial tension and interfacial roughness could not be obtained as long as the experiments by dynamic anisotropy and the excitation energy transfer dynamics. Therefore, molecular-scale interfacial roughness could be governed by not only interfacial tension (as a macroscopic property), but also the nature of the organic solvent.

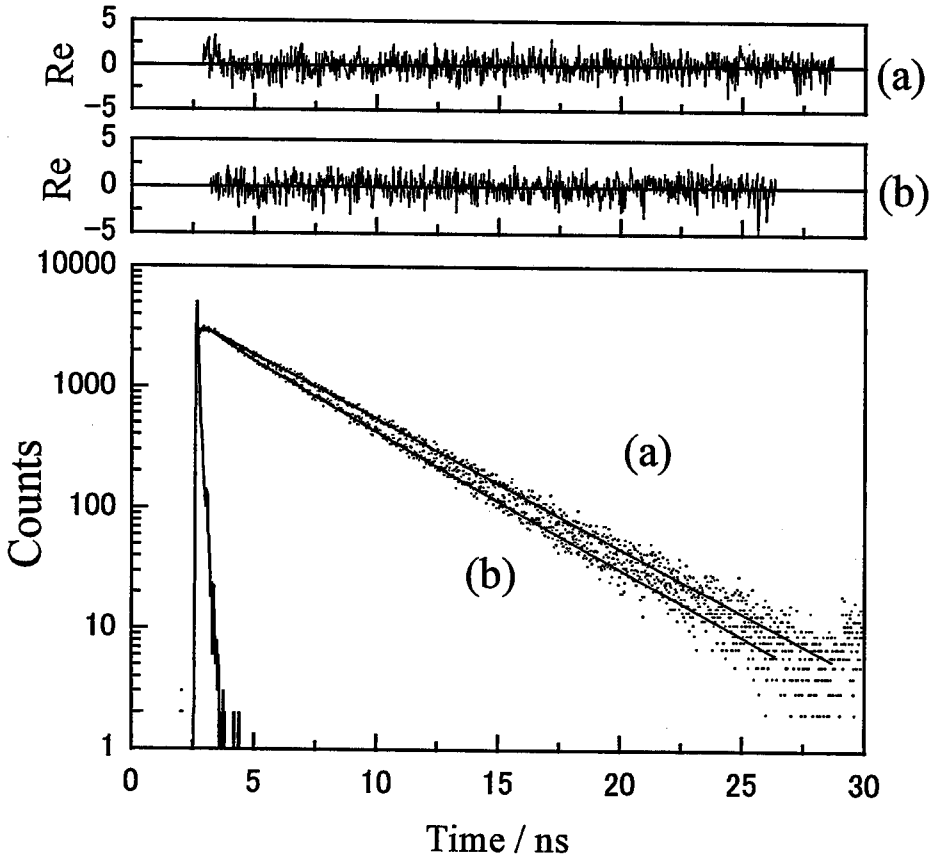

Figure 5-2 Fluorescence decay profiles of SR101 at a water/Cyclohexane interface in the absence and presence of AB1: (a) [AB1] = 0, (b) 4.0×10^{-9} M. The solid curve shows the best fit by eq 4.3.

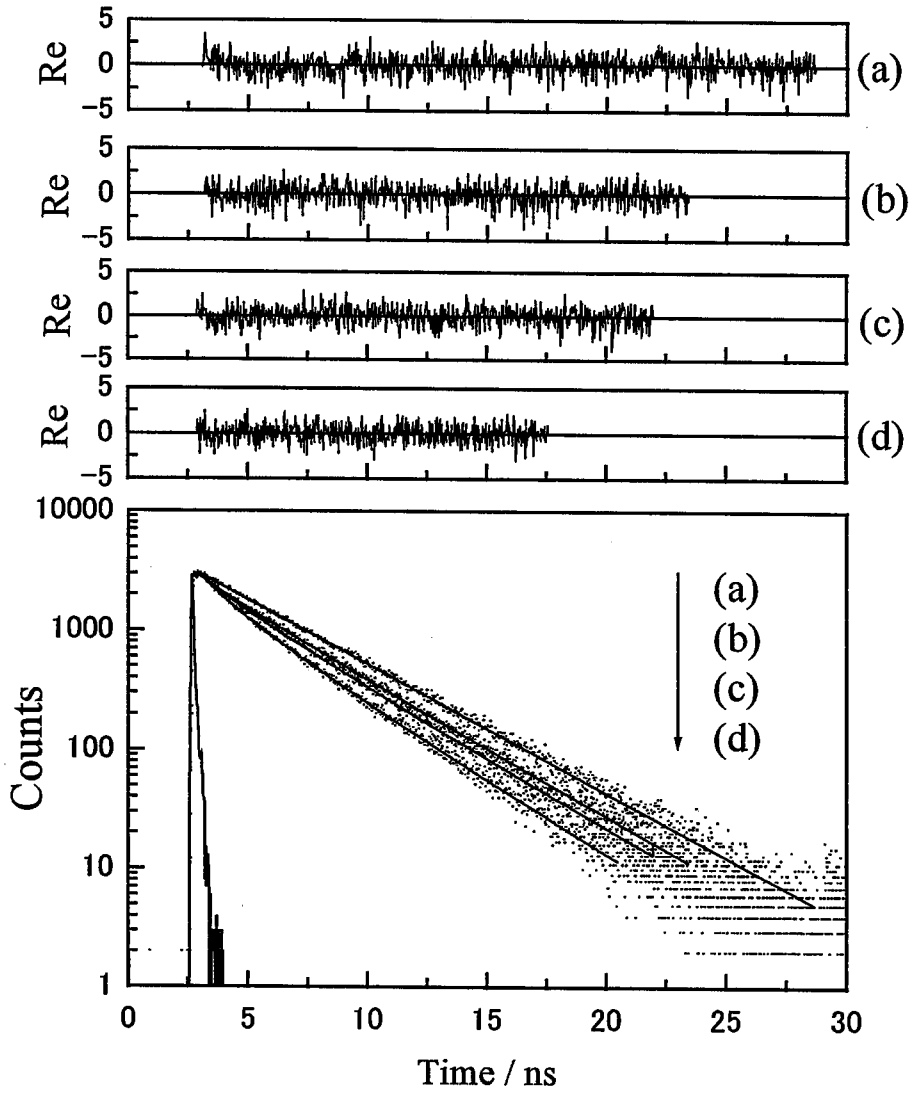

Figure 5-3 Fluorescence decay profiles of SR101 at a water/Toluene interface in the absence and presence of AB1: (a) [AB1] = 0, (b) 1.91×10^{-9}, (c) 3.82×10^{-9}, (d) 5.73×10^{-9} M. The solid curve shows the best fit by eq 4.3.

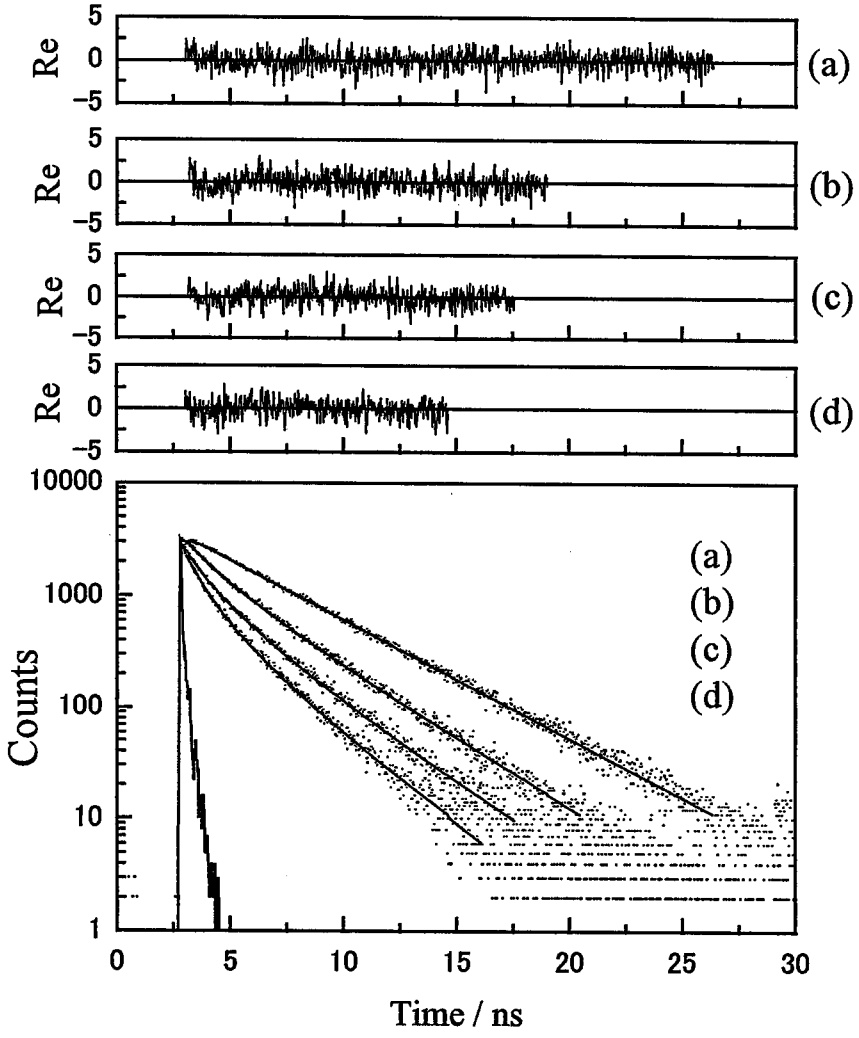

Figure 5-4 Fluorescence decay profiles of SR101 at a water/CB interface in the absence and presence of AB1: (a) [AB1] = 0, (b) 1.91×10^{-9}, (c) 3.82×10^{-9}, (d) 5.73×10^{-9} M. The solid curve shows the best fit by eq 4.3.

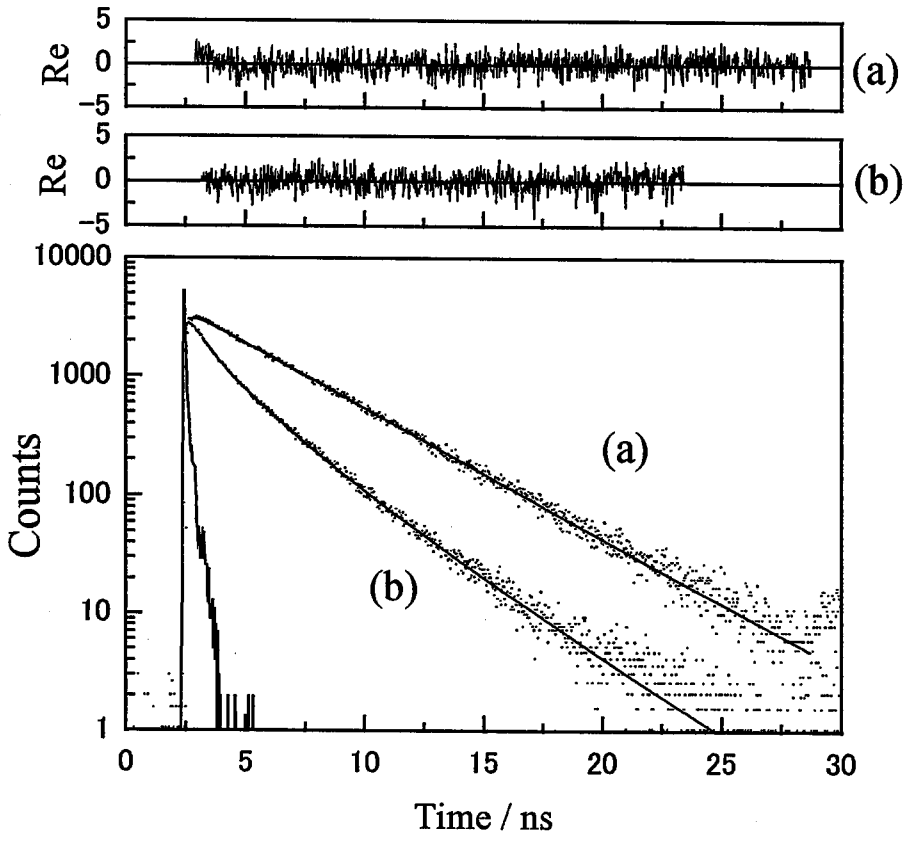

Figure 5-5 Fluorescence decay profiles of SR101 at a water/DCB interface in the absence and presence of AB1: (a) [AB1] = 0, (b) 1.91×10^{-9}, (c) 3.82×10^{-9}, (d) 5.73×10^{-9} M. The solid curve shows the best fit by eq 4.3.

5.3.2 *Solvent Polarity Dependence of the Non-radiative Decay Rate Constant of SRB in Water-Dioxane Mixtures*

For the dynamic anisotropy and excitation energy transfer experiments, SR101 was used as a probe. However, the fluorescence properties of SR101 are not sensitive enough to micropolarity.[23] Therefore, SRB was used as a probe for interfacial polarity measurements. Before describing the results on TIR fluorescence of SRB at the water/oil interfaces, one should discuss the effects of a solvent polarity on the non-radiative decay rate constant of SRB in a bulk solution, which is the fundamental basis for the further discussion on the interfacial structures.

The photophysical properties of a xanthene dye have been extensively studied.[12, 13, 23-26] In order to explain a relationship between the non-radiative decay rate constant (k_{nr}) of the dye and a solvent polarity parameter $E_T(30)$, Quitevis et al. proposed a two-state model.[12, 13] In the model, a fluorescent state A*, which can only decay radiatively to the ground state S_0, is in rapid equilibrium with a non-emissive state B*, which can only decay to S_0 via internal conversion. According to the model, k_{nr} is given by

$$k_{nr} \propto \exp\{-(\beta/RT + \kappa)(E_T(30) - 30)\}\exp(-\Delta G_{A^*B^*}{}^0/RT) \qquad (5.2)$$

where β and κ are constants and, $\Delta G_{A^*B^*}{}^0$ is the Gibbs free energy difference between A* and B* in a non-polar solvent. If eq 5.2 holds, a plot of $\ln k_{nr}$ vs. $E_T(30)$ should be linear with the slope value being equal to $-(\beta/RT + \kappa)$. In practice, Quitevis et al. succeeded in explaining solvent effects on the photophysical characteristics of rhodamine B in various alcohols and nitriles. The physical meaning of eq 5.2 is not straightforward and will be better to consider as an empirical equation. Nonetheless, the relation is useful to explain

solvent effects on the spectroscopic properties of a xanthene dye. Therefore, an applicability of the model to the photophysical properties of SRB was checked in water-dioxane mixtures and several alcohols. (data are shown in Figure 5-6, 5-7)

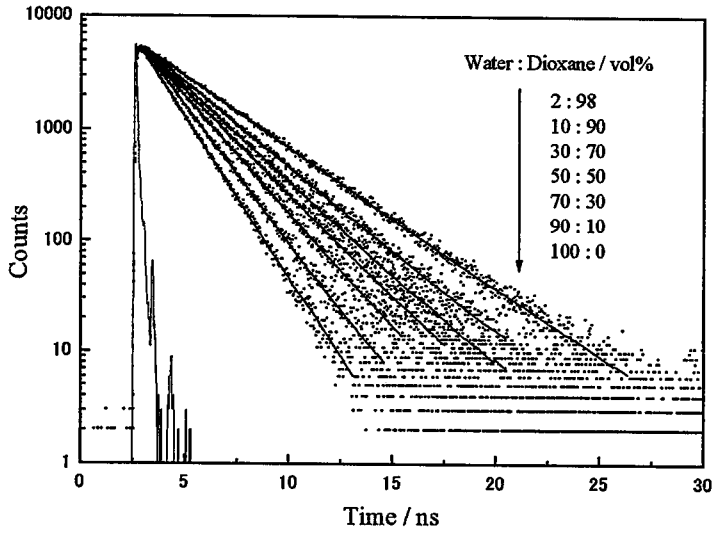

Figure 5-6 Fluorescence decay profiles of SRB in water and dioxane mixtures. The solid curves show the best fit by a single-exponential function, and fitting parameters are listed in a Table 5-2.

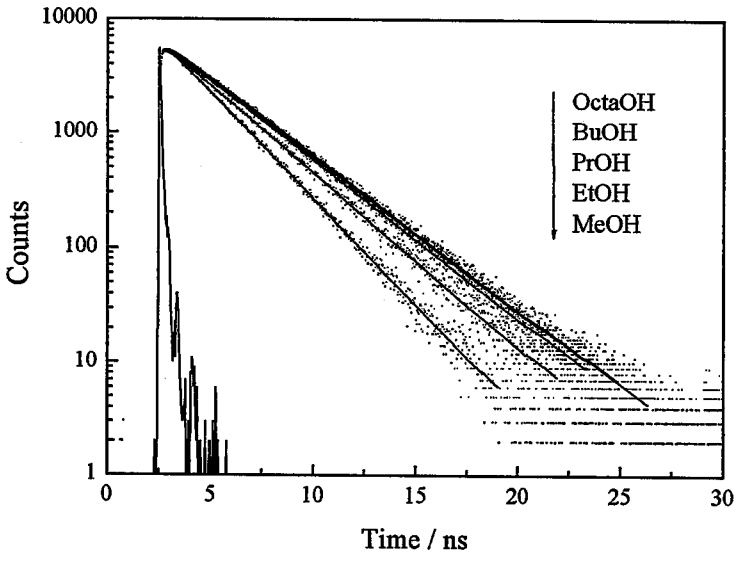

Figure 5-7 Fluorescence decay profiles of SRB in alchols. The solid curves show the best fit by a single-exponential function, and fitting parameters are listed in a Table 5-2.

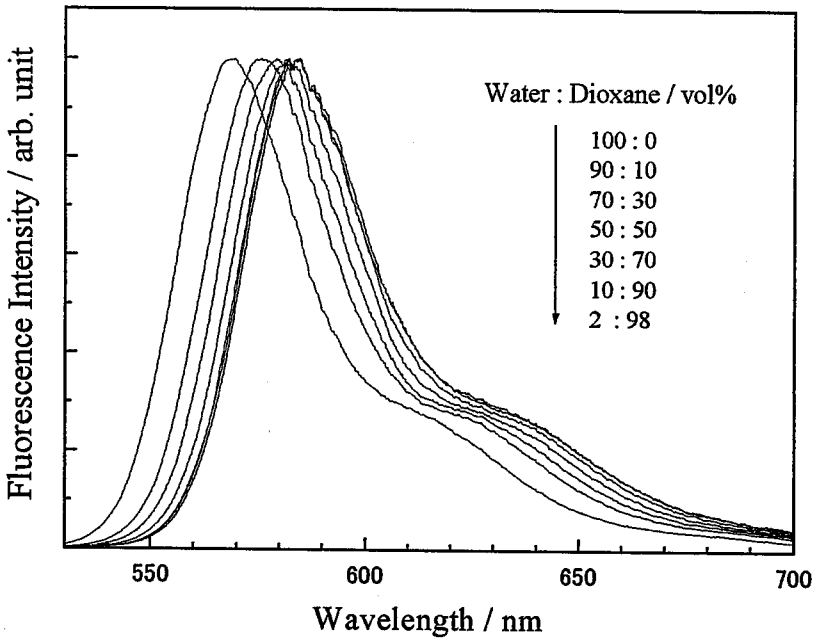

Figure 5-8 Normalized Fluorescence spectra of SRB in water-dioxane mixtures.

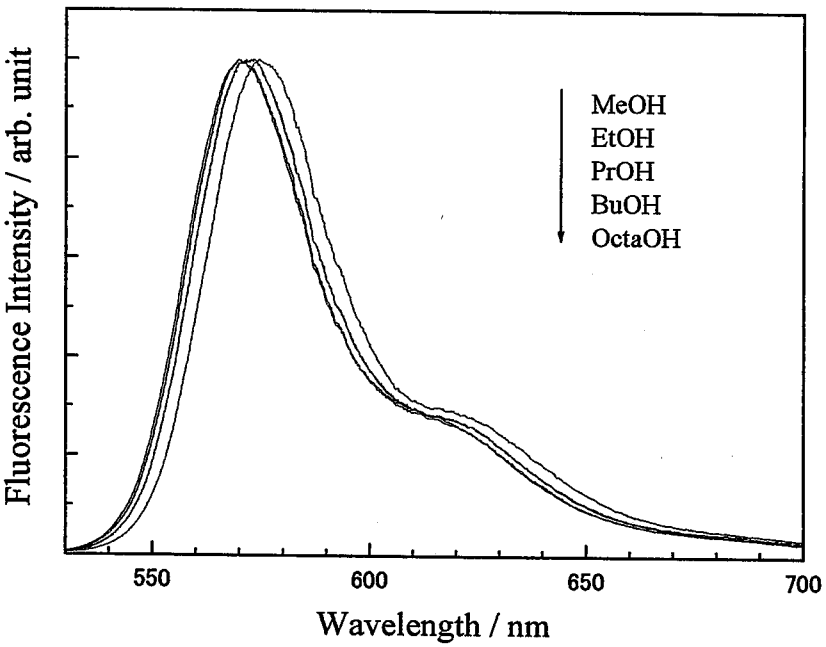

Figure 5-9 Normalized Fluorescence spectra of SRB in alcohols.

Table 5-2. Photophysical Parameters of SRB in Water-Dioxane Mixtures and Alcohols

solvent	$E_T(30)$[a] /kcal mol^{-1}	λ_{em}[b] /nm	τ / ns	k_r /10^8 s^{-1}	k_{nr} /10^8 s^{-1}	Φ[c]
H_2O : Dioxane /vol%						
100 : 0	63.1	583	1.50	2.61	4.08	0.39
90 : 10	61.1	584	1.75	2.78	2.95	0.49
70 : 30	57.1	583	2.07	2.46	2.37	0.51
50 : 50	53.6	582	2.33	2.54	1.76	0.59
30 : 70	50.9	579	2.56	2.33	1.58	0.60
10 : 90	46.7	576	2.85	2.20	1.31	0.63
2 : 98	41.4	569	3.38	2.24	0.72	0.79
Alcohol						
MeOH	55.4	574	2.33	2.06	2.24	0.48
EtOH	51.9	572	2.83	1.94	1.63	0.55
PrOH	50.7	570	3.13	1.73	1.47	0.54
BuOH	49.7	570	3.20	1.68	1.44	0.54
OctaOH	48.1	572	3.21	1.90	1.21	0.61

a) The value is calculated on the basis of a volume percentage of H_2O and dioxane.

b) The fluorescence maximum of SRB.

c) The fluorescence quantum yield of SRB relative to the value for SR101 in ethanol.

The fluorescence lifetimes (τ determined at 580 nm) and quantum yields (Φ) of SRB determined in water-dioxane mixtures and a series of an alcohol at 25 °C are summarized in Table 5-2. The non-radiative decay rate constant (k_{nr}) thus calculated from τ and Φ is also included in Table 5-2. The k_{nr} value varied with the medium in the range of (4.1 ~ 0.7) × 10^8 s^{-1}, whereas the radiative decay rate constant (k_r) was rather insensitive to the medium properties (2.8 ~ 1.7) × 10^8 s^{-1}. The relationship between $\ln k_{nr}$ and $E_T(30)$ is shown in Figure 5-10. As seen clearly, all the data fall on a straight line and the slope value of the plot was 0.074 ± 0.01. Although the slope value is somewhat smaller than that determined for rhodamine B in alcohols (0.12 ± 0.02),[12] the photophysical properties of SRB and eq 5.2 are applicable to probe the polarity at a water/oil interface.

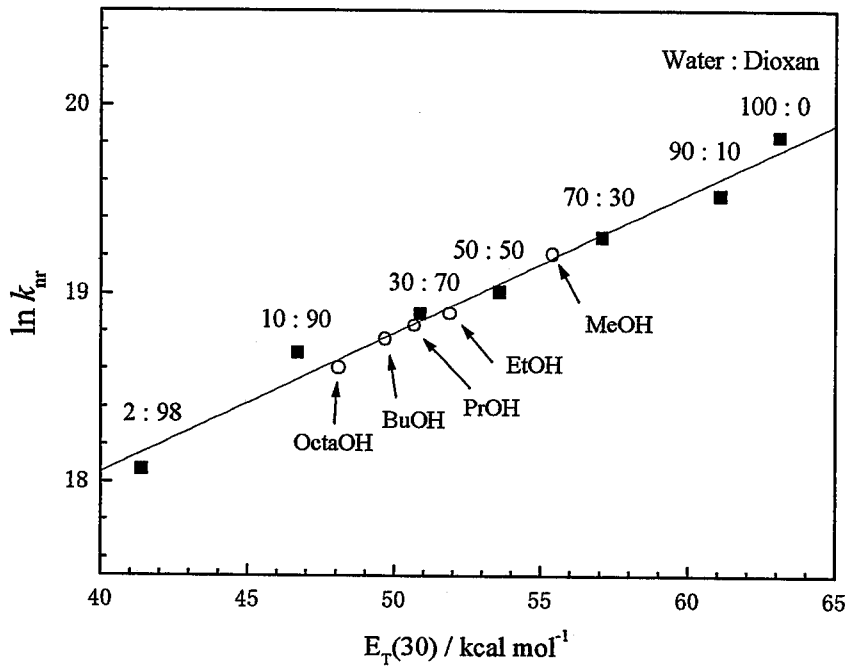

Figure 5-10 Relationship between the natural logarithm of k_{nr} (determined in water-dioxane mixtures and alcohols) and $E_T(30)$.

5.3.3 Solvent Polarity Dependence of the Non-radiative Decay Rate Constant of SRB at Water/Oil Interface

In order to estimate the polarity at a water/oil interface by means of TIR fluorescence spectroscopy, a probe molecule should be highly surface active and adsorb on the interface, so as to exclude fluorescence of the probe molecule from the bulk phase.[27] In practice, SRB is highly surface active and adsorbed on the water/oil interfaces. Therefore, the contribution of the fluorescence from bulk water phase, which is excited by an evanescent wave, to the observed fluorescence is negligible. Figure 5-11 shows fluorescence spectra of SRB in an aqueous solution and at a water/DCE interface. The peak position of the TIR fluorescence spectrum at the interface (579 nm) is slightly blue-

shifted compared to that in a dilute aqueous solution (583 nm). This result suggests that the water/DCE interface is less polar than the bulk aqueous solution.

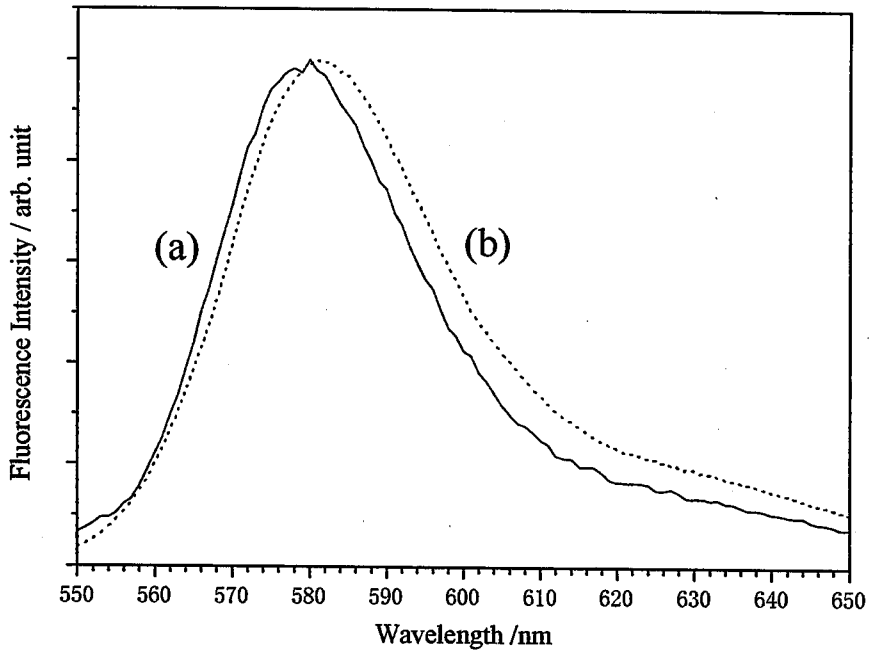

Figure 5-11 Fluorescence spectra of SRB at a water/DCE interface (a) and in water (b).

Figure 5-12 shows the fluorescence decay profiles of SRB at the water/DCE interface and in an aqueous solution, together with the relevant Re for each single-exponential fit. Analogous results were obtained for other water/oil systems (data are shown in Figure 5-13 ~ 5-17), and the τ values determined are summarized in Table 5-3. It is noteworthy that the TIR fluorescence decay curve observed at each water/oil interface was reasonably fitted by a single-exponential function as judged by Re, and their lifetimes were longer than that in an aqueous phase (1.5 ns). The single-exponential fit indicates that the local solvation structure around SRB adsorbed on the interface is almost uniform. Nevertheless, as discussed in the preceding section, the structural dimension of the water/DCB or water/DCE interface is larger than 2, demonstrating that excitation energy transfer quenching of the SR101 fluorescence takes place other than the lateral direction. If the

water/oil interfacial layer is thick (> 1 nm) and the water/oil composition varies gradually within the layer, the TIR fluorescence of SRB should decay multi-exponentially. On the other hand, short-range structural information about the interface obtained by the fluorescence dynamic anisotropy experiments suggested that the interface is three-dimensional-like. These results can be understood only by the fact that the water/DCB and water/DCE interfaces are thin (~ 1 nm), but is rough with respect to the spatial resolution of the excitation energy transfer quenching method (~ 7 nm), as discussed later again.

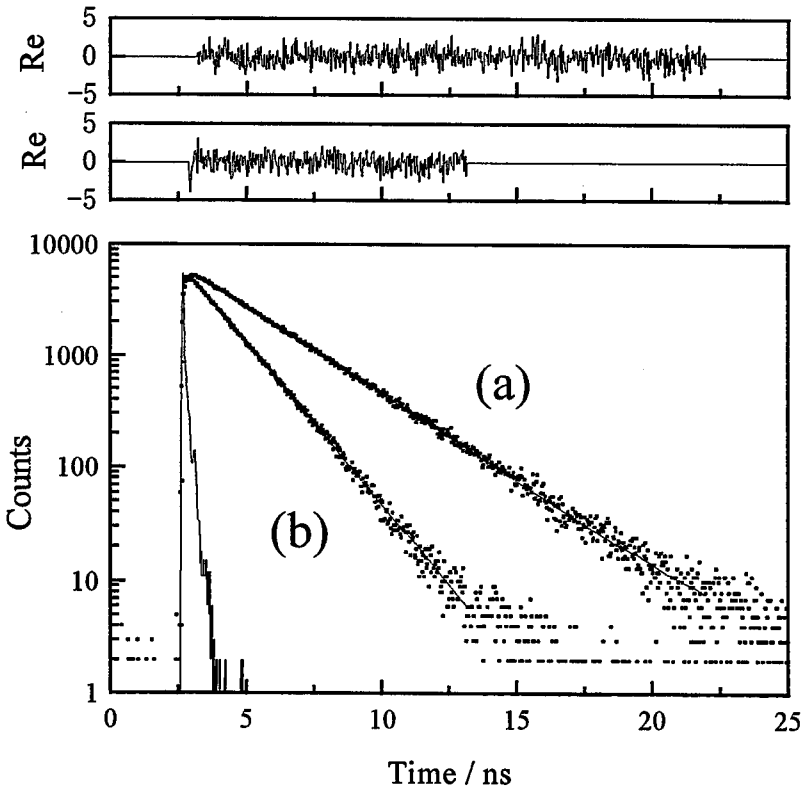

Figure 5-12 Fluorescence decay profiles of SRB at a water/DCE interface (a) and in water (b). The solid curve shows the best fit by a single-exponential function.

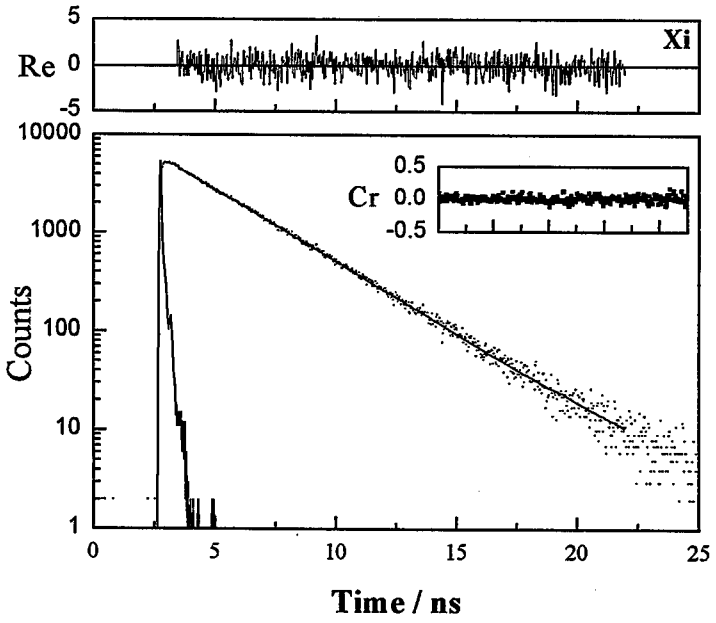

Figure 5-13 Fluorescence decay profiles of SRB at a water/cyclohexane interface. The solid curve shows the best fit by a single-exponential function.

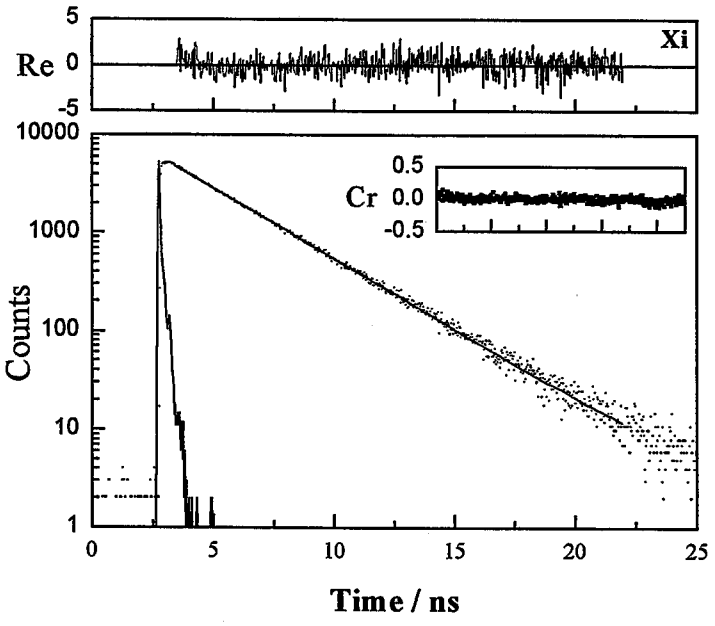

Figure 5-14 Fluorescence decay profiles of SRB at a water/CCl_4 interface . The solid curve shows the best fit by a single-exponential function.

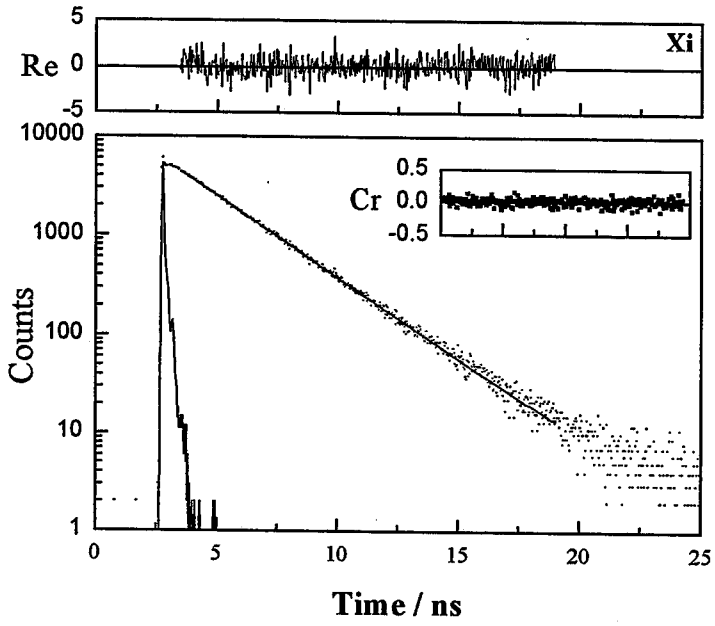

Figure 5-15 Fluorescence decay profiles of SRB at a water/toluene interface . The solid curve shows the best fit by a single-exponential function.

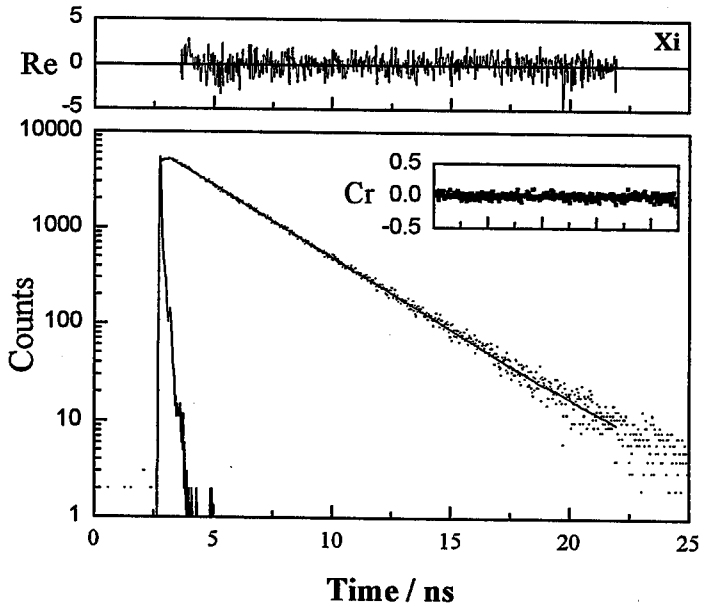

Figure 5-16 Fluorescence decay profiles of SRB at a water/CB interface . The solid curve shows the best fit by a single-exponential function.

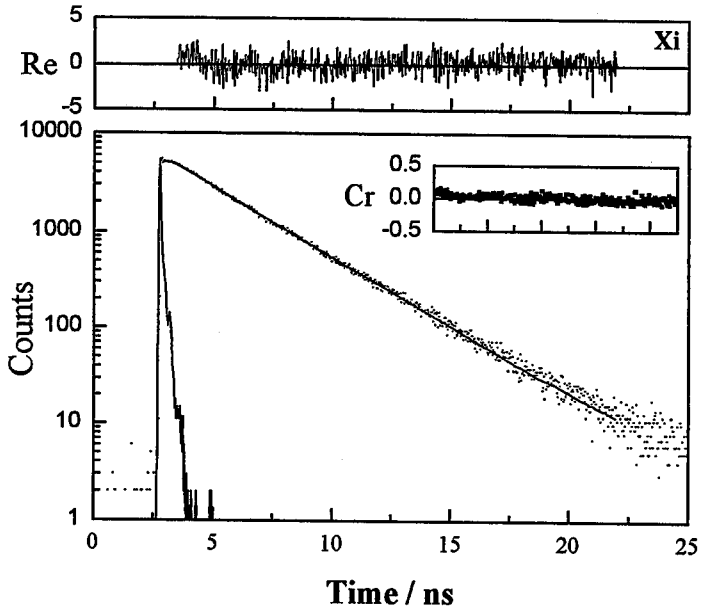

Figure 5-17 Fluorescence decay profiles of SRB at a water/DCB interface . The solid curve shows the best fit by a single-exponential function.

Table 5-3. Photophysical Parameters of SRB and Polarities at the Water/Oil Interfaces

Org. Phase	$E_T(30)^{a)}$ /kcal mol^{-1}	τ /ns	k_{nr} /10^8 s^{-1}	$E_T(30)_{int}$ /kcal mol^{-1}	$E_T(30)_{calc}$ /kcal mol^{-1}
Cyclohexane	30.9	3.00	1.13	46.7	47.0
CCl_4	32.4	2.95	1.18	47.4	47.8
Toluene	33.9	2.84	1.32	48.8	48.5
CB	36.8	2.89	1.25	48.1	50.0
DCB	38.0	3.00	1.13	46.7	50.6
DCE	41.3	2.78	1.39	49.5	52.2

a) The value for the oil.

Table 5-2 indicates that k_r is not sensitive to solvent environments compared to k_{nr}. Assuming k_r being constant at the average value (2.21×10^8 s^{-1}) of those in the bulk solutions (Table 5-2), k_{nr} of SRB at the interface was calculated: $k_{nr} = \tau^{-1} - k_r$. The interfacial polarity $E_T(30)_{int.}$ in each water/oil system was then estimated on the basis of the relevant k_{nr} value and the relationship in Figure 5-6. The results are summarized in Table 5-3 and Figure 5-18, together with calculated interfacial polarity $E_T(30)_{calc}$ as the arithmetic average of $E_T(30)$ of the water and organic phases. These data demonstrate that $E_T(30)_{int}$ observed takes always an intermediate value between $E_T(30)$ of water and the relevant organic phase. However, a close inspection of the data in Figure 5-18 indicates that the discrepancy between $E_T(30)_{int}$ and $E_T(30)_{calc}$ becomes larger with an increase in $E_T(30)$ of the oil itself. In the case of a relatively low polarity solvent (cyclohexane, CCl_4, or toluene), namely, $E_T(30)_{int}$ agreed very well with $E_T(30)_{calc}$. According to the results of dynamic fluorescence anisotropy of SR101 at the interfaces, when the polarity of the organic phase is low, the water/oil interface is thin with respect to the molecular size of SR101 (< 1 nm). In such a case, it is concluded that the interfacial polarity is well predicted by the arithmetic average of the polarities of the water and organic phases (eq 5.1). In the case of a relatively high polarity solvent (CB, *o*-DCB or DCE), on the other hand, $E_T(30)_{int.}$ was always lower than $E_T(30)_{calc}$. It is worth noting that, although thickness of the interfacial layer in these water/oil systems is ~1 nm as estimated by fluorescence dynamic anisotropy, the interfacial polarity deviates from $E_T(30)_{calc}$. Therefore, it is concluded that eq 5.1 dose not hold in these systems. Benjamin et al. predicted that the interfacial polarity was determined by both long-range interfacial solute-bulk solvent and local solute-interfacial solvent interactions (first shell).[10, 11] If this is the case, the interfacial polarity of a water/CB or water/DCE interface determined by Eisenthal et al. using SHG spectroscopy should also deviate from $E_T(30)_{calc}$. Nonetheless,

their observations do not agree with such a prediction. It is suspected that the origin of the present results on the water/oil systems would be due to the orientations of SRB adsorbed on the interface, as discussed below.

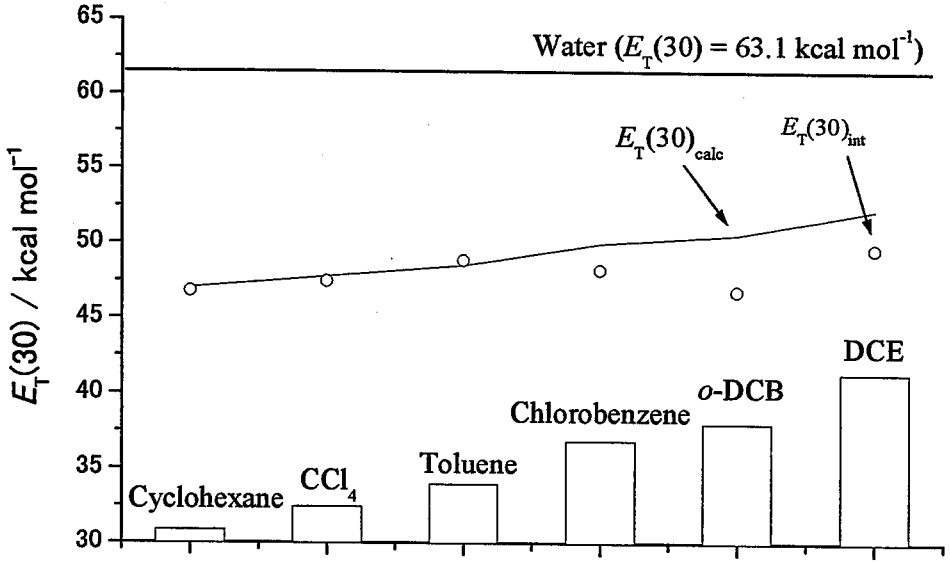

Figure 5-18 Relationship between $E_T(30)_{int}$ and $E_T(30)_{calc}$. Open circles and solid curve represent $E_T(30)_{int}$ and $E_T(30)_{calc}$, respectively.

The observed interfacial polarity agrees roughly with $E_T(30)_{calc}$ irrespective of an experimental method (SHG, ATR absorption, TIR fluorescence) as well as a probe molecule used (DEPNA, DPP, SRB). Therefore, it is concluded that the interfacial polarity is governed predominantly by long-range dipole-dipole interactions between solute and solvent molecules, as predicted by eq 1. When the interface is relatively flat and sharp with respect to the molecular size of SR101 (< 1 nm), the rotational freedom of the dye at the interface becomes two-dimensional-like. Therefore, the orientational distribution of the probe molecule at such an interface could be very narrow, as

schematically illustrated in Figure 5-19 (a). As reported previously, a xanthene dye is adsorbed on a water/heptane interface with the long axis of the xanthene ring being tilted about 70° to surface normal, while the $-SO_3^-$ group of the dye being directed to the water phase.[16] When the interface is molecularly sharp, the interface becomes two-dimensional-like. Therefore, the orientational distribution of the dipole moment governing the photophysical characteristics of SRB at the interface would be aligned with respect to surface normal. The electric field generated across the water/oil interface stabilizes the dipole of the probe molecule, since the direction of the electric field is parallel to the dipole moment of the dye (Figure 5-19 (a)). In such a case, the interfacial polarity coincides to $E_T(30)_{calc}$. On the other hand, when interfacial roughness is comparable to the molecular size of SR101 (~ 1 nm), three-dimensional-like rotational freedom of SR101 at the interface would render a random distribution of the dipole moment of the dye at the interface. The rough interface also leads to randomization of the direction of the electric field at the interface (Figure 5-19 (b)). As the result, the probe molecule adsorbed on the rough interface is less influenced by the electric field, leading to the interfacial polarity being smaller than $E_T(30)_{calc}$.

It is worth pointing out that the present results on the polarity at the water/CB and water/DCE interfaces do not agree with those demonstrated by SHG spectroscopy. It is suspected that SHG spectroscopy dose not necessary reflect all molecules adsorbed on the interface, since the signal is generated only by SHG active molecules aligned at the interface. On the other hand, Benjamin et al. predicted that the interfacial polarity at a rough interface became higher than that at a sharp interface. In their MD simulations, a probe molecule is assumed to be located at the interface of an oil side. In such a case, they demonstrated that the probe molecule was more likely to interact with water molecules at a rough interface compared to that at a sharp interface. However, this also

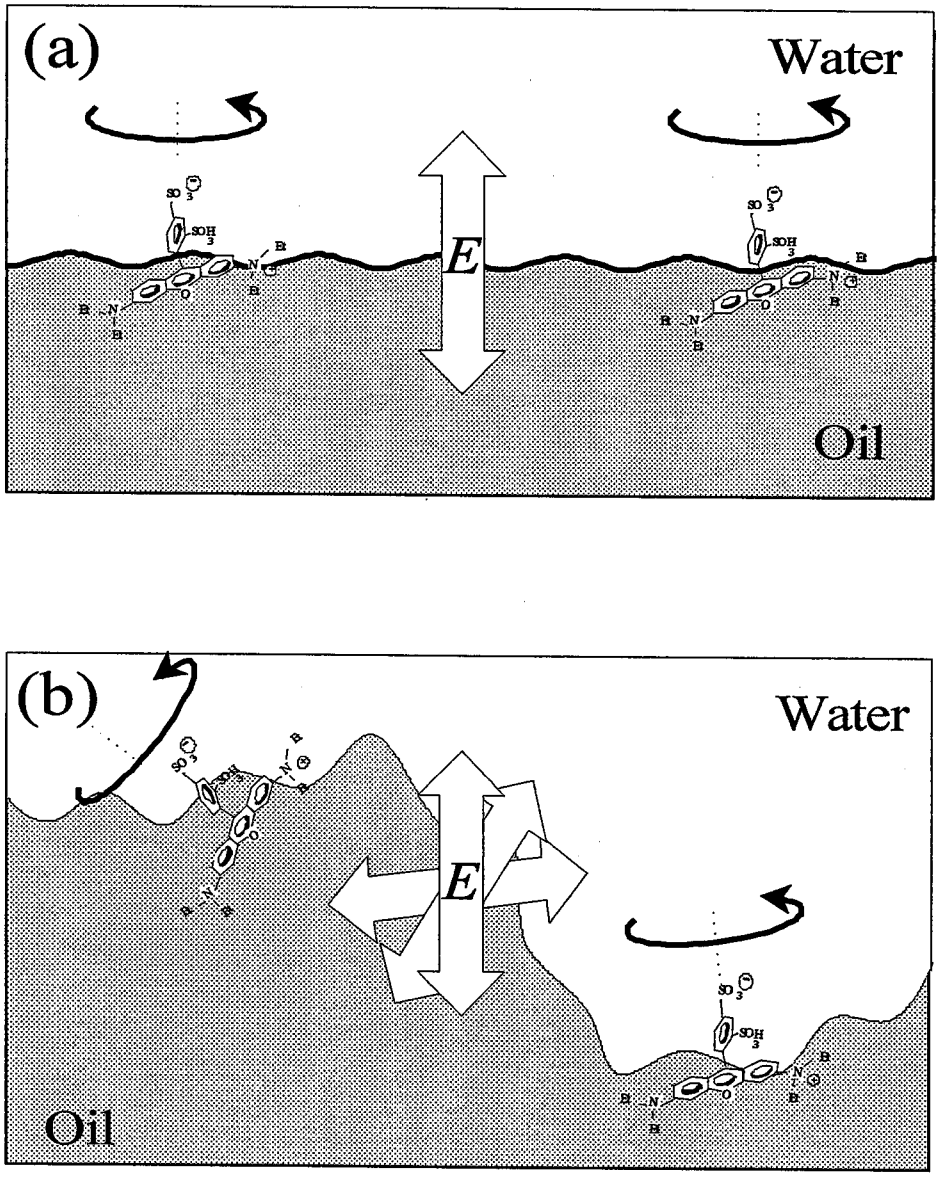

Figure 5-19 Schematic illustrations of sharp ((a)) and rough ((b)) water/oil interfaces. *E* denotes the direction of the electric field generated across the water/oil interface.

contradicts to the present experimental results for the rough interfaces. If their prediction is valid, the present results may indicate that SRB is adsorbed on the interface of the water side, by which interfacial roughness makes it more feasible to interact SRB with oil molecules. In the present discussions, although a role of short-range solute-solvent interactions was neglected, this would also play an important role in determining the excited state energy of SRB and, thus, the interfacial polarity reported by the probe molecule. A comparative study on the same liquid/liquid system by TIR, SHG, and MD simulations could reveal further molecular-level properties of the interface.

Conclusions

A study on excitation energy transfer dynamics of SR101 adsorbed on water/oil interfaces showed that water/DCB and water/DCE interfaces were rough (~7 nm), while the TIR fluorescence decay profiles of SRB adsorbed on the these interfaces demonstrated that the solution structures around the dye was uniform in the interface. According to these results, it was concluded that these liquid/liquid interfaces were sharp (~ 1nm), but rough in the range of ~7 nm (i.e., critical energy transfer distance). In the case of an oil having a relatively low solvent polarity, the relevant water/oil interfacial layer is thin (< 1 nm) and the interfacial polarity becomes to be equal to the arithmetic average of the polarities of the adjoining bulk phases. For a rough water/oil interface, on the other hand, the interfacial polarity observed dose not agree with $E_T(30)_{calc}$, probably due to random orientations of the probe molecule at the interface. The interfacial polarity is governed by not only the long-range interfacial solute-bulk solvent interactions, but also by local solute-interfacial solvent interactions (first shell).

References and Notes

(1) Watarai, H.; Sasaki, K.; Sasaki, S. *Bulll. Chem. Soc. Jpn.* **1990**, *63*, 2797–2802.

(2) Shioya, T.; Nishizawa, S.; Teramae, N. *Langmuir* **1998**, *14*, 4552–4558.

(3) Shioya, T.; Nishizawa, S.; Teramae, N. *Langmuir* **1999**, *15*, 2575–2579.

(4) Perera, J. M.; Stevens, G. W.; Grieser, F. *Colloids Surf. A* **1995**, *95*, 185–192.

(5) Zachariasse, K. A.; Phuc, N. V.; Kozankiewicz, B. *J. Phys. Chem.* **1981**, *85*, 2676–2683.

(6) Drummond, C. J.; Grieser, F.; Healy, T. W. *Faraday Discuss. Chem. Soc.* **1986**, *81*, 95–106.

(7) Warr, G. G.; Evans, D. F. *Langmuir* **1988**, *4*, 217–224.

(8) Bessho, K.; Uchida, T.; Yamauchi, A.; Shioya, T.; Teramae, N. *Chem. Phys. Lett.* **1997**, *264*, 381–386.

(9) Wang, H.; Borguet, E.; Eisenthal, K. B. *J. Phys. Chem. B* **1998**, *102*, 4927–4932.

(10) Michael, D.; Benjamin, I. *J. Phys. Chem. B* **1998**, *102*, 5145–5151.

(11) Michael, D.; Benjamin, I. *J. Chem. Phys.* **1997**, *107*, 5684–5693.

(12) Casey, K. G.; Quitevis, E. L. *J. Phys. Chem.* **1988**, *92*, 6590–6594.

(13) Casey, K. G.; Onganer, Y.; Quitevis, E. L. *J. Photochem. Photobiol. A: Chem.* **1992**, *64*, 307–314.

(14) Ishizaka, S.; Habuchi, S.; Kim, H.-B.; Kitamura, N. *Anal. Chem.* **1999**, *71*, 3382–3389.

(15) Beaumont, P. C.; Johnson, D. G.; Parsons, B. J. *J. Chem. Soc., Faraday Trans.* **1998**, *94*, 195–199.

(16) Ishizaka, S.; Nakatani, K.; Habuchi, S.; Kitamura, N. *Anal. Chem.* **1999**, *71*, 419–426.

(17) O'Connor, D. V.; Phillips, D. *Time-Correlated Single Photon Counting*; Academic Press: New York, 1986.

(18) (a) Klafter, J.; Blumen, A. *J. Chem. Phys.* **1984**, *80*, 875–877. (b) Klafter, J.; Blumen, A. *J. Lumin.* **1985**, *34*, 77–82.

(19) Buff, F. P.; Lovett, R. A.; Stillinger, F. H. *Phys. Rev. Lett.* **1965**, *15*, 621–623.

(20) Wirth, M. J.; Burbage J. D. *J. Phys. Chem.* **1992**, *96*, 9022–9025.

(21) Piasecki, D. A.; Wirth, M. J. *J. Phys. Chem.* **1993**, *97*, 7700–7705.

(22) Simpson, G. J.; Rowlen, K. L. *Chem. Phys Lett.* **1999**, *309*, 117–122.

(23) Karstens, T.; Kobs, K. *J. Phys. Chem.* **1980**, *84*, 1871–1872.

(24) Arbeloa, I. Lopez; Rohatgi-Mukherjee, K. K. *Chem. Phys Lett.* **1986**, *128*, 474–479.

(25) Arbeloa, I. Lopez; Rohatgi-Mukherjee, K. K. *Chem. Phys Lett.* **1986**, *129*, 607–614.

(26) Chang, T.-L.; Borst, W. L. *J. Chem. Phys.* **1990**, *93*, 4724–4729.

(27) Nakatani, K.; Ishizaka, S.; Kitamura, N. *Anal. Sci.* **1996**, *12*, 701–705.

(28) Reichardt, C. *Chem. Rev.* **1994**, *94*, 2319–2358.

(29) Israelachvili; J. N. *Intermolecular and Surface Forces*, Academic Press Ltd., 1992.

Chapter 6

Summary

Summary

In this thesis, several experimental approaches were proposed to obtain structural information about liquid/liquid interfaces at a molecular level and, the chemical and physical characteristics of the interfaces were discussed on the basis of time-resolved total-internal reflection fluorescence spectroscopy.

In order to apply the present experimental ideas to liquid/liquid interfacial systems under TIR conditions, interfacial adsorption of a probe molecule was a key point as discussed in Chapter 2. Fluorescence spectroscopy is intrinsically a high sensitive method compared to other optical methods. This is an advantage of the present method. Under TIR conditions, however, this sometimes disturbs the study on liquid/liquid interfacial systems. If a probe molecule possesses a high fluorescence quantum yield, namely, the dye fluorescence from a bulk phase excited by an evanescent wave is superimposed more or less to that from the interface. Therefore, a probe molecule should be highly surface active. Throughout the present study, surface-active fluorescence probes such as 1-pyrene sulfonate, sulforhodamine 101 and sulforhodamine B were employed, which was essential basis to obtain information about liquid/liquid interfaces.

In order to obtain structural information about liquid/liquid interfaces at a molecular level, two different approaches were introduced successfully to the study. One is a magic angle dependence of the TIR fluorescence decay profile of SR101 adsorbed on a liquid/liquid interface. First, this experimental idea was introduced to study water/PE interfacial systems (in Chapter 3). The observed rotational reorientation times of the dye provided molecular-level information about specific adsorption modes of SR101 on water/PE interfaces and, rotational freedom of SR101

observed at the interfaces also revealed that the water/PE interfaces were considered to be sharp in respect to the molecular size of SR101 (~1 nm). This method was shown to be a potential means to discuss the thickness of the interfacial layer in the spatial resolution of the order of ~1 nm. The other approach was a structural dimension analysis of excitation energy transfer dynamics between dye molecules adsorbed on water/oil interfaces. This method was also shown to have high potential to elucidate the thickness and roughness of the interfacial layer in the spatial resolution of the critical energy transfer distance (~7 nm) between an energy donor and an acceptor (Chapter 4). By using these two methods, the water/CCl_4 interface was demonstrated to be very sharp with respect to molecular dimension of SR101. On the other hand, the water/DCE interface was shown to be rougher than the water/CCl_4 interface. It is worth noting that the present results are first experimental proof of the structural difference between the water/CCl_4 and water/DCE interfaces. These approaches are very meaningful in respect to comparative discussion on the same systems by both experiments and available computer simulation data. Furthermore, it has been suggested that roughness of the water/DCE interface is caused by thermal fluctuation of the sharp (~ 1 nm) interface in the range of ~7 nm as described in Chapter 5. These results support a "sharp boundary model" described in Chapter 1.

These methodologies were also extended to study other liquid/liquid interfacial systems with the properties of an oil being varied (in Chapter 5). Such a systematic study on liquid/liquid interfaces has been scarcely explored up to the date and, therefore, the present study contributes to further advances in the relevant researches. Systematic investigations on liquid/liquid interfaces are the fist step to reveal factors governing structural and physical characteristics of liquid/liquid interfaces. Usually, interfacial roughness is explained in terms of the thermal capillary waves propagating at the interface, which are related to interfacial tension of the system. However, the thermal

capillary wave theory has been derived from macroscopic properties of a liquid/liquid interface, so that the theory is not necessarily sufficient to explain interfacial roughness at a molecular level. Actually, any clear relationship between interfacial tension and interfacial roughness could not be obtained in this study. The results clearly suggest that molecular-scale interfacial roughness would be governed by not only interfacial tension (as a macroscopic property), but also chemical/physical nature of an organic solvent itself. Liquid/liquid interfacial structures would be governed by several factors such as dipole moment, dielectric constant, hydrogen bonding, density, molecular shape of a liquid, and so forth, so that interfacial roughness and nature of a liquid could be correlated in a very compled manner. Further experimental and theoretical studies including a molecular dynamic simulation will reveal detailed characteristics at a liquid/liquid interface.

Various chemical processes at or across liquid/liquid interfaces are governed by the molecular level structures of the interfaces. For example, a relationship between interfacial thickness/roughness and the polarity at the interface was discussed in this thesis (in Chapter 5). Also, interfacial roughness may influence mass/electron transfer processes across liquid/liquid interfaces. In separation sciences, such a process is very important as a typical example being solvent extraction, liquid chromatography, and so on. Although flat liquid/liquid interfaces were studied in this thesis, the results and methodologies introduced by this study will contribute to further researches in the chemistry at liquid/liquid interfaces.

Acknowledgments

I would like to express my sincere gratitude to Professor Noboru Kitamura for his invaluable suggestions and helpful discussions and encouragement throughout this study. I would like to express my sincere gratitude to Dr. Kiyoharu Nakatani for his continuous guidance and invaluable suggestions and encouragement throughout the duration of this study. I am much grateful to Associate Professor Haeng-Boo Kim for his valuable discussions and advices. I also would like to thank Dr. Hiroshi Yao for their beneficial discussions and hearty encouragement. I am much grateful to Professor Kohei Uosaki, Professor Masatsugu Shimomura and Professor Iwao Yamazaki for the examination of this thesis.

I wish to thank colleagues in the Kitamura laboratory for their kind assists and cooperation.

I would like to express special thanks to my parents, wife and daughter for their supports and encouragement.

Shoji Ishizaka

Publication Lists

1) Nakatani, K., Ishizaka, S. and Kitamura, N. : "Time-resolved Total Internal Reflection Fluorometry of 1-Pyrene Sulfonate Anion at a Liquid/Liquid Interface", Analytical Science, 12: 701-705 (1996)

2) Kitamura, N., Ishizaka, S. and Kim, H.-B. : "Effects of Light-Scattering Coefficient of Absorbent in Diffuse Reflectance Spectroscopy of Dye-Doped Microparticles", Analytical Science, 13: 791-796 (1997)

3) Ishizaka, S., Nakatani, K., Habuchi, S. and Kitamura, N. : "Total-Internal Reflection Fluorescence Dynamic Anisotropy of Sulforhodamine 101 at a Liquid/Liquid Interface: Rotational Reorientation Times and Interfacial Structures" Analytical Chemistry, 71: 419-426 (1999)

4) Yoshimura, T., Ishizaka, S., Umakoshi, K., Sasaki, Y., Kim, H.-B. and Kitamura, N. : "Hexarhenium(III) Clusters $[Re_6(\mu_3\text{-}S)_8X_6]^{4-}$ (X = Cl^-, Br^-, I^-) are Luminescent at Room Temperature" Chemistry Letters, 7: 697-698 (1999)

5) Ishizaka, S., Habuchi, S., Kim, H.-B. and Kitamura, N. : "Excitation Energy Transfer from Sulforhodamine 101 to Acid Blue 1 at a Liquid/Liquid Interface: Experimental Approach To Estimate Interfacial Roughness" Analytical Chemistry, 71: 3382-3389 (1999)

6) Yoshimura, T., Ishizaka, S., Sasaki, Y., Kim, H.-B., Kitamura, N., Naumov, N. G., Sokolov, M. N. and Fedorov V. E. : "Unusual Capping Chalcogenide Dependence of the Luminescence Quantum Yield of the Hexarhenium(III) Cyano Complexes $[Re_6(\mu_3\text{-}E)_8(CN)_6]^{4-}$. E=$Se^{2-}$ > S^{2-} > Te^{2-}" Chemistry Letters, 10: 1121-1122 (1999)

7) Kobayashi, N., Ishizaka, S., Yoshimura, T., Kim, H.-B., Sasaki, Y. and Kitamura, N. : "Photoredox Ability of Hexarhenium(III) Cluster $[Re_6(\mu_3\text{-}S)_8Cl_6]^{4-}$" Chemistry Letters, 3: 234-235 (2000)

8) Yoshimura, T., Umakoshi, K., Sasaki, Y., Ishizaka, S., Kim, H.-B. and Kitamura, N. : "Emission and Metal- and Ligand-Centered Redox Characteristics of the Hexarhenium(III) Clusters, *trans*- and *cis*-$[Re_6(\mu_3\text{-}S)_8Cl_4(L)_2]^{2-}$, Where L is Pyridine Derivative or Pyrazine" Inorganic Chemistry, vol. 39, No. 8, 1765-1772 (2000)

9) Chen, Z.-N., Yoshimura, T., Abe, M., Sasaki, Y., Ishizaka, S., Kim, H.-B. and Kitamura, N.: "Chelate Formation around a Hexarhenium Cluster Core by the Diphosphane Ligand, $Ph_2P(CH_2)_6PPh_2$" Angewandte Chemie International Edition, vol. 40, No. 1, 239-242 (2001)

10) Ishizaka, S., Kim, H.-B. and Kitamura, N. : "Time-Resolved Total Internal Reflection Fluorometry Study on Polarity at Liquid/Liquid Interface" submitted.